AALBORG UNIVERSITET

INSTITUTE OF ENERGY TECHONOLOGY

A FAST METHOD TO EVALUATE ANNUAL ENERGY PRODUCTION OF DIFFERENT OFF-SHORE WIND FARM CONFIGURATIONS CONNECTED TO A VSC-HVDC LINE TRANSMISSION INCLUDING EVALUATION OF A NEW VARIABLE SPEED WIND TURBINE CONCEPT BASED ON RCC-WRIG

CONDUCTED BY GROUP WPS4-1056 and PED4-1038D
SPRING SEMESTER, 2009

Title:	**[A fast method to evaluate annual energy production of different off-shore wind farm configurations connected to a VSC-HVDC line transmission including evaluation of a new variable speed wind turbine concept based on RCC-WRIG]**
Semester:	**[4th]**
Semester theme:	**[Master Thesis]**
Project period:	**[Spring 2009]**
ECTS:	**[ ]**
Supervisor:	**[Ewen Ritchie / Lars Helle]**
Project group:	**[WPS4-1056]**

_____

[Jorge Varela Barreras]

_____

[Fernando Valderrey Sánchez]

SYNOPSIS:

This project is initiated by a proposal from Vestas Wind Systems A/S. The main goal is to develop a fast method to evaluate the energy production of different wind turbines (WT) in an off-shore wind farm (WF) connected to a VSC-HVDC line transmission. The proposal also includes the evaluation of a new wind turbine concept based on a V/f controlled Rotor-Current-Controlled Induction Generator. The evaluation method is based on simplified models of the considered machines and controls, which are solved analytically – without derivative or integrative terms and feedbacks. The converter topology proposed by the manufacturer is a two-level three-phase Voltage Source Converter. A first approach of the evaluation method is implemented in MATLAB/Simulink and it is used to evaluate and compare the performance of several WFs configurations (full scale SPMSG, DFIG, RCC-IG and SCIG) in an off-shore VSC-HVDC WF made up of one hundred 2 MW turbines. Aggregated WT models are employed and different wind speed distributions across the WF are considered. Results from this simulation are presented and discussed. It should be emphasized that specific results and conclusions from simulations can vary if WTs with different characteristics are employed or if e.g. the wind speed distribution across the WF varies. So the most important aspect of this report is to develop a proper fast evaluation method.

Copies:	[3]
Pages, total:	[121]
Appendix:	[YES]
Supplements:	[CD]

By signing this document, each member of the group confirms that all participated in the project work and thereby that all members are collectively liable for the content of the report.

Preface

The present project report entitled "**A fast method to evaluate annual energy production of different off-shore wind farm configurations connected to a VSC-HVDC line transmission including evaluation of a new variable speed wind turbine concept based on RCC-WRIG**" has been conducted by the group WPS4-1056 at the Institute of Energy Technology (IET), Aalborg University.

The project theme was proposed by the company Vestas Wind Systems A/S and is submitted in partial fulfilment of the requirement for the M.Sc.-degree in electrical engineering and wind power systems.

The literature references are mentioned by numbers in square brackets. Detailed information about the literature used in this project is presented in Bibliography. The figures have the format 'Fig.x.y', equations are in format '(x.y)', where 'x' is the chapter number and 'y' is the item number.

The enclosed CD-ROM contains the project report in Word DOC, Adobe PDF format, Matlab and Matlab/Simulink models.

Authors would like to thank their supervisors Ewen Ritchie and Lars Helle for the help and support provided during the project period.

The report is conducted by:

Jorge Varela Barreras

Fernando Valderrey Sánchez

Table of contents

Abbreviations list

Abbreviation	Description
BLDCM	Brushless DC Motor
CTAC	Constant Torque Angle Control
WT	Wind Turbine Generators
DDSG	Direct Drive Synchronous Generator
DE	Denmark
DFIG	Double Fed Induction Generator
DPC	Direct Power Control
DSC	Dynamic Slip-Controlled
EMF	Electromagnetic Force
EU	Europe Union
EWFM	Equivalent WF Model
EWTM	Equivalent WT Model
FOC	Field Oriented Control
FSWTS	Fixed Speed WT System
HV	High Voltage
IG	Induction Generator
IM	*Induction Machine*
IPMSM	*Interior Permanent Magnet Synchronous Machine*
LCC	*Line Commutated Converters*
LV	*Low Voltage*
NL	*Netherlands*
MTPAC	*Maximum Torque Per Ampere Control*
MV	*Medium Voltage*
PE	*Power Electronics*
PEC	*Power Electronics Converters*
PEE	*Power Electronics Equipment*
PCC	*Point of Common Coupling*
PLL	*Phase Locked-Loop*
PMACM	*Permanent Magnet AC Machines*
PMP	*Power Measuring Point*
PMSG	*Permanent Magnet Synchronous Machine*
PWM	*Pulse Width Modulation*
RCC	*Rotor Current Control*
SCIG	*Squirrel-Cage Induction Generator*
SM	*Synchronous Machine*
SPMSM	*Surface Permanent Magnet Synchronous Machine*
SPWM	*Sinusoidal PWM*
SVPWM	*Space Vector PWM*
STATCOM	*Static Synchronous Compensator*
SW	*Sweden*
THIPWM	*Third Harmonic Injection PWM*
UK	*United Kingdom*

VOC	*Voltage Oriented Control*
VRCC	*Vestas Rotor Current Control*
VSC	*Voltage Source Converter*
VSWTS	*Variable Speed WT System*
WECS	*Wind Energy Conversion System*
WF	*Wind Farm*
WP	*Wind Power*
WRIG	*Wound Rotor Induction Generator*
WRSG	*Wound Rotor Synchronous Generator*
WT	*Wind Turbine*

Chapter 1 Introduction

ABSTRACT

This project is initiated by a proposal from Vestas Wind Systems A/S. The main goal is to develop a fast method to evaluate the energy production of different WT configurations in an off-shore WF connected to a VSC-HVDC line transmission. The proposal also includes the evaluation of a new wind turbine concept based on Rotor-Current-Controlled Induction Generator. The method is based on simplified models of the considered machines and controls, which are solved analytically –without derivative or integrative terms and feedbacks. The converter topology proposed by the manufacturer is a two-level three-phase Voltage Source Converter (VSC).

Nowadays there is a great political and social effort to decrease the dependence on fossil fuels as energy sources. Definitely a lot of research on different energy sources is carried out with the wind energy as one of the most developed alternatives. Namely, wind power is the world's energy source with a highest annual growing rate – 30% – and a penetration of 12% of world electricity demand is predicted by 2020 [14].

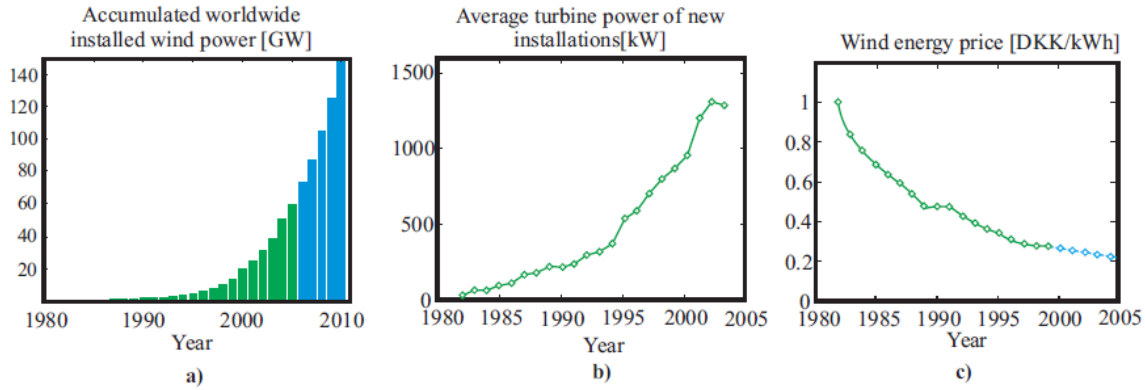

Fig. 1.1 Accumulated worldwide installed Wind Power (WP). b) Average power of new Wind Turbine (WT) installations. c) Estimated costs of wind energy price in Denmark [45]

In fact, wind energy is really a huge resource of power in a world sense – it was estimated that exploiting about the 10% of the total amount of wind power available is enough to cover all the electricity needs of the world [3]. Beyond this, wind energy is not just abundant; it is also renewable, clean and widely distributed. However, the installation of a wind farm (WF) produces certain environmental effects, such as visual impact, noise or danger to birds.

Until now, wind power did not compete against fossil fuels on the same level – it has been supported by public incentives and subsidies. But the price of power produced from wind turbines (WT) is continuously falling, mainly due to the development of power electronics and the increase of the average power of new installations (Fig. 1.1). Thanks to that, wind technology is becoming more and more attractive not only as a renewable source, rather as a competitive energy source [4].

1.1 Expected scenario

A key point to reduce the costs of wind projects is to promote the installation of multi-megawatt WF made of identical technology. The experience of the last twenty years demonstrates that great savings can be achieved in this way, especially on the installation and maintenance of the WF.

It has been stated that at places with good wind characteristics on-shore multi-megawatt WF can be cost-competitive, but the development of these projects is limited by the availability of large areas.

One solution to avoid land congestions and to minimize visual and noise impact is the development of off-shore WF. Furthermore, the installation of a WF far from the shore usually improves the wind characteristics – higher speeds, less turbulence and lower wind-shear.

Since the wind power increases with the cube of the wind speed, an increase of 10% in wind speed implies an increase of more than 30% in wind power available. Moreover less turbulences result on less fatigue loads and less actions of pitch angle controllers of the blades, which improves the reliability of the system.

But on the other hand, off-shore projects still require higher investments due to:

- The marine foundations.
- The corrosion protection.
- The integration into the on-shore AC network.
- The installation procedures.
- The limited access for operation and maintenance.

In general terms, the investment is increased 30% to 50% in comparison with on-shore installations [28].

Despite of this, it is expected that along the next decade significant cost-savings can be achieved, based on the experience gained by the off-shore industry during last 20 years.[45] In fact, many studies have stressed the enormous potential of the off-shore WF and have predicted an enormous growth of the annual wind power installed capacity.

It is foreseen that around 20 to 40 GW of off-shore wind power will be into operation in the EU by 2020 [28].

The design of WT optimized for the off-shore environment – greater sizes and reliability – is one key point in this cost reduction.

EU members as Denmark, United Kingdom, Sweden, Belgium and Germany have already built off-shore WF. The picture below shows the off-shore WF in operation and to be built in 2008-2009 in Europe (Fig. 1.2).

Fig. 1.2 Off-shore WF in operation and to be built in 2008-2009 in Europe [28]

Since off-shore WF are made up of large multi-megawatt aggregations and on-shore connection points are usually relatively weak, the impact of the WF on power system quality and reliability should be carefully considered, especially in relation to WF correlated rushed shutdown of WT. Normally dynamic grid stability is considered the main limiting factor, over other factors as flicker, harmonics and static stability.

Owing to the increase of wind power penetration in power systems, tasks as stabilization and control, traditionally undertook by conventional power plants, becomes a key point on wind power development. [6] [9] In fact, network operators have introduced grid connection requirements for WT worldwide. [10] [11] [12] [13]

A lot of information about stability and control of specific WF topologies can be found in current available literature, mainly focused on "connection and disconnection of the WT, grid disappearance, short circuit power contribution, voltage dips and power quality during the production"[9].

1.2 Wind turbine technology

WT technology has been developed during last 25 years and nowadays there is a wide range of WT configurations. The main components of a WT system are shown in next figure. As it can be seen, some of the components are optional.

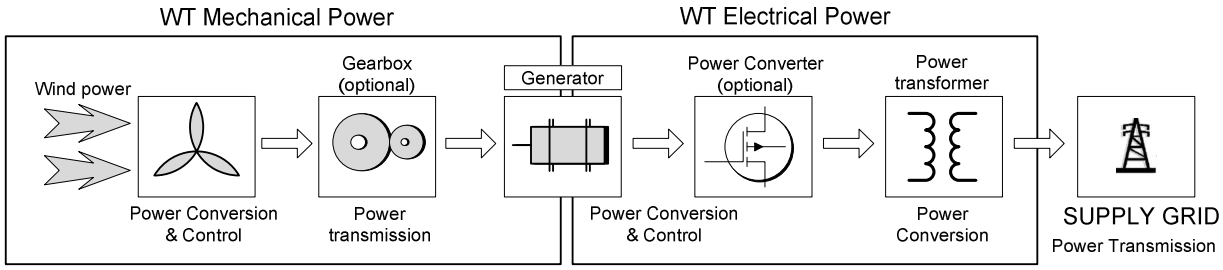

Fig. 1.3 Main components of a WT system.

The wind kinetic energy is converted into mechanical energy by the rotor blades. The number of blades is usually three and the rotor speed increases as the blades radius decreases. The average power delivered by the turbine rotor is limited aerodynamically by stall control, active stall control or pitch control. More details about aerodynamic control are given further.

Since the rotational speed of megawatt WT ranges between 10-15 rpm a gear box is usually employed between the turbine rotor axis and the turbine generator axis. This converts low-speed high-torque power into high-speed low-torque power suitable to standard generators. Multipole generators can be driven directly (without gearbox), but in this case the size and weight of the generator are considerably higher.

The mechanical energy is converted into electrical energy by the generator, and is delivered into the grid through a power electronics converter (optional) and a transformer. The connection of an individual WT or a whole WF at the point of common coupling (PCC) can be made at low, medium, high or extra high voltage, mainly depending on the amount of power to be transmitted – higher currents implies higher transmission losses – e.g. most of single WT are connected at medium voltage while large multimegawatt off-shore WF are connected at high or extra high voltage.

Attending to the wide range of components, many WT configurations are possible and several classifications can be made. But broadly, WT systems are divided into two basic groups: fixed speed WT systems (FSWTS) and variable speed WT systems (VSWTS).

FSWTS have been widely used from the beginning because of their simplicity for power ratings up to 2.3 MW. In fact FSWTS offer a low cost solution, in terms of investment and maintenance, with a high reliability. But there are several drawbacks which are going to limit their use in the expected future scenario.

1.2.1 Fixed speed wind turbine systems

FSWTS, so called “the Danish concept” since they were employed first in Denmark, use squirrel-cage induction generators (SCIG) directly connected to the grid with a transformer (Fig. 1.4).

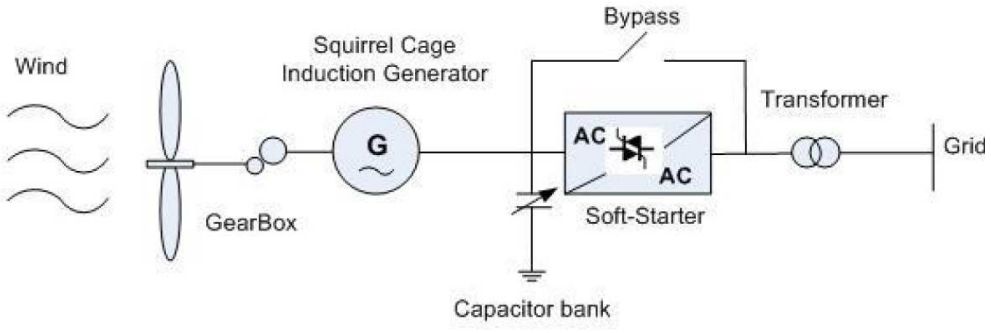

Fig. 1.4 Configuration of fixed speed WT – SCIG.

In case of small WT FSWTS looks most cost competitive technology, but in multi-megawatt WTs suitable for large WFs several drawbacks appear. Next the main problems are explained.

Aerodynamic conversion

A certain amount of the kinetic energy of the wind is converted into mechanical energy by the WT rotor blades. The total power delivered to the shaft of the rotor is given by equation (1.1): [56][57]

$$Pwt = \frac{1}{2}\rho A_v V^3 Cp(\lambda, \theta) \tag{1.1}$$

Where Pwt is mechanical power, ρ is the air density, A_v is the area swept out by the WT blades, V is the wind speed, $Cp(\lambda, \theta)$ is the power coefficient, λ is the tip speed ratio and θ is the pitch angle. As it can be seen the mechanical power depends on a factor called power coefficient which at the same time depends on the tip speed ratio and pitch angle of the rotor blades.

Tip speed ratio can be obtained as a relation between tip of the blade speed and the wind speed (1.2). The typical relation between the tip speed ratio and the power coefficient is illustrated on Fig. 1.5. [57]

$$\lambda = \frac{\Omega}{V} \tag{1.2}$$

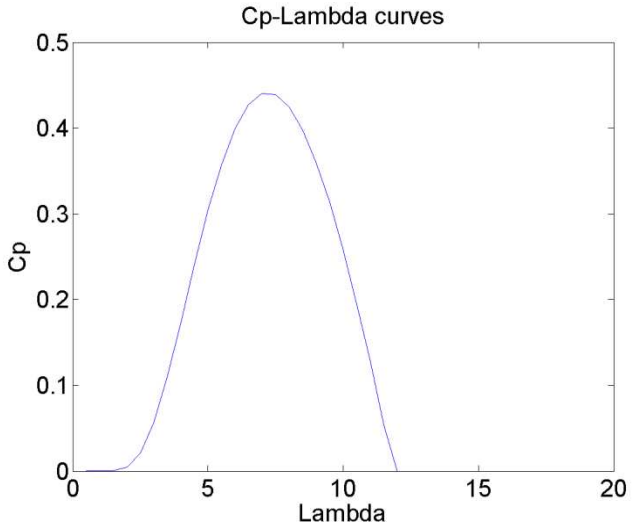

Fig. 1.5 Cp-Lambda curve for θ=0.

The highest effectiveness of the power generation can be obtained following maximum value of Cp curve[1]. The only way to operate with maximum output power is to adjust rotor speed to wind speed (Fig. 1.6), using variable speed generators [56][57]**.** This is the main disadvantage of the FSWTS vs. VSWTS.

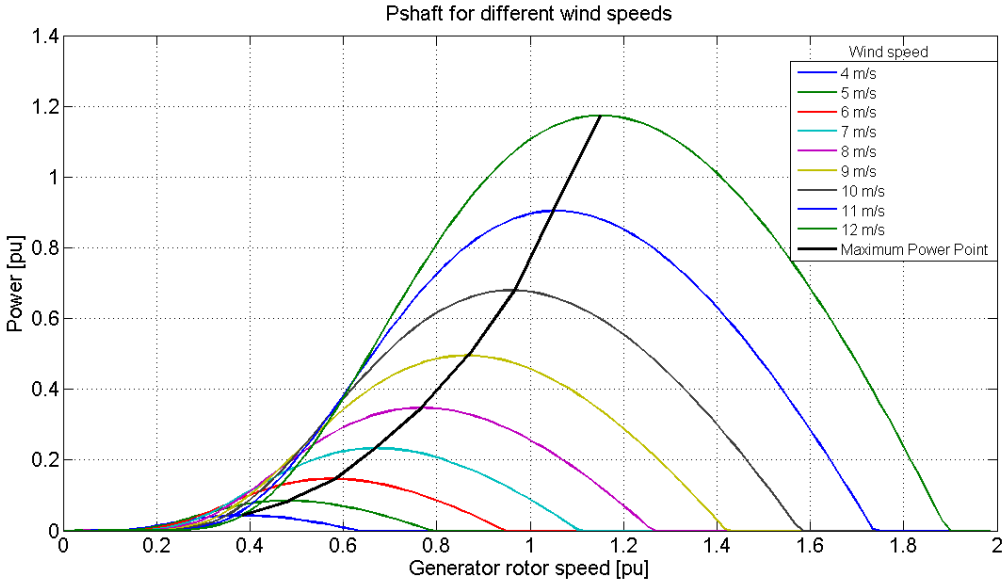

Fig. 1.6 Wind turbine power vs. rotor speed

Next figure (Fig. 1.6) illustrates the previous statement. In literature this idea is broadly supported, e.g. McIver [60] calculated an improvement of 9-15% in energy capture employing VSWTS.

[1] *In 1919 a German physicist, Albert Betz, demonstrated that no WT can convert more than 59.3%* $(^{16}/_{27})$ *of the total kinetic energy in the wind. His theory is known as the Betz's law, and states the theoretical maximum Cp of a WT.[59]*

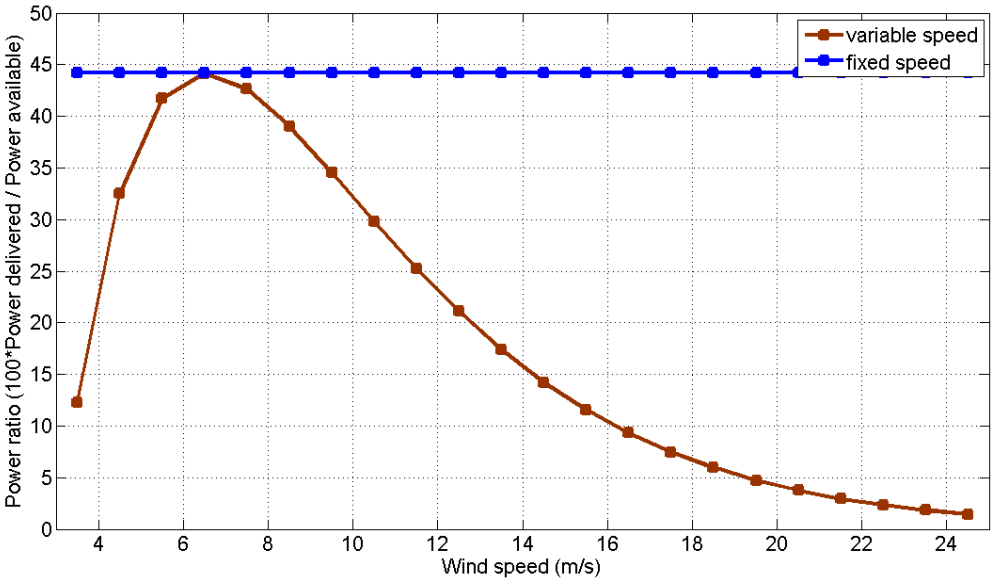

Fig. 1.7 Fixed speed vs Variable speed WTs

Mechanical stress

Since FSWTS operate at constant speed (±1-2% rated speed) high mechanical stress appear on the mechanical system due to torque pulsations caused by strong wind gusts. The next statement can be done:

The peak load conditions of the mechanical system (gear train and gear box) for a FSWTS are higher than for a VSWTS of the same size. So the mechanical dimensions of a VSWTS could be reduced in comparison with a FSWTS. This means less expensive mechanical construction.

In [61] the improvement on the mechanical stress is showed comparing the performance of a FSWTS with a VSWTS.

Power management

Three main problems arise on power management when FSWTS are employed:

- Flicker sensitive: torque pulsations on the drive train are directly translated into voltage flicker on the grid.
- Reactive power consumption: FSWTS do not control reactive power, so an active or passive compensator is needed to reduce the demand of reactive power from the grid.
- Soft starter is needed to limit high currents at start: this is short circuited when the connection is finished.

Moreover FSWTS do not allow *island operation*[2] and do not have full *rolling capacity on grid*[3].

[2] *"The island operation may occur in some situations in case of grid collapse and the ability of operating in such a situation could be useful for minimizing the possible area of blackout". [5]*

[3] *"The rolling capacity on grid means that a WT keeps active when a fault appears in the grid and has the possibility to reduce the power production even though more power is available in the wind and thereby act as a rolling capacity for the power system". [5]*

Owning to the several drawbacks commented, FSWTS penetration on power systems is intrinsically limited.

1.2.2 Variable speed wind turbine systems

On the other hand variable speed WT systems, made up with several generator concepts directly or indirectly connected to the grid, have become more and more important in recent years. This is mainly because variable speed systems allow active and reactive power control – can decouple the speed control from the grid– and comply better with grid requirements: many configurations allow island operation and have full rolling capacity on grid. [5][15]

Decoupling the speed control from the grid also means a reduction of mechanical stress and flicker contribution. Kinetic energy from wind gusts, which appears as torque pulsations, can be stored as mechanical rotational energy in the moment of inertia of the rotor, since the system is capable of keeping the output power constant at variable rotor speed in a certain range.

Furthermore the variable speed WT systems performance presents reduced acoustic noise and is more efficient – can generate more energy for a given wind speed (especially at low speeds). The WT rotational speed is adjusted as a function of wind speed with the purpose of maximizing the output power. But the initial investment is naturally higher than fixed speed due to the presence of power converters and the resulting system is more complex and sensitive.

It should be noted that the method of controlling the converter strongly affects the WT performance.

Variable Speed Wind Turbines With Full-Scale Power Converters

In Direct Driven Synchronous Generators (DDSGs) the stator is connected to the power grid via a full scale power converter and a transformer (Fig. 1.8). Then the stator frequency is variable, allowing the operation at maximum power point for the full power range. The generator can be either a Permanent Magnet Synchronous Generators (PMSG) or a Wound Rotor Synchronous Generator (WRSG). A similar configuration is also employed with SCIG. It should be noted that if standard generators (not multipole) are employed a gearbox is needed. Turbines equipped with this type of configuration are called full-scale WT.

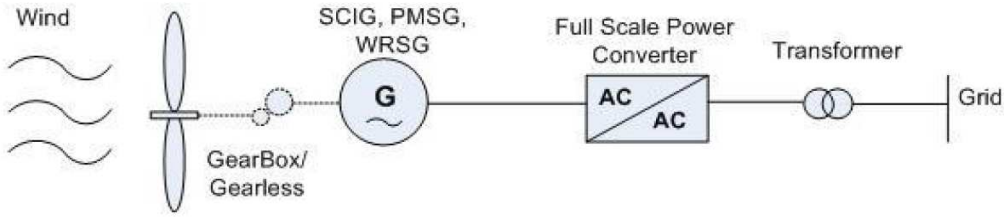

Fig. 1.8 Variable speed configuration: Full-scale WT.

Several configurations can be used for the AC/AC converter Naturally, the AC/AC converter efficiency is a key point on the total system efficiency.

Variable Speed Wind Turbines with Partially Rated Power Converters

A. Double Fed Induction Generator (DFIG) systems

DFIG systems uses medium scale four-quadrant converter connected to the rotor windings via slip rings, while the stator is connected directly to the power grid (Fig. 1.9). As the stator is connected directly to the grid via a transformer, its voltage and frequency are constant. Depending on the working mode, super-synchronous or

sub-synchronous, electric power is delivered to the grid from the rotor and the stator or from the grid into the rotor respectively. Using a converter of 30% of rated nominal power a speed range of ±30% around synchronous speed can be achieved [5].

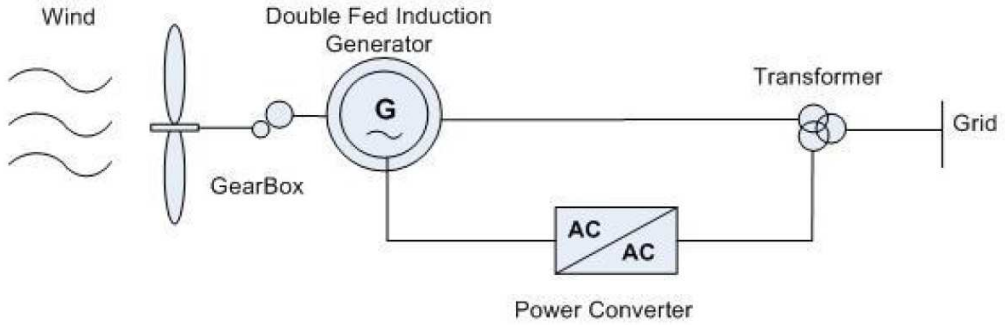

Fig. 1.9 Variable speed configuration: DFIG WT.

DFIG WT systems are cheaper than full-scale WT systems since the nominal power of the converter is only a fraction of the nominal power of the WT: the size of the converter and DC-link capacitor are reduced. But it has the next disadvantages: the operation at maximum power point cannot be done for the full power range, increased maintenance cost due to the slip rings and high sensitivity of the converter to grid faults.

B. Dynamic Slip-Controlled (DSC) Wounded Rotor Induction Generator (WRIG) systems

DSC WRIG WT systems are a variation of fixed speed SCIG WT systems. To reduce the effect of the wind gusts – torque pulsations which produce power fluctuations – a variable extra resistance is added to the wounded rotor (Fig. 1.10).

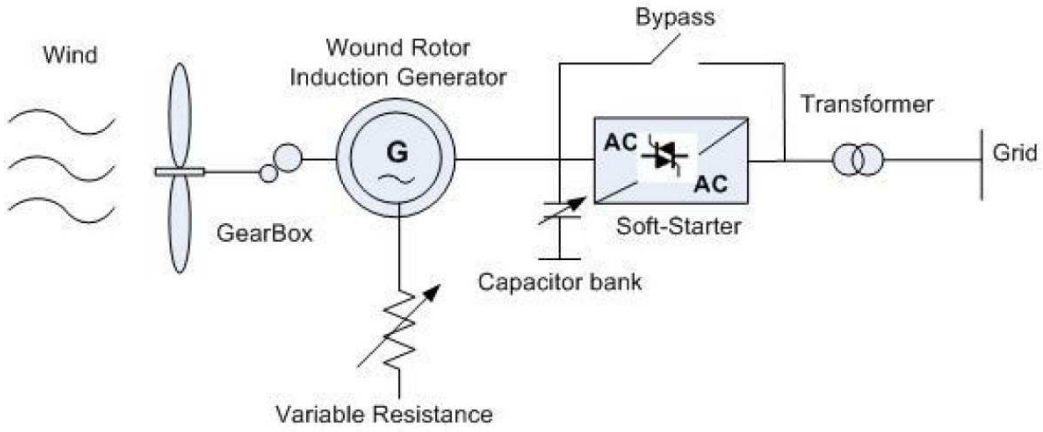

Fig. 1.10 Variable speed configuration: WRIG

Controlling the rotor current with a power electronics device as a chopper is possible to run the generator with semi variable speed – varying the slip – keeping the output power constant. Usually a speed range of 2-5% is obtained [5] (Fig. 1.11). In this way the system efficiency is improved, since the power fluctuations are stored as rotational energy in the rotor.

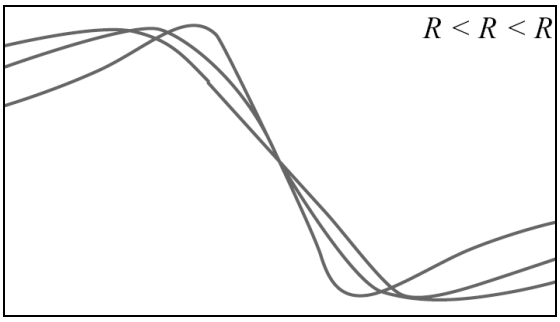

Fig. 1.11 Torque and speed characteristics of DSC WRIG system [5].

DSC WRIG systems improve the performance of fixed speed systems, but still a soft starter and a capacitor bank is needed. Moreover reactive power cannot be controlled since no power is delivered into the rotor windings.

OptiSlip® system [18] [19]

Vestas Wind Systems A/S has developed a commercial DSC WRIG system called OptiSlip®, which can achieve a variable speed range up to 10% without ring-brushes and an improved quality of delivered power (compare to fixed speed systems).

Since the ring-brushes and specially the power converter are avoided, OptiSlip® maintenance and investment costs are much lower than DFIG or DDSG.

Next table shows the world market share of different wind systems (Table 1.1). It can be seen that OptiSlip® covers a considerable amount of the market.

Wind System	Market Share
Fixed Speed / Stall	23%
OptiSlip® / Pitch	11%
DFIG / Pitch	50%
DDSG / Pitch	16%

Table 1.1 World market share of different wind systems. Source: BTM Consults 2001 [20].

The WRIG integrates a Vestas Rotor Current Controller (VRCC) rotating with the rotor. The VRCC is made up of resistances, IGBTs, Diodes Bridge, current sensors and a microprocessor control and has a fast dynamic response. Communication and control signals are sent through an optical link. In this way the ring-brushes are avoided (Fig. 1.12).

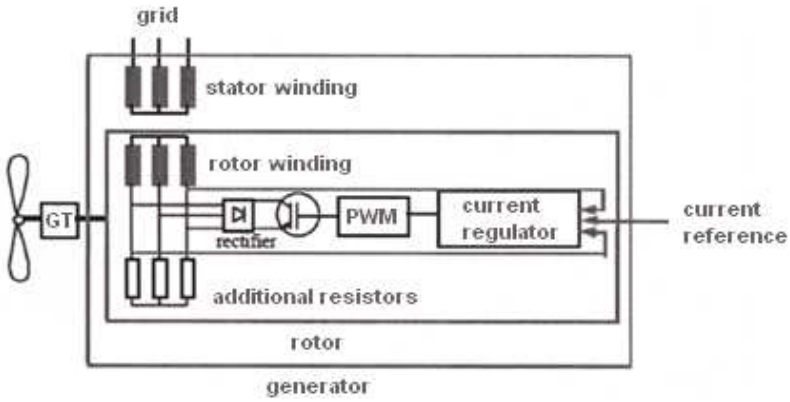

Fig. 1.12 OptiSlip® VRCC.

1.2.3 WT State of the art

Today the major WT manufacturers are developing turbines with capacities on order of 3-6 MW, all based on variable speed WT systems with pitch control employing doubly-fed induction generator – most of them – or direct-driven synchronous multipole generator [16]-[18]. FSWTS with stall control are considered unfeasible for this range of power [15].

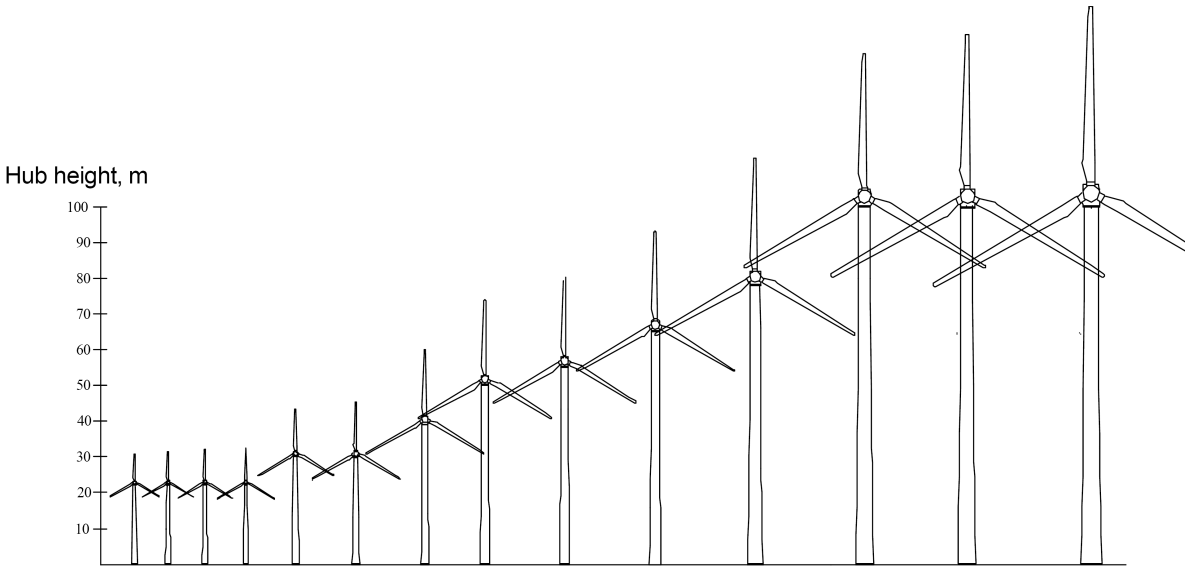

Capacity	55 kW	75 kW	90 kW	100 kW	200 kW	225 kW	500 kW	600 kW	660 kW	850 kW	1750 kW	2000 kW	3000 kW
First install.	1981	1984	1986	1987	1988	1989	1991	1995	1997	2000	1999	2000	2002
Rotor	15/16 m	17 m	19 m	20 m	25 m	27/29 m	39 m	44 m	47 m	52 m	66 m	80 m	90 m
Control	Stall	Stall	Stall	Stall	Stall	Pitch	Pitch/OptiSlip	Pitch/OptiSlip	Pitch/OptiSlip	Pitch/OptiSpeed	Pitch/OptiSpeed	Pitch/OptiSpeed	Pitch/OptiSpeed
Tow er	22 m	22 m	22 m	31 m	31 m	39 m	50 m	50 m	55 m	49- 65 m	60-78 m	60-100 m	80 m
MWh/year	217	265	301	346	662	860	1671	1904	2372	2998	5303	7041	

Fig. 1.13 Vestas WT development [9].

1.3 Electrical topologies of wind farms

As it has been stated before it is expected that in the near future off-shore WF will play an important role on the grid power quality and control. The development of technological solutions based on Power Electronics Equipment (PEE) is a cornerstone to achieve the present and future grid demands.

Next figure shows the general topology of an off-shore WF (Fig. 1.14).

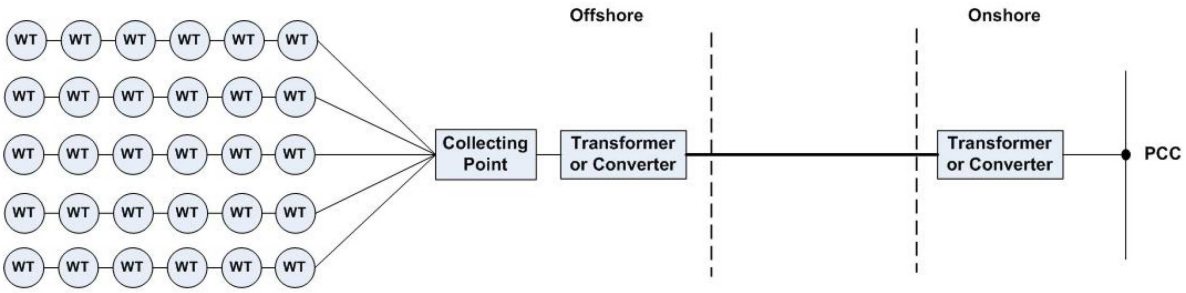

Fig. 1.14 General topology of an off-shore WF [28].

The wind park or WF is made up of many WT – from tens to more than 100 – aggregated in long arrays. Typically the WT generates in low voltage (LV), then a low/medium voltage (LV/MV) transformer or converter is employed to connect each WT to the medium voltage (MV) internal electrical network of the WF. This MV common line connects each group of WT to the collecting point of the WF substation, where a medium/high voltage (MV/HV) converter or transformer converts the electricity at high voltage (HV). Then a HV submersible transmission line connects the off-shore substation to an on-shore substation, where a transformer or converter adapts the power characteristics to the demands of the PCC.

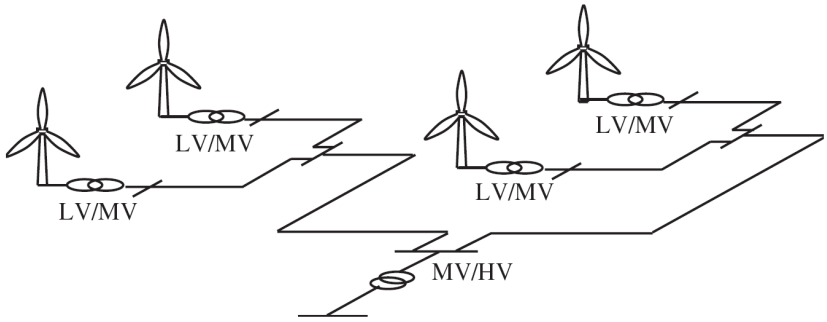

Fig. 1.15 Example of internal electrical network of a WF [27].

WF control includes control of each individual WT and the control of the entire WF. The strategies of control depend on the WF topology, which is defined by the kind of technology employed in the WT and the off-shore/on-shore transmission line.

WFs equipped with Power Electronic Converters (PEC) can regulate at the PCC voltage and frequency and both active and reactive power, and can control the speed of the WT in order to maximize the energy conversion and to minimize the voltage fluctuations, the fatigue loads and the acoustic noise.

One variable speed WT solution based on DFIG is shown in next figure (Fig. 1.16). This layout, with an AC grid connection, is employed in Horns Rev off-shore WF. This WF is made up of 80 WT able to deliver 160MW and is located in the North Sea, 14 kilometers west of Denmark.

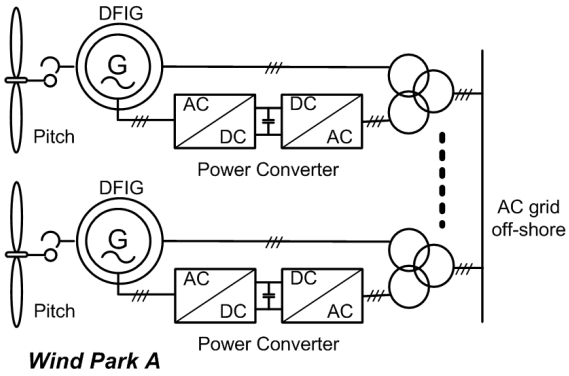

Fig. 1.16 Off-shore WF with AC grid transmission line based on DFIG variable speed WT [33].

A fixed speed WT solution ("Danish Concept") is shown in Fig. 1.17. This layout requires lower maintenance and initial investment, but presents worse features acting as a power station to the grid. Soft starter and reactive power compensation are needed.

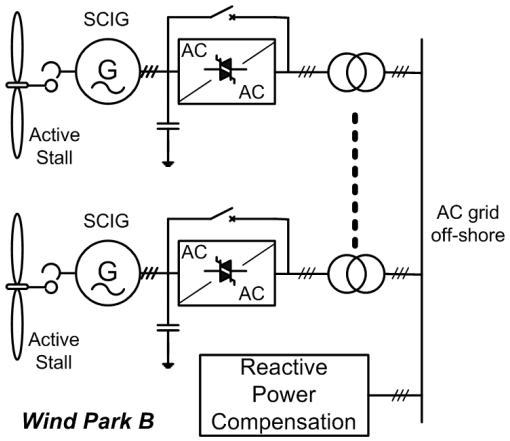

Fig. 1.17 Off-shore WF with AC grid transmission line based on SCIG fixed speed WT [33].

Wind Park A and B are based on HVAC transmission systems between the off-shore and the on-shore substations. Nowadays most of the WFs in operation are based on these systems, e.g. Horns Rev – 160MW (DK), Nysted – 170MW (DK), Horns Rev II – 200MW (DK), Lynn and Inner Dowsing – 194MW (UK), Burbo Bank – 94MW (UK) or Prinses Amalia – 120MW (NL).

The current trend is to develop much larger WFs. Some approved projects are London Array – 1GW (UK), Greater Gabbard – 500MW (UK), Kriegers Flak I – 330MW (DE), Kriegers Flak II – 640MW (SW) or Kriegers Flak III – 450MW (DK) [29] [30]. For the level of power of these off-shore WFs the employment of HVDC transmission lines (classical or based on Voltage Source Converter (VSC)) is being considered.

A fixed speed WT solution ("Danish Concept") with a VSC-HVDC transmission line is shown below (Fig. 1.17). The AC WF grid frequency and voltage are the same for all the WT. A soft starter is included in the layout, but is not mandatory. This topology can be also applied with variable speed WT solutions as full-scale, DFIG or RCC [31] [32].

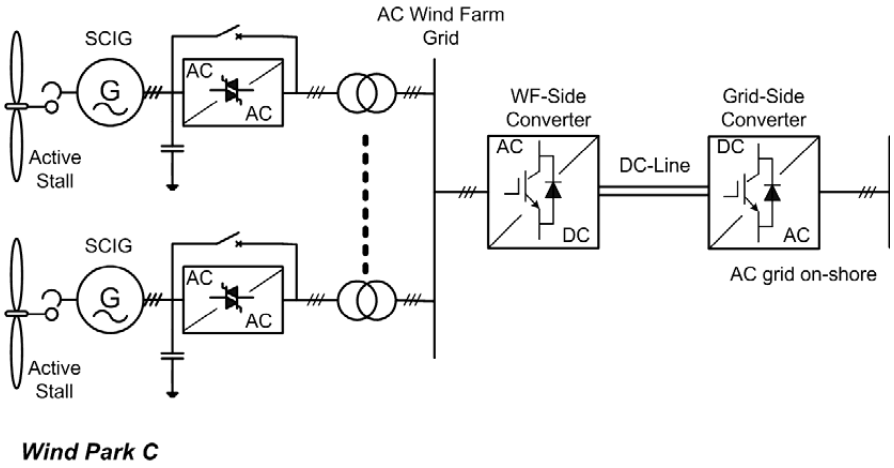

Fig. 1.18 Off-shore WF with HVDC grid transmission line based on SCIG fixed speed WT [33].

VSC-HVDC transmission of wind power is currently in operation on pioneer projects as Tjaereborg by Eltra (DK) and Gotland by ABB (SW). [26] [42]

All the off-shore WF topologies proposed in this project employ the WF configuration depicted on Fig. 1.18.

Another VSC-HVDC solution, presenting a common DC WF grid, is given in Fig. 1.19. Using this topology full-scale variable speed operation can be achieved. The principal advantage of WF type D is that no DC/AC converters and substation platform are needed off-shore.

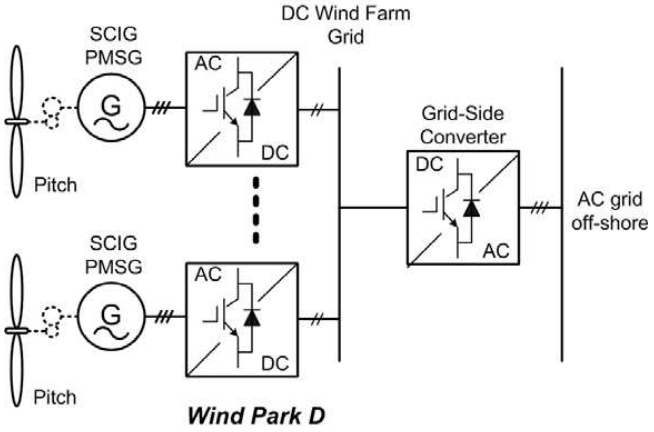

Fig. 1.19 Off-shore WF with HVDC grid connection based on full-scale variable speed WT [33].

A general comparison between the presented WF topologies is shown in next table.

	Wind Park A	Wind Park B	Wind Park C	Wind Park D
Individual speed control	Yes	No	Yes	No
Control active power electronically	Yes	No	Yes	Yes
Control reactive power	Yes	Centralized	Yes	Yes
Short circuit (active)	Partly	Partly	Yes	Yes
Short circuit power	Contribute	Contribute	No	No
Control bandwidth	10-100 ms	200ms - 2s	10 -100 ms	10 ms – 10 s
Stand by-function	Yes	No	Yes	Yes
Soft-starter needed	No	Yes	No	No
Rolling capacity on grid	Yes	Partly	Yes	Yes
Redundancy	Yes	Yes	No	No
Investment	+	++	+	+
Maintenance	+	++	+	+

Table 1.2 Comparison between WF topologies [33].

Finally, a multiple way to connect an off-shore WF to the grid is shown (Fig. 1.20). VSC-HVDC and HVAC transmission lines are implemented at the same time. This allows choosing between each connection, depending on the generated wind power, in order to maximize the power delivered to the grid. Also both systems could be employed together. This topology might appear more often if current WFs are enlarged.

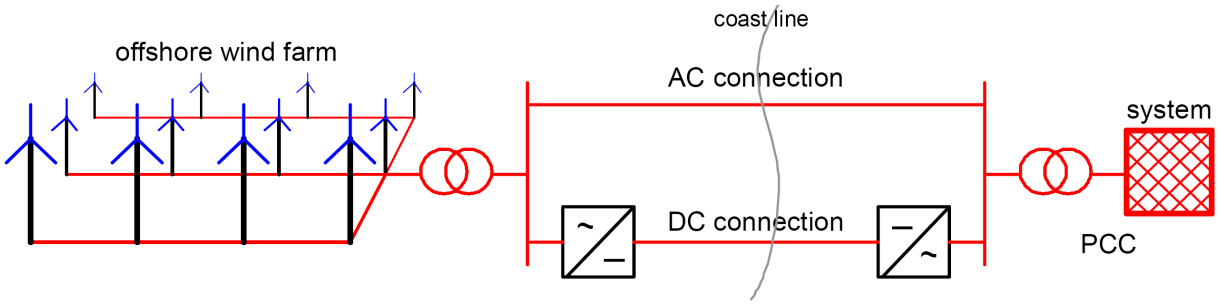

Fig. 1.20 Off-shore WF with HVAC and HVDC transmission [39].

1.4 Off-shore wf connection

Nowadays, due to the expected large capacity of the new off-shore WF, issues related to the connection of the WF to the grid system are becoming more interesting. New investigations are centered on transmission power losses, transmission faults, power quality or investment costs.

As above stated, there are four basis connections systems: HVAC, classical HVDC, VSC-HVDC and the combination of the previous.

1.4.1 HVAC

By now, HVAC transmission lines are the common solution adopted in transmission lines, but many studies stress on VSC-HVDC as “a very promising technology, especially from a technical viewpoint” for off-shore WF [39].

HVAC systems are simple passive systems up to 170kV with sea cables, which represent the most reliable and cheap solution when the off-shore WFs are relatively small and relatively close to the PCC. As the distance and the size of the WFs increase the power losses increase too and the reactive power active compensation becomes a requirement. “The AC transmission cables capability is limited by the capacitive charging current and

a long AC cable can cause system instability" [39]. HVAC transmission capacity is represented in next figure (Fig. 1.21). In this case is considered that "the critical distance is achieved when half of the reactive current produced by the cable reaches nominal current at the end of one cable" [41].

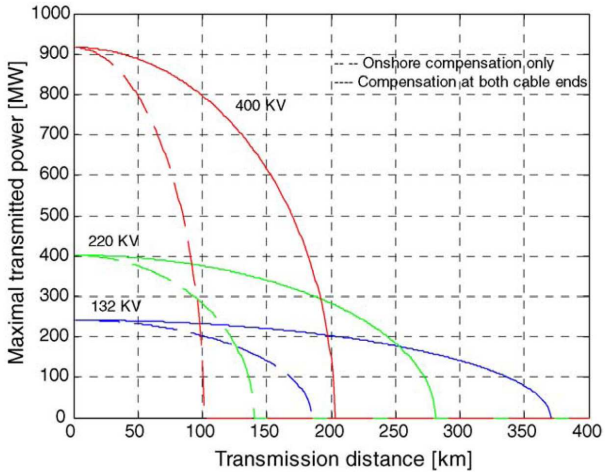

Fig. 1.21 HVAC transmission capacity for three voltage levels [41].

1.4.2 Classical HVDC

Classical HVDC transmission systems are based on line commutated converters (LCC). Originally these systems were based on arc valves, but during the early 1970s they started to be replaced by thyristors [43].

Since the first commercial installation in Gotland (SW) in 1954, LCC based HVDC systems have been employed both on land and submarine in lot of long-distance projects around the world up to 800kV and a power range up to 6000MW. [26] [39] [41] [44]

The advantages are lower transmission power losses, grid decoupling in case of failure, no synchronization required between WF and grid and certain active and reactive power control [39]. The main drawbacks of this technology are the need of the reactive power for the thyristor valves and the possible harmonic injection (need of AC filters) [41].

Certain reactive power control is commonly achieved with the installation of capacitor banks or STATCOM (Static Synchronous Compensator). However independent control of reactive power is impossible since the thyristor are line-conmutated devices (only two quadrant control is achieved).

Due to the cost of converter stations is not employed for short distances and small power.

1.4.3 VSC-HVDC

VSC-HVDC transmission systems are a very promising technology which is being widespread since it was used first for transmission in 1997 in Gotland (SW) [26]. They are based on state of the art power semiconductor devices, the last generation of IGBTs. IGBTs can be switched on and off by a very low power gate signal.

Fig. 1.22 shows a standard four-units bipolar HVDC arrangement made up of four three-phase Pulse Width Modulation (PWM) converters – two of them in the off-shore substation and another two in the on-shore. While Fig. 1.23 shows a standard two-units bipolar HVDC transmission system.

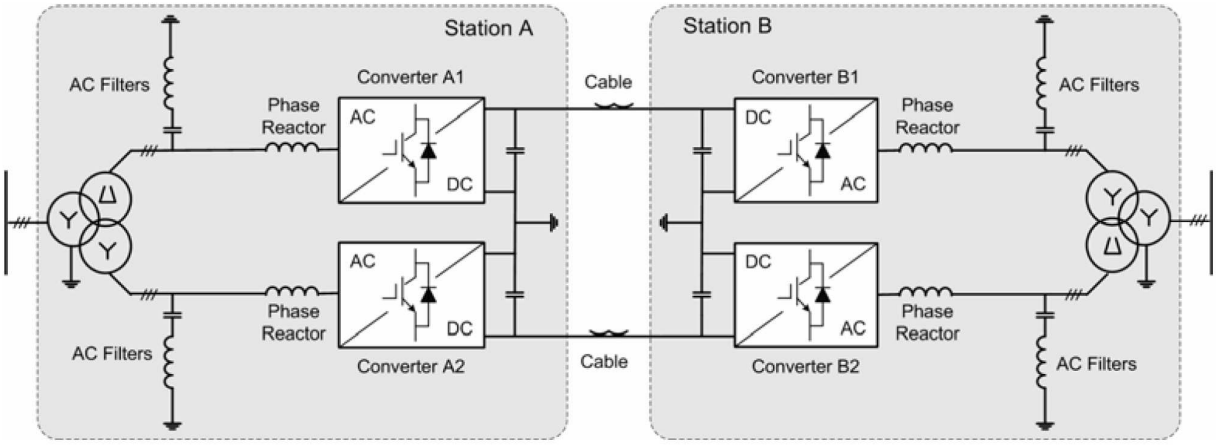

Fig. 1.22 DIAGRAM 1: 4 units bipolar HVDC transmission system [42]

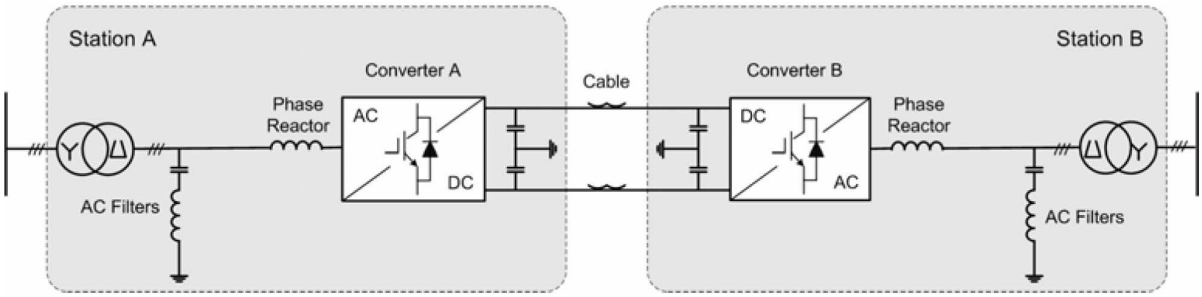

Fig. 1.23 DIAGRAM 2: 2 units bipolar HVDC transmission system [42]

The main advantages of this technology are: its ability to carry out independent active control of voltage, active and reactive power to handle power system stability (four quadrant operation), the injection harmonics is lower – directly related with PWM performance – which means that the need of AC filters is reduced (lower space and weight), the reduction of transmission power losses, the complete decoupling between WF network and the grid and the remote operation.

Thanks to IGBTs characteristics, VSC-HVDC systems can operate in four quadrants in the P-Q plane, allowing independent active control of active and reactive power (Fig. 1.24). Currents can be carefully controlled, even allowing operation at zero current.

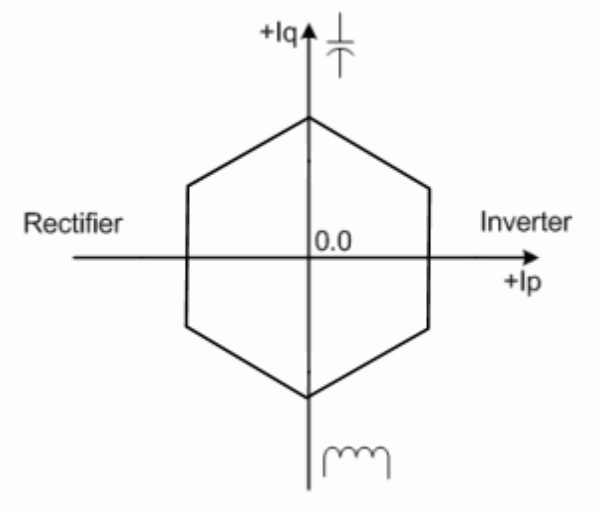

Fig. 1.24 Four quadrants operation [44].

Compared to classical thyristor based HVDC, PWM VSC-HVDC present higher power losses mainly due to the IGBTs operation with much higher switching frequency (over 20 times higher).

1.4.4 HVAC vs. PWM VSC-HVDC for large WF

The major drawback of PWM VSC-HVDC is the higher initial cost than HVAC due to the cost of converter stations. But as the connection distance and the size of the WFs increase this is compensated with the reduction of the transmission power losses (Fig. 1.25).

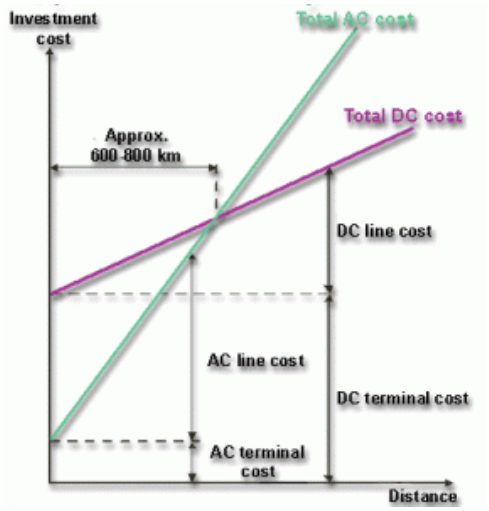

Fig. 1.25 HVAC and HVDC transmission losses cost [39].

The estimated distance above the HVDC system which achieves the lowest cost is so called the “break-even-distance”. This distance is lower in the case of transmission lines implemented with submarine cables than for overhead lines.

But the break-even-distance is not the only important factor that should be evaluated in the selection between HVAC and HVDC. Furthermore the next advantages of VSC-HVDC against HVAC should be taken into account:

- Enables connection between networks with different frequency or phase angle.

- Can be implemented with underground cables, which is easier and faster than overhead lines not only in a technical meaning, also in bureaucratic meaning. This is also an important feature to protect sensitive wildlife environments and reduce visual impact.

- Allows variable speed operation of the WF.

- Achieves less power transmission losses for long distances.

- Ensures active control of voltage, active and reactive power to handle power system stability.

- No reactive compensators needed – only AC filtering. So required space and weight are lower (important in off-shore).

- Can operate in an unsymmetrical network (e.g. during AC network faults) providing unbalance control to compensate unsymmetrical loads.

- Offers robust performance respect to AC grid faults.

- Is a modular concept –short installation and commissioning period.

1.4.5 VSC-HVDC state of the art

Mainly two different topologies of VSC-HVDC are in the market, HVDC Plus by Siemens and HVDC Light by ABB , with power ratings commonly from tenths of megawatts up to over 1000MW with sea cables. [42] [43] [44]

HVDC Light concept presents a rating for one bipolar unit up to 1200MW and ±320kV with sea cables, while HVDC Plus offers up to 1000MW and ±150kV. [42]

HVDC Plus by Siemens employs a multilevel approach to generate a smaller voltage step in comparison with existing two or three-level PWM converters. In this way the harmonic distortion and the HF noise are reduced, so the need of AC filtering is lower [44]. HVDC Plus basic topology is shown before in diagram 1 (Fig. 1.22).

On the other hand ABB has developed its own concept based on PWM two-level three-phase VSC. ABB offer commercialize this system with the two basic topologies shown in diagram 1 and 2 (Fig. 1.22 and Fig. 1.23).

1.5 Problem statement

WHAT IS THE OBJECTIVE?

Out of the many issues related to the stabilization and control problems, this report focuses on annual energy production comparison between different multi-megawatt off-shore WF connected to VSC-HVDC transmission line.

It is well known that the transmission system between the off-shore WF and the on-shore AC network is characterized in general by high power (>100MW) and long distances. Under this main requirement, HVDC may be a lower cost solution than HVAC.

Moreover, since a VSC-HVDC transmission line can decouple the AC transmission system from the WF AC grid, a WT concept less complex than a full-scale or DFIG may be used successfully off-shore, e.g. the RCC IG.

The purpose of this report is to develop a new fast method to evaluate the energy production of different WT configurations in an off-shore WF connected to a VSC-HVDC line transmission (Fig. 1.26).

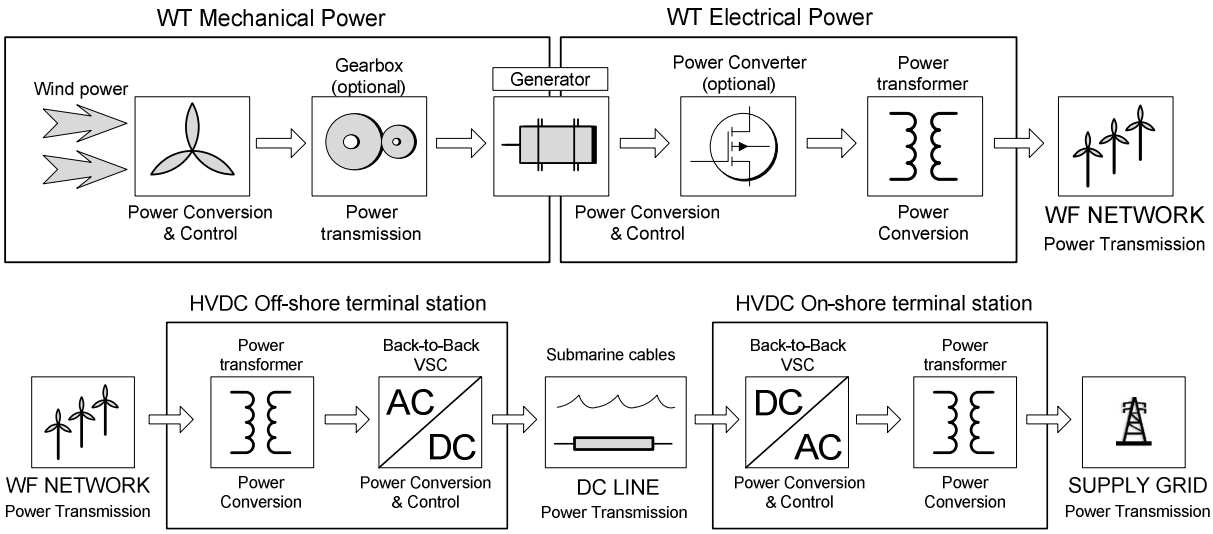

Fig. 1.26 Overview of the studied system.

WHY IS INTERESTING?

As stated previously a lot of information about stability and control of specific topologies can be found in current available literature, but just a few references deal with comparison between different ones. As is stated in [46] this fact is confirmed on the technical report "Conceptual survey of Generators and Power Electronics for Wind Turbines" from Risø National Laboratory [13].

This can be explained taking into account the really fast evolution of wind power technology – WT size and complexity – during last years. In some way, specific technical solutions are adopted along based on background knowledge instead of optimization criteria.

Interesting investigation on comparison between WT topologies have been done by the next authors – their contribution means an invaluable inspiration and support in this report.

- Grauers [62]. He compared three variable speed wind generator systems, obtaining the highest efficiency for a multipole-PMSG. He did not take into account the converter losses, which is a key point on efficiency evaluation.
- Hoffman et al. [63]. They presented an energy production study based on different blade control approaches.
- Helle [45]. He evaluates the efficiency of different converter topologies in VSWTS and develops a new fast tool suitable for determining the power capability of certain converter design. The VSWTS studied is a DFIG and the converter topologies are: back-to back two-level VSC, matrix converter and back-to-back three-level VSC .
- Helle and Munk-Nielsen [46]. They presented a method to evaluate two converter topologies (back-to back two-level VSC and back-to-back three-level VSC) for use in a 2MW DFIG. "From this evaluation it appears that with regards to the efficiency, the two-level VSC is the most suitable solution for the rotor side inverter while at the grid side, both inverter topologies show approximately the same efficiency. The evaluation method is validated with experimental results".

- Ackermann et al. [41]. They evaluate power losses of HVAC and HVDC transmission solutions for large off-shore WFs.

WHO WILL BENEFIT?

Optimization studies conducted to find the topology which ensures maximum efficiency under certain circumstances are a cornerstone in future multi-megawatt wind power development.

Higher efficiencies mean:

- Lower power losses. If the losses are lower the designs can be more compact (less cooling needed), so the volume and weight are also lower. This reduces the price of the technology (less material cost) and the logistics issues. Taking into account the huge size of actual and expected WTs this could be a key advantage for manufacturers.
- Higher annual energy production, which means directly an economic profit for the wind park owner.

HOW WILL BE DONE?

A comparison taking into account different WT systems and different converter topologies is a huge task that cannot be carried out in this report. To reduce this task, considering previous investigations, it seems a reasonable choice to use a single topology for the existing converters – back-to-back two-level VSC – and focus the investigation on the evaluation of different WT systems: full-scale SPMSG, DFIG and VRCC IG.

About modeling

The accuracy of a simulation relies on detailed modeling of the technology considering the manufacturer specific variations. But in the case of WF made of large aggregations of WT, due to the high complexity of the system, some assumptions to simplify the models are necessary to improve the simulation speed.

Regarding to the WT systems modeling, complete predefined WT models are available in professional software as PSCAD, DigSilent or PSS, but their use is limited by the difficulty to know their assumptions and limitations, and their flexibility to introduce new assumptions. Because of that, this project is based in self developed models, which can be built to any level of detail.

MATLAB/Simulink® – a widely known and recognized program – is the tool chosen for this task.

The chosen method includes simplified models of the considered generators and controls which are solved analytically –without any derivative or integrative terms and without feedbacks – and converter models based on ideal switches. More details about model assumptions are included in section 1.7.

A first approach is based on lossless models – the complete descriptions of the losses can be included later based always on analytical expressions.

Regarding the WF modeling, to improve the computation time, equivalent WF models based on aggregated WT models are commonly applied. This task is not trivial – depends on the kind of study to be performed and the WF location and configuration.

In this thesis aggregated WT models are developed to simulate the performance of the several off-shore WFs proposed by VESTAS.

The best way to validate the correctness of the own models is to employ real measurements. But of course this is a difficult task if no information is freely available. Another simpler way to verify the developed models is

to compare them with the available predefined models. For the present project the built-in models included in the SimPowerSystems library of MATLAB/Simulink® could be employed.

1.6 Investigated systems

In followings the basic topologies of the investigated WFs are presented, including specific control strategies and converter topologies.

1.6.1 WF topologies

All investigated topologies are based on WT with standard generators –not multipole– so a gear box is needed between the rotor blades and the generator shaft.

In next figures, the gear train is represented as the block GT.

Only two WTs are represented in each figure, but the WF network is made up of 100 turbines connected in parallel.

It should be also noted that:

All DC/AC-AC/DC converters considered are PWM two-level three-phase VSC.

This choice is discussed further on in chapter 3.

Furthermore:

All WTs are equipped with a pitch control system in order to limit the output power when the wind becomes too high.

Some details about control are included in next section.

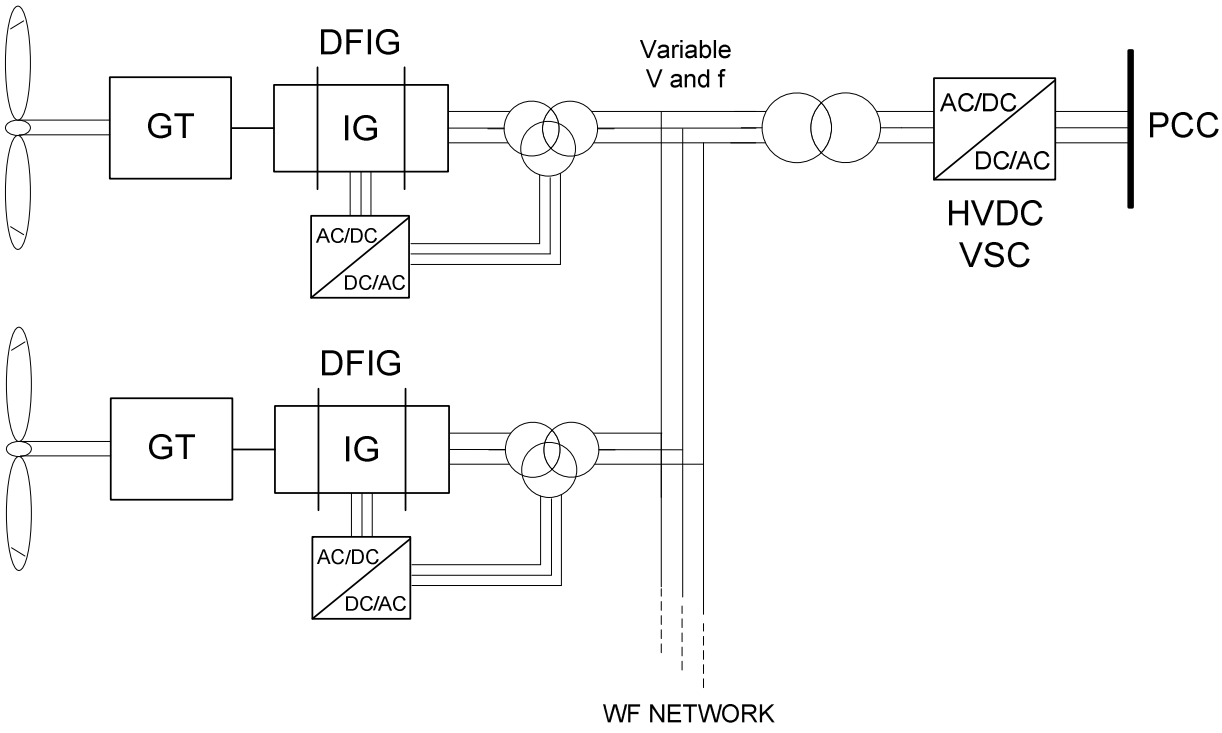

Fig. 1.27 Variable speed pitch controlled HVDC off-shore WF with DFIG

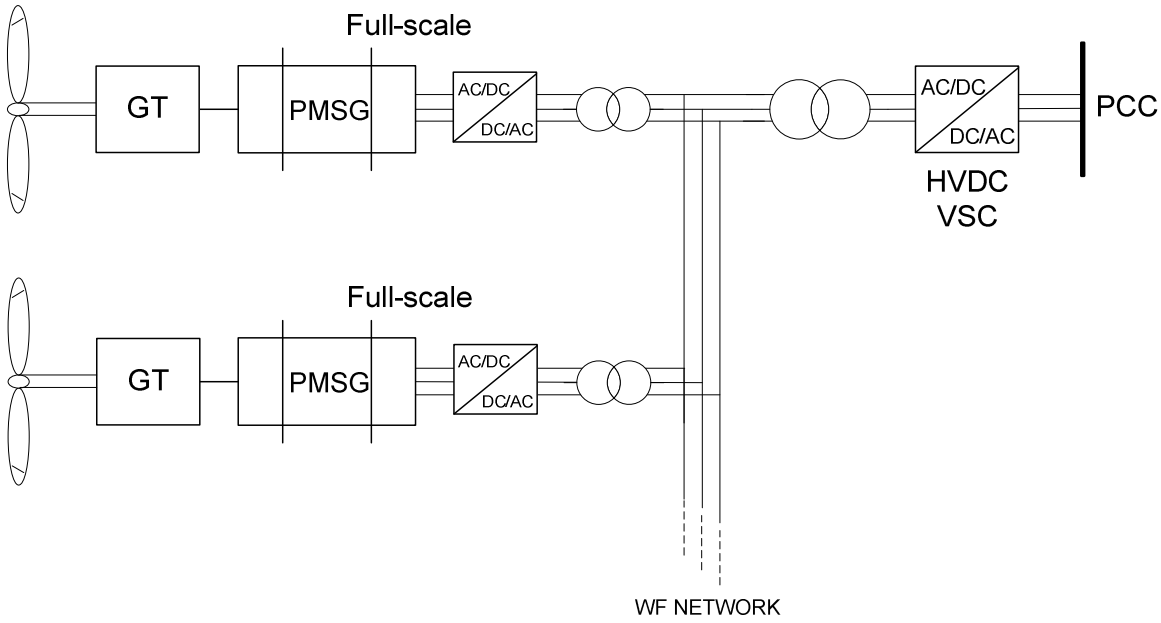

Fig. 1.28 Variable speed pitch controlled HVDC off-shore WF with full-scale SPMSG

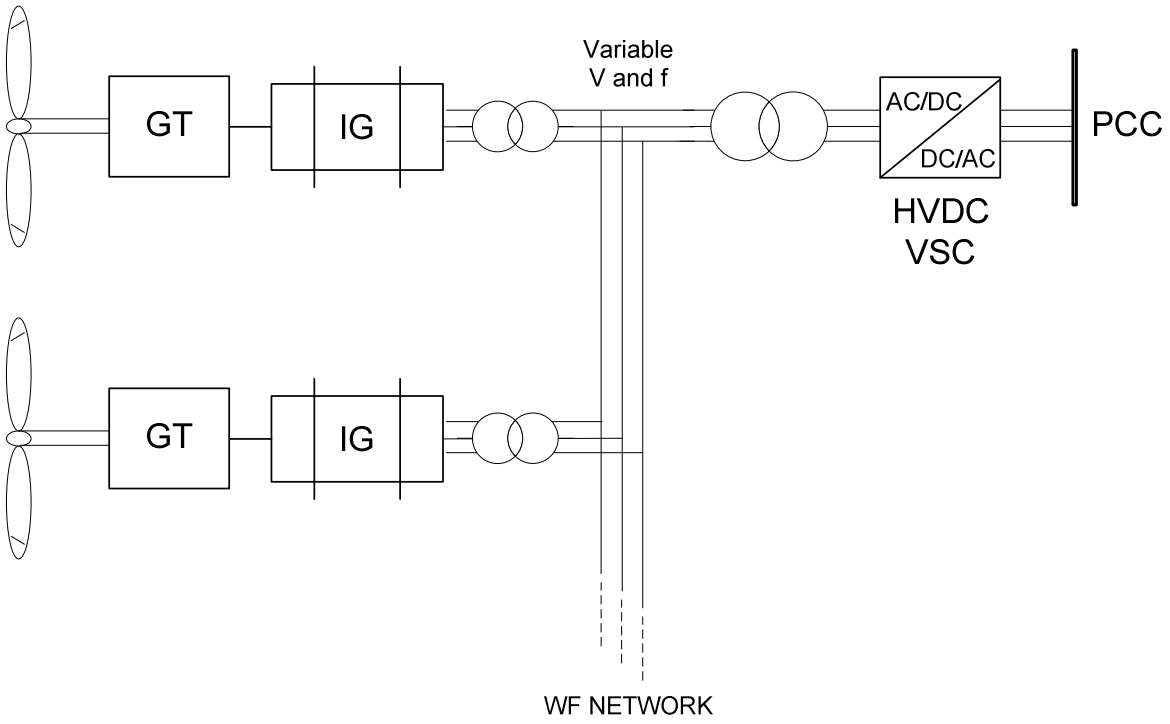

Fig. 1.29 Variable speed pitch controlled HVDC off-shore WF with IG

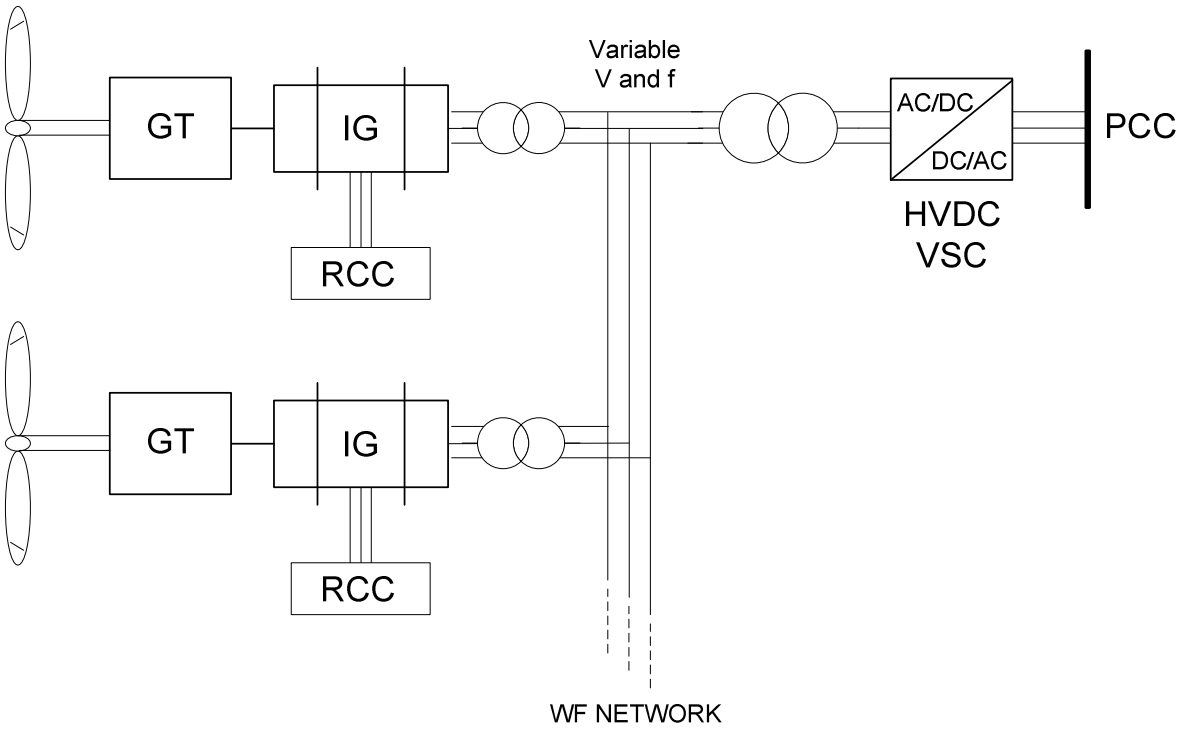

Fig. 1.30 Partial-scale Variable speed pitch controlled HVDC off-shore WF with RCC-IG

1.6.2 Control strategies

Two main stages of control can be stated in a modern variable speed pitch controlled based WF with VSC-HVDC link grid connection: WT control and Power electronic devices control.

1.6.2.1 WT control

This stage of control is responsible of the power control, grid synchronization and monitoring modules and logic and safety functions.

A. Power Control

The basic purpose of the power control is to maximize the wind power production according to wind variations following a reference point given by a control center (or locally). Moreover the power control system must be able to limit the output power when the wind becomes too high, as the power of the wind is directly proportional to the cube of the wind speed.

In this project, since the purpose is to evaluate annual power production, the WFs are supposed to deliver always maximum available power following wind speed variations. This means that not external power reference point is given.

Regarding to power limitation, three different aerodynamic solutions are widely used in WTs. Two of them achieve power limitation generating a stall along the turbine blades, either turning the rotor blades (active stall) or due to certain aerodynamic design of fixed blades (passive stall). On the other hand pitch control systems achieve power limitation turning the rotor blades out of the wind (opposite to active stall).

Next figure presents a comparison of the performance of the three methods for a fixed speed WT [5].

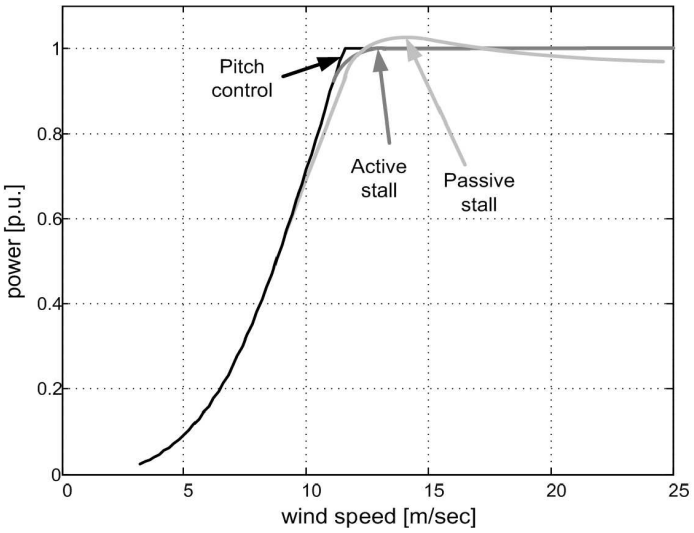

Fig. 1.31 Power characteristic for different power limitation methods.

It can be observed a small overshoot in passive stall system – the value of this overshoot depends on the aerodynamic design of the blades.

In this project a pitch control system is employed in each WT. Below rated rotor speed (nominal rotor speed) the WT basically changes its speed proportionally with the wind speed keeping the pitch angle of the blades fixed in a certain position (blade angle equal to zero). Over nominal rated speed the pitch angle system acts as a speed controller, keeping the rotor speed constant at its nominal value(Fig. 1.32).

In this way the system achieves less mechanical stress in normal operation and in emergency situations. Mechanical brakes are not necessary since the blades are set in flag position at disconnection speed.

Small variations of the blades pitch angle have a strong effect on delivered torque, so the pitch system has to be controlled carefully. Since the pitch system is a mechanical system it has relatively low dynamics.

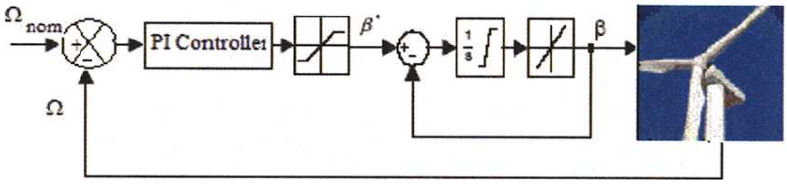

Fig. 1.32 Typical block diagram of a pitch controller system.

It can be stated that the pitch control is the key controller in the design of a WT control, since it is the slowest. It can be assumed that the rest of the controllers can follow the reference signal almost instantaneously, affecting slightly the final behavior of the WT in dynamic-state.

As is shown further on, the previous statement is a cornerstone for the development of the simulation models in this project.

B. Grid synchronization

Initially, during the 80s, SCIG fixed speed WT were connected directly to the grid. So there was no control of active or reactive power (only output power limitation), which are usually the main control signals employed to regulate voltage and frequency. This becomes a network problem when the wind power installed increases over certain levels (depending on the network topology).

Nowadays, thanks to power electronics development, active and reactive power control at the PCC is possible. In fact, this feature has become a requirement in grid codes. Moreover, variable speed performance reduces (or eliminates) output power pulsations due to sudden wind variations. All these features can allow wind power to behave as a conventional active energy source, not only as a renewable energy source. Lot of research is still being done on the field of grid synchronization, being voltage grid angle estimation a main point.

Accurate voltage grid angle estimation is a key point on the performance of grid-side converters. In this project taking into account the steady-state simulation requirements, a simple Phase Locked Loop (PLL) technique for estimation of phase angle of grid voltage could be a feasible solution. A block diagram of the basic structure for a PLL system for grid synchronization is shown in next figure.

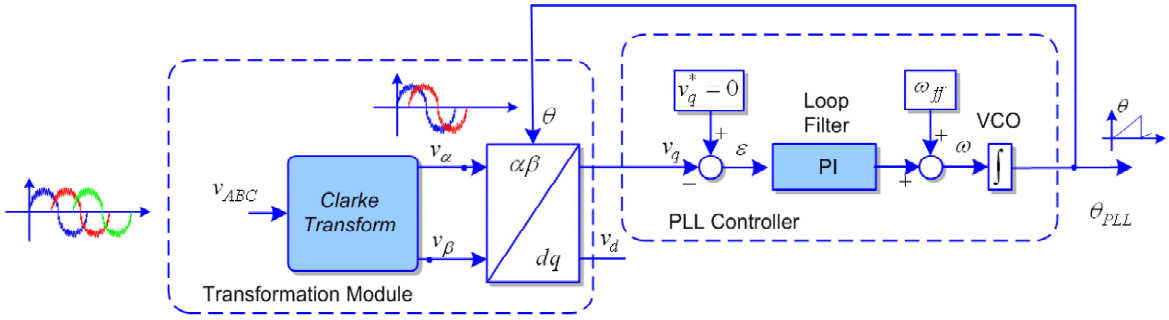

Fig. 1.33 Basic structure of a PLL system for grid synchronization [65]

Further on, the no need of simulating the PLL system is explained based on general modeling assumptions.

C. Grid monitoring

The performance of the WF is subjected to certain operating conditions. These conditions are stated in grid codes requirements of each country.

Due to steady-state simulation model requirements no considerations are made about grid monitoring in this project.

It is important to remark that the focus in this project is the evaluation of energy production – deep research on power system stability and reliability or WT stress is out its reach – so grid monitoring issues are not tackled.

1.6.2.2 Power electronic devices control

The other stage of control consists on power electronics equipment (PEE) control, including the WT PEE and the HVDC VSC control.

The specific control strategies of the PEE vary for different WF configurations, depending on the WT concept. It should be noted that the method of control can affect strongly the WT performance.

The specific chosen strategies are presented in following chapters, as well as the specific assumptions employed in those simulations.

1.7 Limitations - Steady-state general modeling assumptions

Since only the steady-state WFs performances are studied in this project, important general assumptions are made in order to simplify the simulation models. The main objective is to avoid integration blocks and closed-loops in order to improve simulation time.

The employment of next assumptions limits the validity of the developed method to proposed simulation requirements, so the developed method is not suitable to study dynamic-behavior. For example, the WF behavior during voltage disturbances cannot be represented accurately with the presented reduced model.

Next the main general assumptions employed in this project are stated:

General Assumption 1
The pitch control system is properly designed, achieving an accurate control of the rotor speed.

Employing this first assumption the performance of the pitch controller is simulated through the aerodynamic power equation. Constant pitch angle (zero) is supposed until maximum power is reached. Then the aerodynamic power is just limited to this maximum value using a conditional statement. Furthermore when nominal rated speed is reached the rotor speed is just limited to this nominal value using another conditional statement. In this way PI controllers and feedbacks are avoided.

Using this approach the next rotor speed and power in the shaft characteristics are obtained:

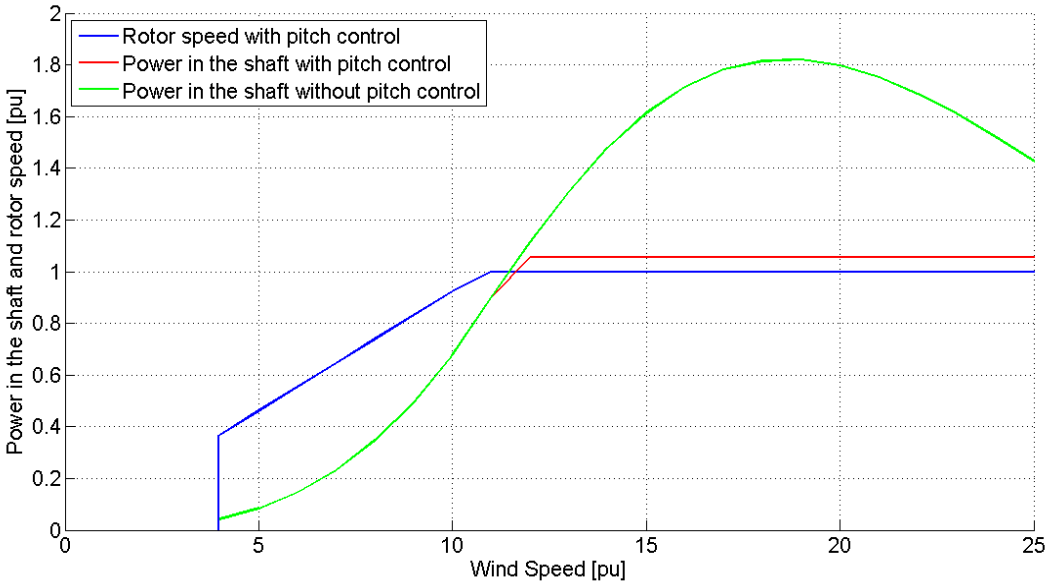

Fig. 1.34 Rotor speed and power in the shaft characteristics with the considered pitch control system.

General Assumption 2
Since the pitch controller is properly designed and is the slowest (low dynamics) it is assumed that the rest of the controllers can follow the reference signal instantaneously.

The result of this second assumption is that no PI controllers and feedbacks are employed to implement each specific control strategy on each converter. Reference signals represent directly steady-states in the machine models.

General Assumption 3
As the pitch control system, the PLL system is properly designed, ensuring accurate estimation of voltage grid angle.

According to this third assumption there is no need to include the PLL system on WF models – a perfect estimation is assumed.

Then, from previous assumptions it can be stated that:

General Assumption 4
An ideal performance of all converter control systems is assumed.

For example, the currents drawn from the converters to the grid (either from the generator to the WF network or from the WF network to the power grid) are considered sinusoidal and in phase with respective phase voltages satisfying the unit power factor condition - it is assumed an ideal performance of all the grid-side converters control.

General Assumption 5
All three-phase machines are star-connected.

This means that in abc currents are always line values and voltages are always line-to-neutral values.

General Assumption 6
The proportional factor of the space phasor is chosen equal to 2/3.

As stated in [24][64] a value of the proportional factor equal to 2/3 deals with amplitude-invariant transformation – the length of the voltage, current and flux space vectors in abc and dq0 reference frame is the same. However, the torque and power conservation is lost.

General Assumption 7
The motor convention is used in rotating machines models.

This means that in the models currents are inputs, active and reactive power have negative sign when are fed into the grid and the slip is negative in generator region. However, it should be noted that in plots generator convention is employed.

General Assumption 8
Rotor resistance and rotor leakage inductance are referred to stator in equivalent models.

General Assumption 9
The DC-link voltage of the back-to-back converters is constant.

According to this assumption the DC-link completely separates both VSCs, allowing independent control of each one. In real dynamic operation there are DC-link voltage variations, which result in apparition of high frequency terms in the output signals [24].

General Assumption 10
The VSCs filters are well-designed and the switching frequency of the VSC is sufficiently large to ensure that the reference voltage and the obtained voltage are equal in the operating frequency range.

Based on assumptions 9 and 10 the whole VSC system PWM operation can be replaced by a much simpler system, which generates sinusoidal waveforms exactly equal to the reference waveforms [24].

Finally, it should be emphasized that:

The most important issue of this project is the evaluation method rather than specific results from simulations.

1.8 Outline of the report

The report is divided into three main parts. The first one – PRELIMINARIES – deals with the introduction to wind power scenario, wind turbine technology, off-shore wind farms topologies and HVDC connection. Moreover the general problem statement is presented as well as project limitations.

The second part – WIND FARM MODELING – is dedicated to the specific modeling of each WF component.

Finally the third part – EVALUATION AND CONCLUSSIONS – is aimed to the evaluation of the developed method through comparison of different WF configurations and the presentation of the main conclusions and future work.

A secondary fourth part – APPENDICES – is also included covering certain number of appendices.

Next figure depicts the structure of the project Fig. 1.35.

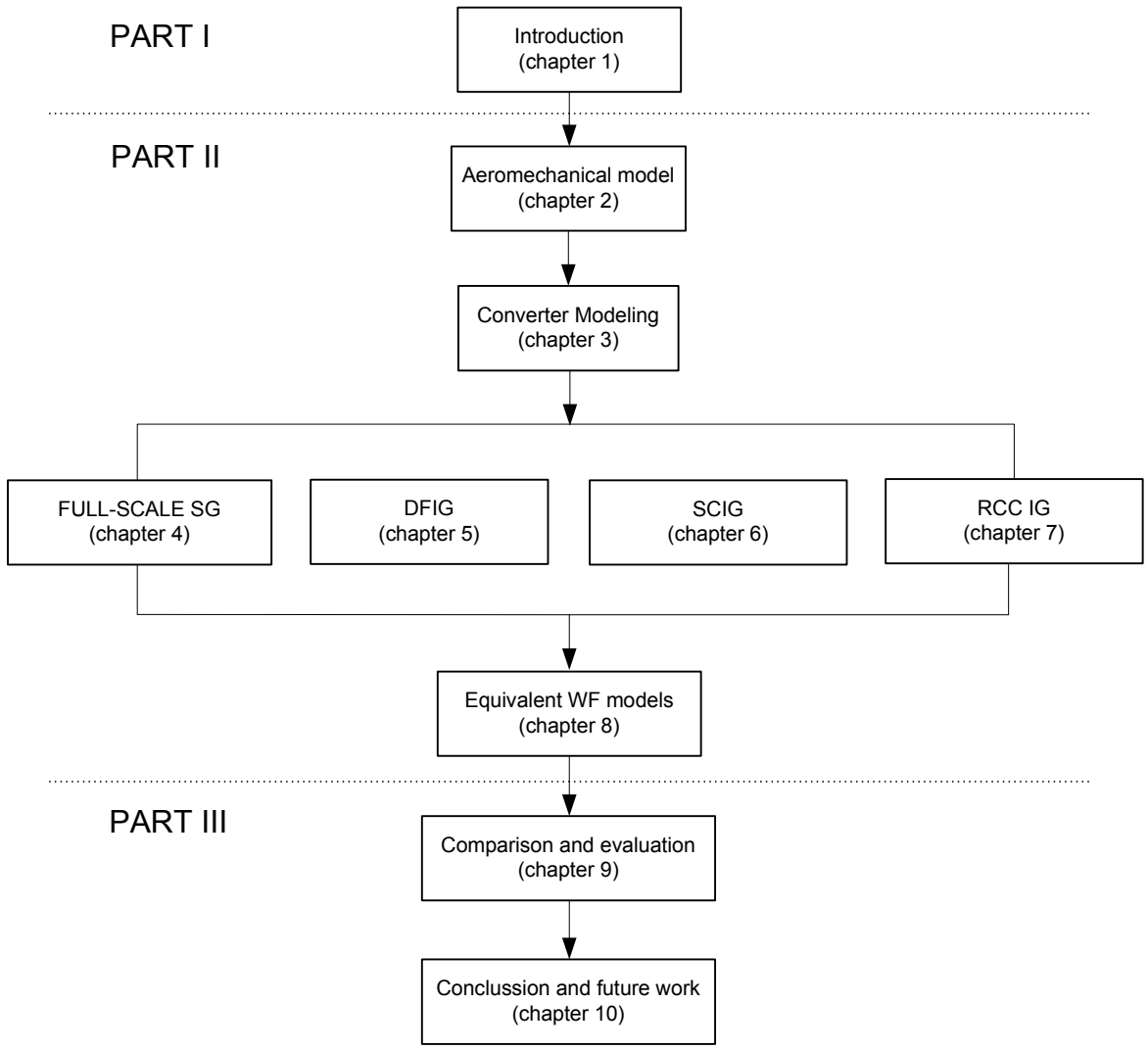

Fig. 1.35 Delineation of the project.

Chapter 2 AEROMECHANICAL MODEL

ABSTRACT

Next chapter deals with the modeling of the wind speed distribution used in the wind farm simulation and the modeling of the wind turbine gear train. Firstly, the basic theory behind the aerodynamic conversion process is presented. Then a wind speed model based on the Weibull distribution is presented. Finally a model to estimate the gear train power losses based on analytic equations is described.

2.1 Aerodynamic conversion

As discussed in chapter 1, a certain amount of the kinetic energy of the wind is converted into mechanical energy by the WT rotor blades. The exact quantity of power delivered to the shaft of the rotor mainly depends on the wind speed, the rotor swept area, the shape of the blades and the pitch angle (for a pitch controlled WT). Total mechanical power extracted from the wind (Fig. 2.1) is given by equation ((2.1):[56][57]

$$Pwt = \frac{1}{2}\rho R V^3 Cp(\lambda, \theta) \tag{2.1}$$

Pwt - mechanical power
ρ - air density
R - blade radius
V - wind speed
Cp - power coefficient
λ - tip speed ratio
θ - pitch angle

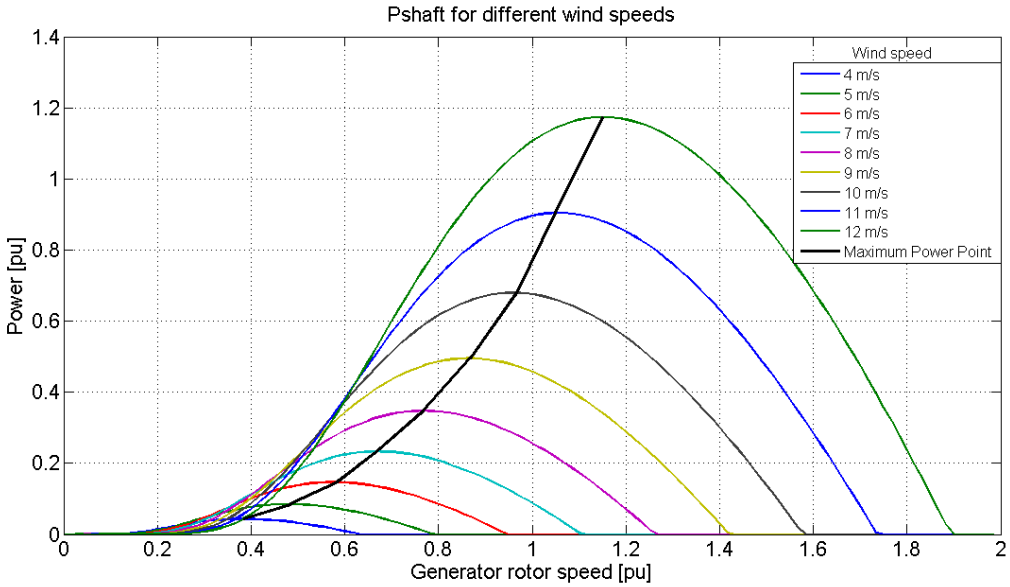

Fig. 2.1 Wind turbine power vs. generator rotor speed

As it can be seen, the mechanical Power is dependent in a factor called power coefficient (Cp). This coefficient is dependent on the tip speed ratio λ, the shape of the blades and the pitch angle of the rotor blades θ.

First parameter can be developed as a relation between tip of the blade speed and the wind speed:

$$\lambda = \frac{\Omega R}{V} \quad (2.2)$$

In order to calculate the Cp curve, equation ((2.3) is used [56]

$$C_p = c_1\left(\frac{c_2}{\lambda_i} - c_3\theta - c_4\theta^{c_5} - c_6\right)e^{-\frac{c_7}{\lambda_i}} \quad (2.3)$$

Where

$$\frac{1}{\lambda_i} = \frac{1}{\lambda + c_8\theta} - \frac{c_9}{\theta^3 + 1} \quad (2.4)$$

Values of c1 to c9 have been taken from [56]; $c_1 = 0.73, c_2 = 151, c_3 = 0.58, c_4 = 0.002, c_5 = 2.14, c_6 = 13.2, c_7 = 18.4, c_8 = 0.02, c_9 = 0.003$

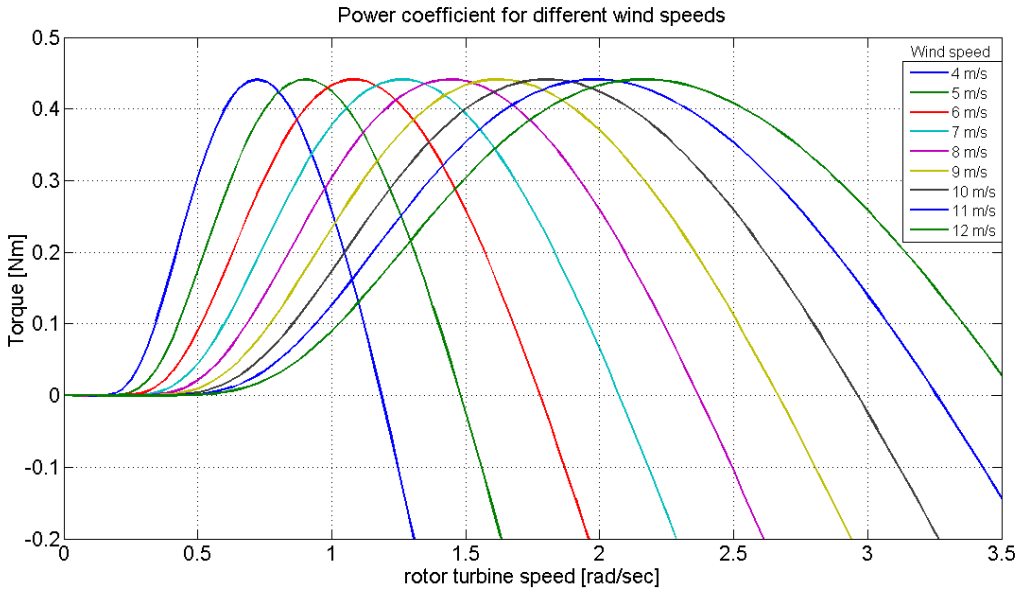

Fig. 2.2 Cp curve, presented as a relation between rotor turbine speed and wind speed

For a certain wind speed, Cp curve can be shown as a function of rotational speed which is assigned to power efficiency value. The Cp curve is represented in the figure Fig. 2.3. [57]

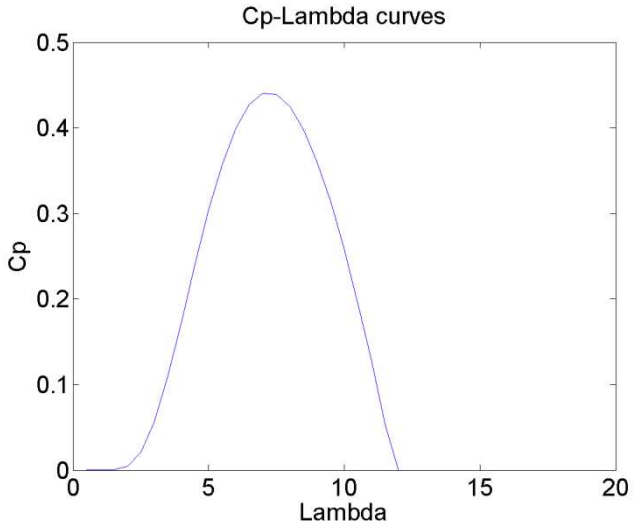

Fig. 2.3 Cp-Lambda curve for θ=0

The highest effectiveness of the power generation can be obtained following maximum value of Cp on the Cp curve. Adjusting rotor speed to wind speed (Fig. 2.4), using variable speed generators, and pitching the blades (pitch control) the turbine can be operated operate with maximum output power.[56][57].

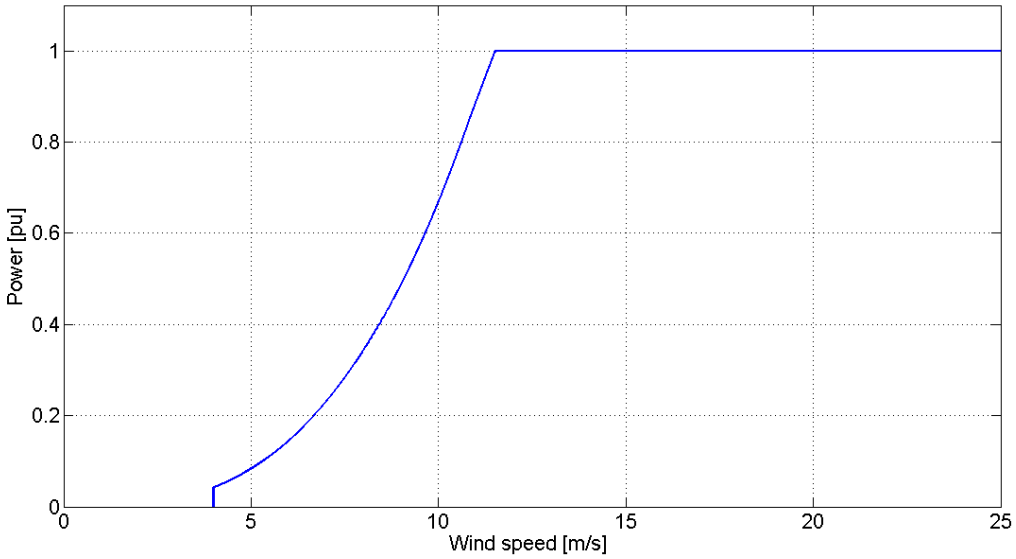

Fig. 2.4 Maximum Power Point Tracking for Cpmax

It is concerned that output of electrical power given as a product of torque (T) and rotational speed (ω) is converted from mechanical power on the shaft. The relation between torque and rotational speed is represented in Fig. 2.5.

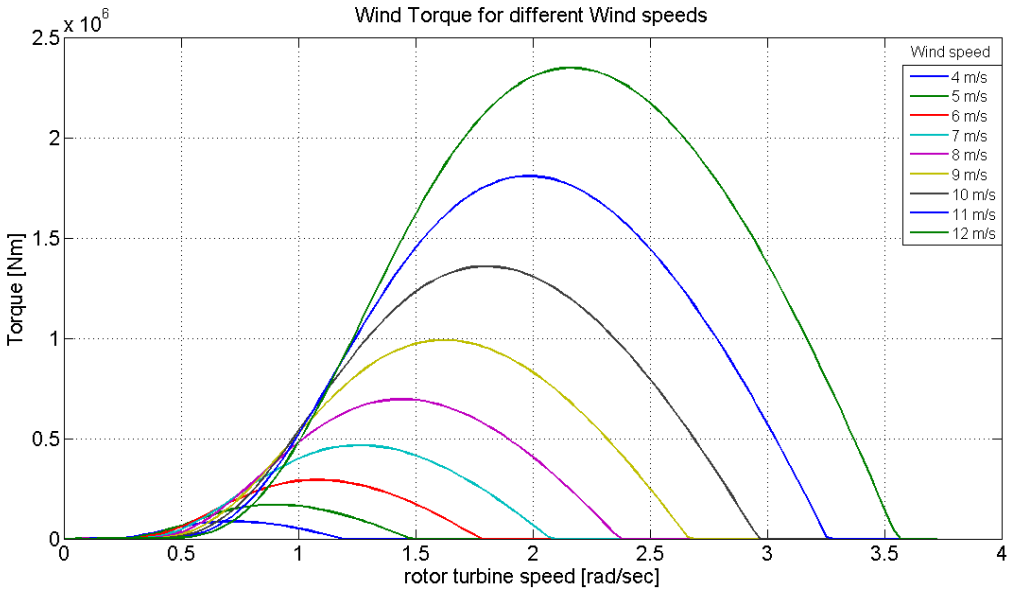

Fig. 2.5 Wind turbine torque vs. rotor turbine speed characteristic

The torque has small value at the initial speed w=0, it reaches maximum and slightly falls close to zero line for a high rotational speeds. At that point wind turbine blades turns almost exactly with the same speed as the wind.

In order to reach maximum wind turbine efficiency, tracking of the maximum power output point is an issue. Maximum power point floats with the wind speed change – this is the reason why the rotor speed has to be continuously adjusted. [58]

The mechanical power generation is given by the equation (2.5).

$$P_m = T_m \Omega_m \tag{2.5}$$

Where, T_m is the mechanical torque in the generator shaft and Ω_m the rotor speed.

2.2 Model of wind distribution [45]

The variability of the wind is its most notable characteristic, from the wind energy point of view. The wind is extremely variable in time and in location, besides it persists over a wide range of scales.[59]

In order to model the power in the wind two components must been taken in to account:

The macro-scale air flow (average wind speed)

The micro-scale air flow (rapid wind speed changes)

The macro-scale air flow is determined by the local high and low pressure zones, it is characterized for showing slowly varying conditions. The micro-scale air flow is determined by characteristics of the terrain, like obstacles, which results on fast fluctuations in the wind speed.

2.2.1 Short term distribution

In the short term distribution as it was said before represents the rapid wind speed changes (micro-scale) and the hourly varying (macro-scale). Next figure (Fig. 2.6) shows the wind speed with a turbulence of 0.1, for a mean wind speed of 15 m/s.

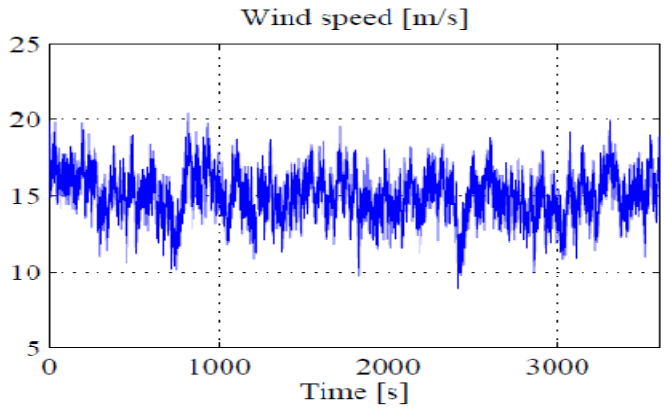

Fig. 2.6 Short term wind speed. Average wind speed 15 m/s

This way of modeling is suitable for a short period of evaluation of the wind farm, taking in to account dynamic behavior of the turbines. For the purpose of this project, where evaluation of the annual production is the scope, this model is not the most suitable.

2.2.2 Long term distribution

In the long term the annual wind speed distribution is represented. This term can be estimated by using the Weibull distribution function given by:

$$P(\bar{V}_{wind}, c, a) = \frac{c}{a^c} \bar{V}_{wind}^{c-1} e^{-\left(\frac{\bar{V}_{wind}}{a}\right)^c} \quad (2.6)$$

Where $\bar{V}_{wind}$ is the wind speed range where the wind distribution is evaluated, and a and c are parameters of the distribution. These values are taken from the classification given by the International Electrotechnical Commision (IEC).

For an offshore wind farm annual average wind speed $a = 11.38$ and $c = 2$. With this parameters and equation (2.6) the annual wind distribution is obtained (Fig. 2.7).

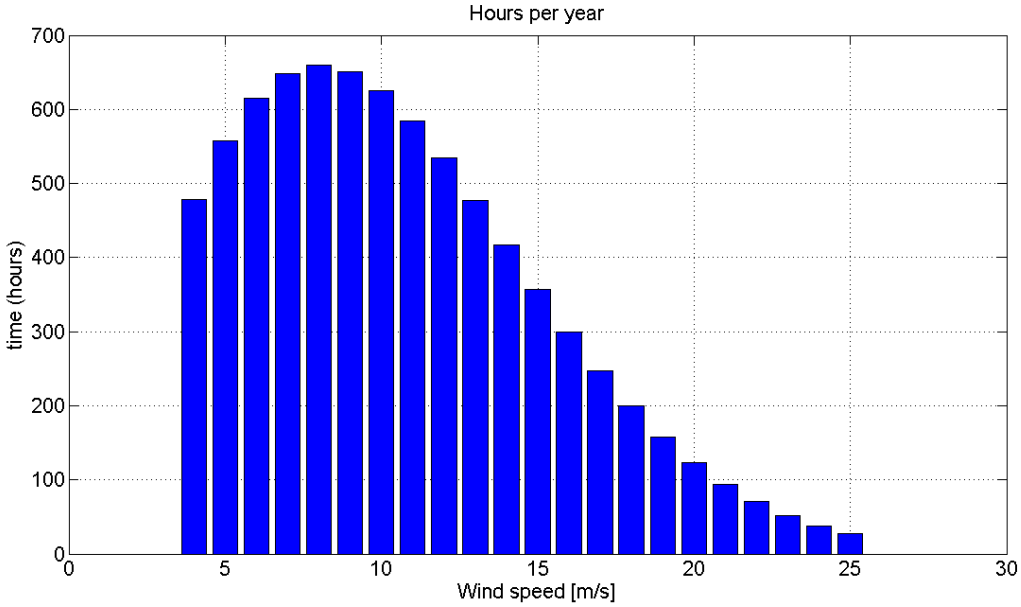

Fig. 2.7 Annual wind distribution of an off-shore site

From the previous wind speed Weibull distribution next wind speed characteristic is derived (Fig. 2.1). This characteristic is used, as average wind speed, in the simulation models.

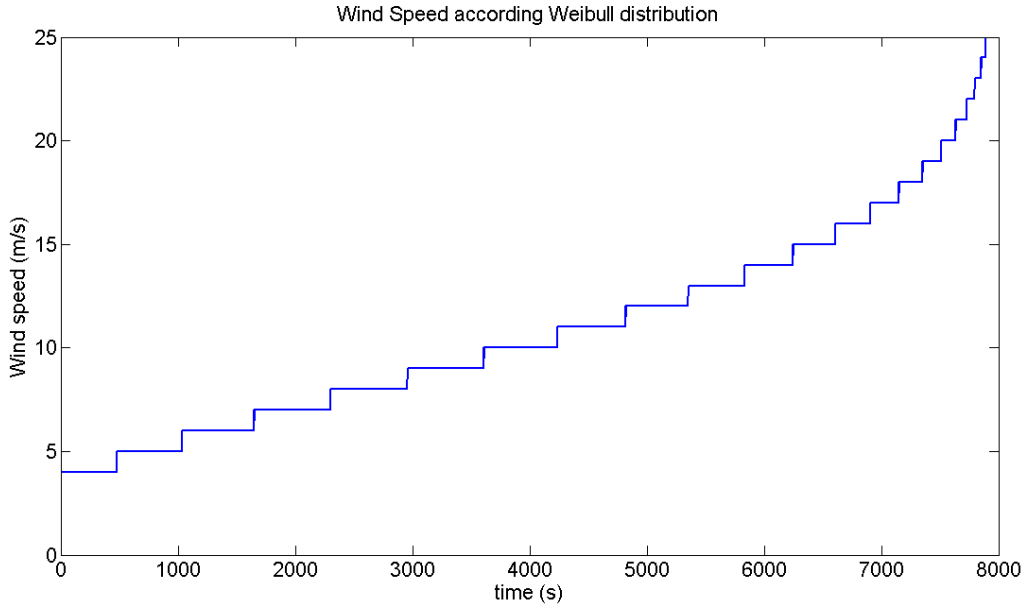

Fig. 2.8 Wind Speed distribution used in the WF simulation

2.3 Model of drive train

The function of the gearbox in a WT is to increase the speed of the rotor to a suitable value for standard generators [59]. Turbines containing gearbox have a considerable part of the losses dissipate in this element. Since the operating speed area depends in the chosen topology, losses and hence generated energy may change. [45]

2.3.1 Gear losses

Gearboxes have as inputs the applied torque and the rotational speed produce by the wind in the blades (main shaft) and as output, the rotational speed and applied torque of the generator shaft. In order to calculate these outputs equation must be use in order to model the gearbox losses.[46]

$$P_{gear,loss} = k_{g1}\omega_{r0}^2 + k_{g2}\omega_{r0} + k_{g3}\omega_{r0}T_{r0} + k_{g4} \tag{2.7}$$

Where, $k_{g1}$is the viscous friction coefficient, k_{g2} is the static fiction coefficient, k_{g3} is the mesh friction coefficient and k_{g4} the constant loss, this last constant represents the power used for cooling and circulation of the gearbox.

In steady state the speed in the generator ω_{gen} is simply related to the speed of the main shaft ω_{r0} by the gearbox ratio N_{gear}:

$$\omega_{gen} = N_{gear}\omega_{r0} \tag{2.8}$$

The torque applied to the generator shaft T_{gen}, in steady state, is then given by:

$$T_{gen} = \frac{\omega_{r0}T_{r0} - P_{gear,loss}}{\omega_{gen}} \tag{2.9}$$

2.4 Summary

It can be stated that the main objectives of this chapter were successfully achieved: modeling of the wind speed distribution used in the wind farm simulation and modeling of the wind turbine gear train based on analytic equations.

Chapter 3 Converter Modeling

ABSTRACT

Taking into account that the only converter topology considered in this report is the PWM two-level three-phase VSC, the purpose of this chapter is to present a non-ideal model of this converter, which takes into account the switching and conducting losses of switches as well as the reactor losses. The idea, under simulation requirements, is to develop a loss-model based on analytical expressions. This analytical model is verified in [45] through comparison with a non-ideal dynamic model.

3.1 Introduction

Two main stages of the studied systems can include power electronics AC/AC converters. The first one, which is presented in all the studied topologies, is the HVDC transmission system and the second one, which is presented in DFIG WT and full-scale PMSG WT, is the wind energy conversion system (WECS) of each WT. RCC IG WT also includes a PEC, but is just a simple chopper to control rotor currents – its modeling is discussed in chapter 6.

HVDC AC/DC/AC Converter

As it has been explained in chapter 1 several topologies are available for HVDC systems, each one with their own advantages, disadvantages and limitations. Due to time constraints in this report only one of these topologies is considered.

In this report the HVDC transmission system considered is based on PWM two-level three-phase VSCs – one of them in the off-shore substation and another one in the on-shore (Fig. 3.1).

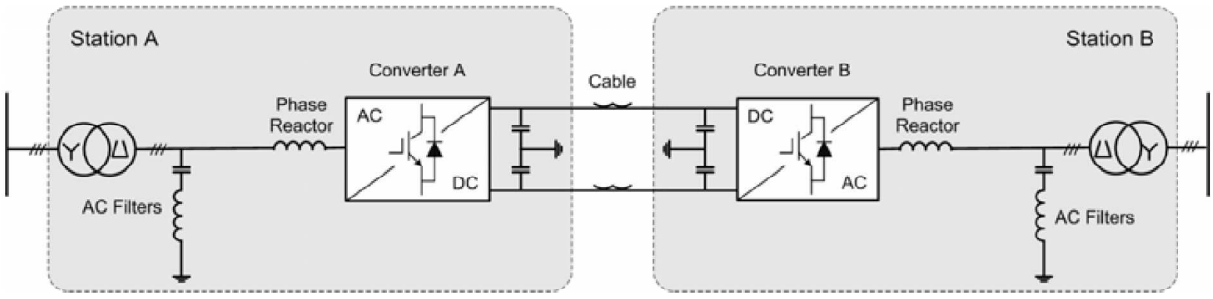

Fig. 3.1 Two units bipolar VSC-HVDC transmission system [42].

WT AC/AC Converter

On the other hand, many different generator-converter topologies are also available for WECS. A complete review of power converter topologies for wind generators can be found in [47]. Since detailed description of each topology is an overwhelming task this is not the scope of this report, so just a brief summary is presented.

Next table from [47] summarizes the available WECS. It can be stated that the cost of the generator-converter system increases directly with the complexity of the PEC. As well the complexity of the controller design influences the overall costs. But at the same time the employment of more complex PEC and controllers may improve the performance of the system from several points of view: controllability, efficiency or fault response.

Generator (Power Range)	Converter Options	Device Count (Semiconductor cost)
PMSG (kW)	Diode Bridge/SCR Inverter/Compensator	DC-Link Cap. 12 Controllable Switches (Moderate)
	SCR Rectifier/SCR Inverter	DC-Link Cap. 12 Controllable Switches (Moderate)
	Diode Bridge/ Switching Inverter	DC-Link Cap. 6 Controllable Switches (Low)
	Diode Bridge/DC Boost/ Switching Inverter	DC-Link Cap. 7 Controllable Switches (Low)
	Back-to-Back Switching Inverters	DC-Link Cap. 12 Controllable Switches (Moderate)
	Back-to-Back Switching Inverters (Reduced Switch)	2 DC-Link Caps. 8 Controllable Switches (Low)
DFIG (kW-MW)	Diode Bridge/SCR Inverter	DC-Link Cap. 6 Controllable Switches (Low)
	SCR Rectifier/SCR Inverter	DC-Link Cap. 12 Controllable Switches (Moderate)
	Back-to-Back Switching Inverters	DC-Link Cap. 12 Controllable Switches (Moderate)
	Matrix Converter	18 Controllable Switches (High)
IG (kW-MW)	Back-to-Back Switching Inverters	DC-Link Cap. 12 Controllable Switches (Moderate)
SG (kW-MW)	Diode Bridge/DC Boost/ PWM Switching Inverter	DC-Link Cap. 7 Controllable Switches (Low)
	Back-to-Back Switching Inverters	DC-Link Cap. 12 Controllable Switches (Moderate)

Table 3.1 Summary of available WECS [47].

During the late nineties, the employment of back-to-back two level VSC in large WT has become widespread by WT industry. This decision was mainly based on the gathered experience by the drives industry for more than a decade [45].

Nowadays, as commented in chapter 1, most of the manufacturers are developing WT with capacities on order of 3-6 MW, all based on variable speed WT systems with pitch control employing doubly-fed induction generator or direct-driven synchronous multipole generator [16-18]. Most of these designs are still based on the conventional back-to-back two level VSC.

Taking into account the previous considerations and due to time constraints in this report only the conventional back-to-back PWM two level VSC topology is considered.

In this report the WECSs considered are based on PWM two-level three-phase back-to-back (Fig. 3.2).

Moreover, using equivalent topologies in the HVDC system and the WECSs allows the development of only one single tool and method to evaluate the converter performance of all systems.

3.2 Two level pwm three-phase voltage source converter

The whole converter topology studied is made up of two single two level PWM three-phase VSCs interconnected via a DC-link.

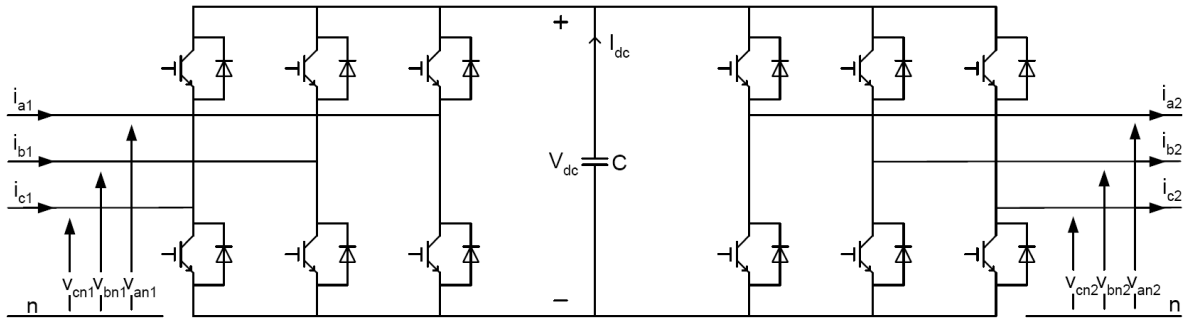

Fig. 3.2 Back-to-back converter topology [24].

The converters of both sides are controlled with PWM, which allows amplitude and phase control of each three-phase voltage in order to satisfy each three-phase current demand.

PWM allows amplitude and phase control of each three-phase voltage in order to satisfy each three-phase current demand.

This topology has been employed widely in drives, being implemented in one single bi-directional power converter unit so called back-to-back converter.

An equivalent topology can be employed in off-shore HVDC systems, with one VSC in the off-shore substation and another one in the on-shore, both interconnected via a submarine DC-cable.

The DC-link separates both VSCs, allowing independent control of each one. Since the operation of each of the VSCs is controlled individually the performance analysis can be just based on the performance of one single converter.

Basically the PWM of a converter control of the power sent to a load modulating its duty cycle. In fact, the PWM is just a method to generate switching sequences.

The PWM VSC is built with three legs (a, b and c), each of them with two switching power devices. The control of the upper and lower switches of each leg is complementarily done through the switching signals (q_a , q_b and q_c) . If the upper switch is opened then the lower switch is closed and vice versa.

An example of the basic principle of a carrier based modulator is shown in next figure. A reference voltage (Vref) which represents the desired output voltage is compared with a triangular carrier waveform (Vtri).

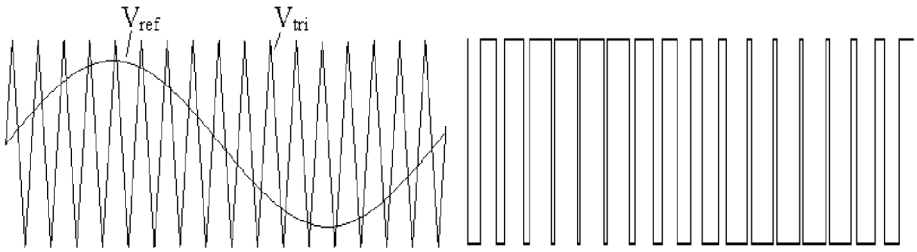

Fig. 3.3 PWM and switching signal for one-phase of the VSC [24].

From this comparison a square switching signal is obtained. If Vref>Vtri the value of the switching signal is 1 (the upper switch is closed). If Vref<Vtri the value of the switching signal is 0 (the lower switch is closed). This results in pulsating voltages at the AC side.

PWM methods always employ a square switching signal which pulse width is modulated to control the VSC: the on/off states of the semiconductor switches are controlled through the discrete on/off states of the modulation.

The PWM signals can be generated by analog system or digital devices. But nowadays digital devices offer several advantages over analog systems:

- Stability (no drift, offsets, temperature or aging effects)
- Precision (noise immunity)
- Flexibility (can be customized by changing software)
- More compact (fewer devices)

As shown in previous figure, PWM carrier based methods as Sinusoidal PWM (SPMW) and Third Harmonic Injection PWM (THIPWM) just require a comparator between a sinusoid reference signal and a triangle or a sawtooth waveform to generate the PWM. So PWM carrier based methods are conceptually simple and easy to implement in a digital system in comparison with direct digital methods, but require longer computation times since the sinusoidal reference signal have to be computed or found in a table. Thus it can be stated that employing direct digital methods this computation process is simplified, so less computation time is required and the performance is improved, although a deeper knowledge of the theory is needed for the implementation task.

Based on the previous reasoning, in this report is assumed that a direct digital PWM method should be chosen to be implemented in digital devices.

Many direct digital PWM methods have been developed but in this report, due to time constraints, the converter loss performance is only studied for Space Vector PWM method (SVPWM).

3.2.1 Control analysis

Usually, in drives applications vector-control scheme are applied on both converters. One of the converters (grid side) carries out independent DC-link voltage control and reactive power control ensuring sinusoidal grid currents. The other is controlling active and reactive power generation (generator side converter).

In off-shore HVDC applications the off-shore converter (WF network converter) is equivalent to the generator side converter.

In general terms it can be stated that independently on the WT concept all the vector-control schemes applied to the grid side converters are almost equivalent.

On the other hand, the specific control schemes applied to the other converter (rotor side converter for DFIG, stator side converter for PMSG or WF network side converter for HVDC) differ depending on the application.

Since the VSC-HVDC transmission system is the same for all the studied WFs, it is decided to explain the VSC-HVDC control scheme in followings, while the analysis of the specific control schemes of machine-side converter for DFIG and PMSG is explained in chapter 5 and 4 respectively.

3.2.1.1 VSC-HVDC control scheme

Independently on the WT concept, for all proposals, the topology and control approach of the HVDC system is the same.

The HVDC system proposed (Fig. 3.4) is basically made up of a transformer, a filter, a WF-grid-side converter (two level three phase VSC with 6 controllable switches), a DC-link (an off-shore capacitor bank, a sea transmission line and on-shore capacitor bank), a grid-side voltage source converter (another two level three phase VSC with 6 controllable switches), another filter, another transformer and a transmission line (typically an overhead line) to the PCC.

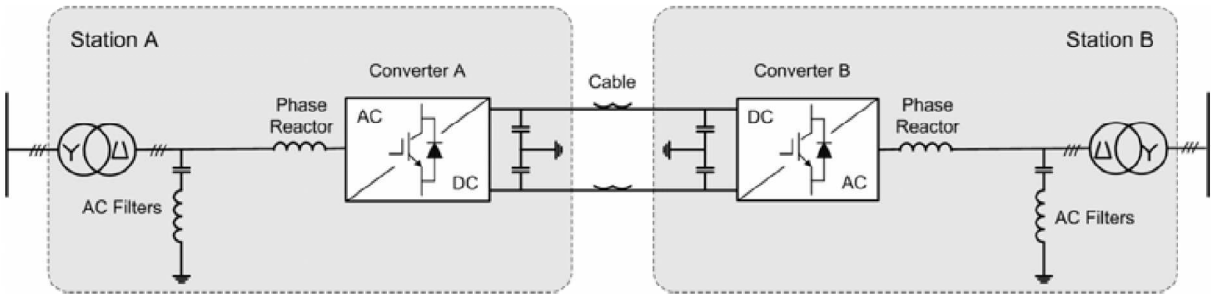

Fig. 3.4 Several control strategies can be employed for each back-to-back converter.

HVDC grid side converter vector control (on-shore substation)

A review of grid-side converter control strategies is presented in [reference]. In this review is stated that for the HVDC grid side VSC a Voltage Oriented Control (VOC) with PI controllers and a simple PLL for the voltage grid angle estimation can ensure high steady-state performance. A block diagram of a possible VOC with PI controllers is given in Fig. 3.5.

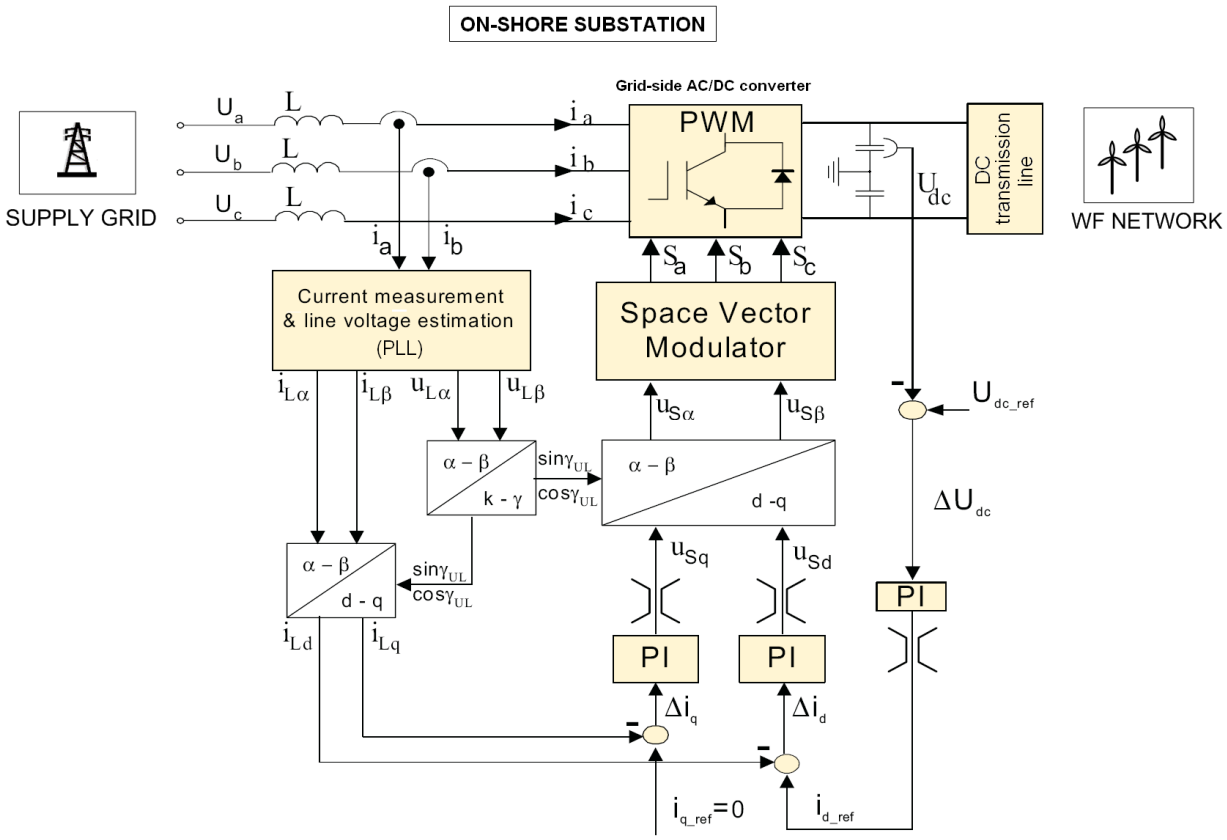

Fig. 3.5 Block diagram of the VOC of the HVDC grid-side converter.

This control structure is based on d-q decoupled control, using the d-axis component of the current for DC-link voltage control and the q-axis component of the current for reactive power control.

This control structure is widely employed in drives on grid-side converters. In this project all grid-side converters used in drives employ the same basic structure as the HVDC grid-side converter (the DFIG WF-network side converter and the full-scale SPMSG WF-network side converter).

HVDC WF-network side converter V/f control (off-shore substation)

On the other hand, depending on the WT concept, the WF-network side converter keeps the voltage and frequency of the WT network constant – for DFIG and full-scale SPMSG – or not – in case of SCIG and RCC-WRIG.

The nominal rotor speed of an IG depends basically on its synchronous speed and nominal slip. This synchronous speed is determined by the grid frequency, so a certain range of speed control can be achieved varying the frequency of the applied stator voltage. But in order to not increase the maximum flux set by the equation (3.1) the voltage should vary in a proportional way with the frequency ($V_s/f = cte$)[54].

$$\frac{V_s}{f} = \frac{2\pi}{\sqrt{2}} N_1 \phi_{max} \tag{3.1}$$

Next figure (Fig. 3.6) shows how is the Torque-speed characteristic of an IG for different frequencies in a V/f control.

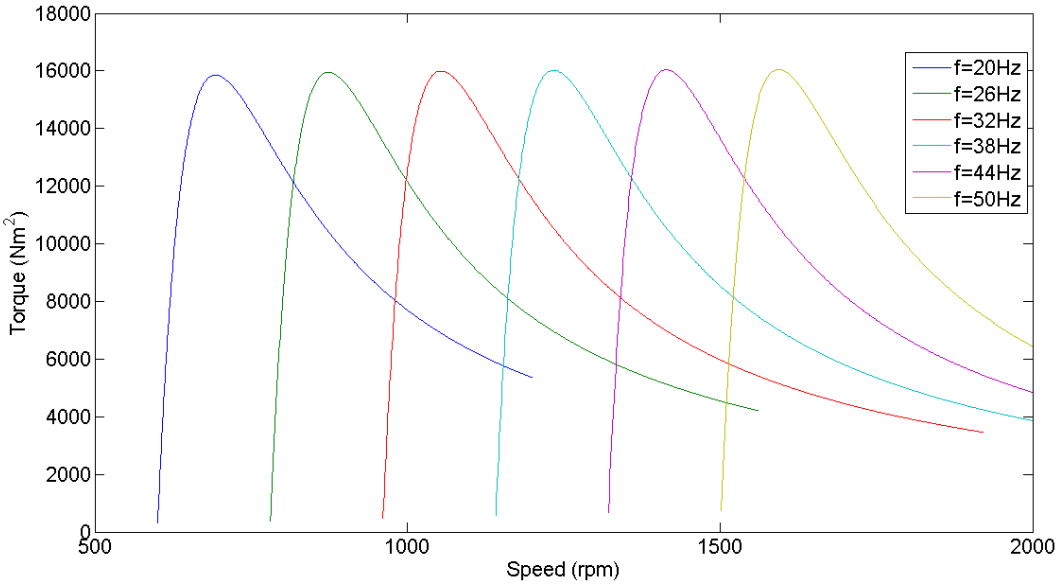

Fig. 3.6 Torque-Speed characteristic for different frequencies

From Fig. 3.6 it can be seen the advantage of using a V/f control in SCIG and RCC-WRIG configurations.

The V/f-control used in the WF-network side HVDC converter, sets the voltage and frequency for the entire WF. A block diagram of the open-loop V/f control strategy implemented is shown next.

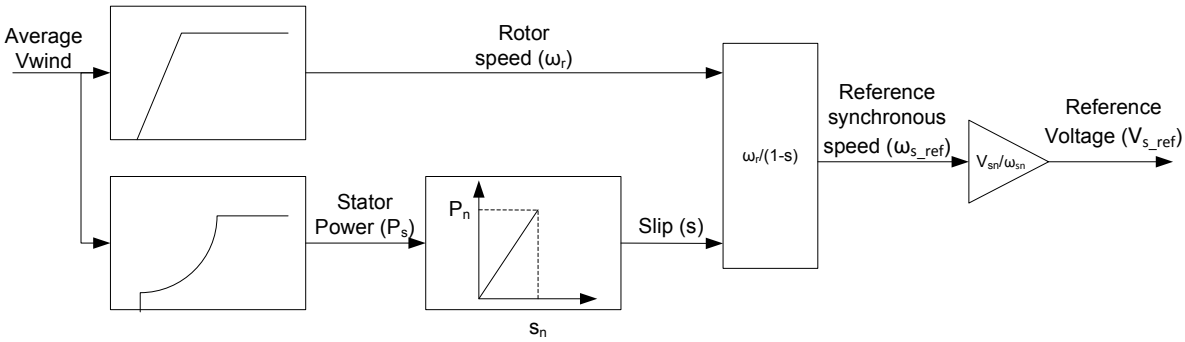

Fig. 3.7 Block diagram of the Open-loop V/f control of the HVDC WF-network side converter.

By introducing the average wind in the wind farm, rotor speed and stator power are obtained. From the stator power, using a linear relationship, the slip for the MPP is derived. Next, from the rotor speed and slip the reference frequency is calculated. Finally, the reference voltage is obtained multiplying the reference frequency by a constant derived from the relationship between nominal frequency and nominal voltage. Output voltage and frequency are limited to the nominal values. The reference voltage signal is sent to the PWM in order to generate the corresponding switching sequences.

For DFIG and full-scale SPMSG WF-network frequency and voltage are just fixed at their nominal values.

3.3 Converter Modelling

Based in the general assumptions presented in chapter 1, the control structure is greatly simplified in simulation models.

- According to general assumption 3 PLL system performance is considered ideal, so perfect line voltage estimation is assumed. Then PLL system is not modeled.
- According to general assumption 2, it is assumed that the controllers can follow the reference signal instantaneously. Then no PI controllers and feedbacks are employed to implement the control strategy. Reference signals represent directly steady-states in the machine models.
- According to general assumption 9 (Chapter 1), the DC-link voltage of the back-to-back converters is considered constant in models. This means that the DC-link completely separates both VSCs, allowing independent control of each one.
- Moreover, general Assumption 10 (Chapter 1) states that the VSCs filters are well-designed and the switching frequency of the VSC is sufficiently large to ensure that the reference voltage and the obtained voltage are equal in the operating frequency range.

Based on these assumptions:

The whole VSC system PWM operation is replaced by a much simpler system, which generates sinusoidal waveforms exactly equal to the reference waveforms [24].

Thus, the modeling of the V/f controlled HVDC WF-network side converter can be easily understood from Fig. 3.7.

And therefore, the modeling of the vector controlled HVDC grid-side converter can be reduced to next equations

$$\begin{aligned} P_{out} &= P_{in} - P_{loss} \\ v_{qout} i_{qout} &= v_{qin} i_{qin} - P_{loss} \\ Q_{out} &= 0 \Rightarrow i_{dout} = 0 \end{aligned} \tag{3.2}$$

3.3.1 Loss evaluation

As explained in the preface of this chapter, the idea, under simulation requirements, is to develop a loss-model based on analytical expressions.

As first approach in all presented simulations the whole losses in the back-to-back converter are just modeled by a static factor μ.

Then the modeling of the vector controlled HVDC grid-side converter is reduced to:

$$\begin{aligned} \mathrm{P_{loss}} &= (1-\mu)\mathrm{P_{in}} \\ \mathrm{P_{out}} &= \mu \mathrm{P_{in}} \\ \mathrm{v_{qout} i_{qout}} &= \mu \mathrm{v_{qin} i_{qin}} \\ \mathrm{Q_{out}} &= 0 \Rightarrow \mathrm{i_{dout}} = 0 \end{aligned} \tag{3.3}$$

A more detailed analytical model is derived and verified in [45] through comparison with a non-ideal dynamic model. This analytical model takes into account the modulation method, the modulation index (M) and the load angle (φ) of the VSC. This analytical model is presented in followings, but is not implemented in simulations.

Next the equations employed in this detailed model are presented.

3.3.1.1 Conducting losses of switches [45]

The conductiong losses of a semiconductor device (transistor and diode) are modeled by next equations:

$$P_{t,cond} = V_{t0}(T) \cdot I_{t,avg} + R_t(T) \cdot I_t^2$$
$$P_{d,cond} = V_{d0}(T) \cdot I_{d,avg} + R_d(T) \cdot I_d^2 \quad (3.4)$$

Where:

$V_{x0}(T)$ is the temperature dependent voltage of component x.

$I_{x\,avg}$ is the average current through component x.

$R_x(T)$ is the temperature dependent resistance of component x,

I_x is the RMS current through the considered component.

The transistor and diode average currents can be calculated through next equations, which are independent of the used modulation method:

$$I_{t,avg} = \left(\frac{\sqrt{2}}{2\pi} + \frac{\sqrt{6}}{12} M\cos(\varphi)\right) I_r$$
$$I_{d,avg} = \left(\frac{\sqrt{2}}{2\pi} - \frac{\sqrt{6}}{12} M\cos(\varphi)\right) I_r \quad (3.5)$$

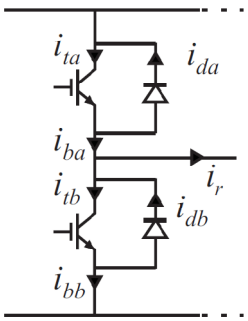

Fig. 3.8 Definition of current direction [45].

Next figures shows the average transistor and diode current as a function of the load angle (φ) for several values of modulation index (M).

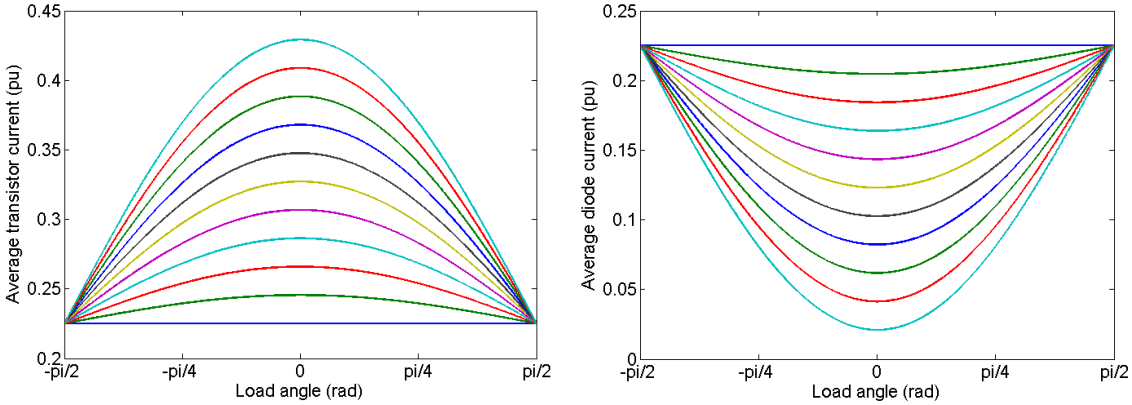

Fig. 3.9 Average transistor (left) and diode (right) current as a function of the load angle (φ) for several values of modulation index (M). M=[0,0.1..1].

The program written in MATLAB script to plot this figures is included in APPENDIX.

The RMS current through the transistor and diode is given by equations that are not independent of the used modulation method. In [45] next equations are derived to evaluate the RMS currents using SVM PWM:

$$I_t = \begin{cases} \left(\frac{-M + 3\pi - 4M\cos(\varphi)^2 + 8\sqrt{3}M\cos(\varphi)}{12\pi}\right)^{\frac{1}{2}} I_r & |\varphi| < \frac{\pi}{6} \\ \left(\frac{2M\left(2 + \frac{\sqrt{3}}{2}\sin(|2\varphi|) - \cos(\varphi)^2 - 2\sin(|\varphi|) + 2\sqrt{3}M\cos(\varphi)\right)}{12\pi}\right)^{\frac{1}{2}} I_r & \frac{\pi}{6} < |\varphi| < \frac{\pi}{2} \end{cases} \quad (3.6)$$

$$I_t = \begin{cases} \left(\frac{1}{2} - \frac{-M + 3\pi - 4M\cos(\varphi)^2 + 8\sqrt{3}M\cos(\varphi)}{12\pi}\right)^{\frac{1}{2}} I_r & |\varphi| < \frac{\pi}{6} \\ \left(\frac{1}{2} - \frac{2M\left(2 + \frac{\sqrt{3}}{2}\sin(|2\varphi|) - \cos(\varphi)^2 - 2\sin(|\varphi|) + 2\sqrt{3}M\cos(\varphi)\right)}{12\pi}\right)^{\frac{1}{2}} I_r & \frac{\pi}{6} < |\varphi| < \frac{\pi}{2} \end{cases} \quad (3.7)$$

Next figures shows the RMS transistor and diode current as a function of the load angle (φ) for several values of modulation index (M) for SVM PWM.

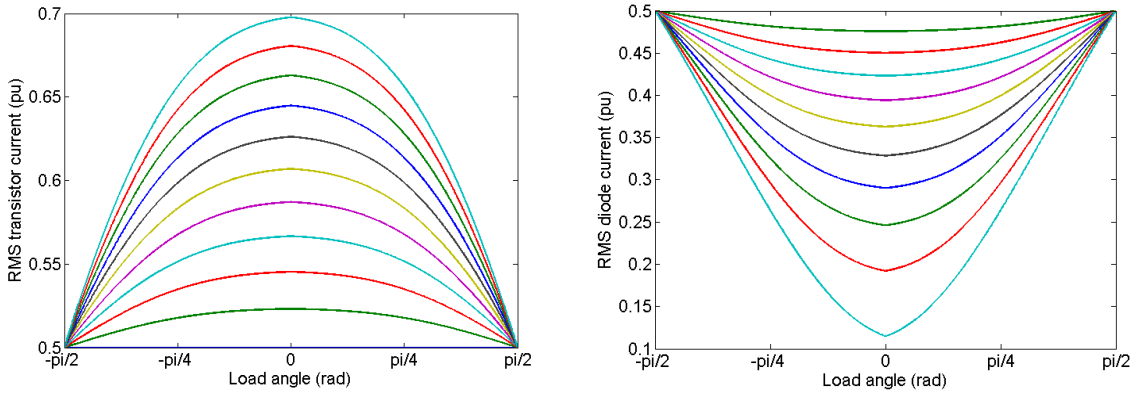

Fig. 3.10 RMS transistor (left) and diode (right) current as a function of the load angle (φ) for several values of modulation index (M) for SVM PWM. M=[0,0.1..1].

The program written in MATLAB script to plot this figures is also included in APPENDIX.

3.3.1.2 Switching losses [45]

In [45] an analytical expression to estimate the converter switching losses is presented. It is assumed that "the switching losses are only proportional to the switched voltage and the switched current and account only for the fundamental component of the load current".

The switching losses of a semiconductor device (transistor and diode) are modeled by next equations:

$$P_{t,sw} = V_{DC} E_{sw0,t} f_{sw} I_{sw,avg} \tag{3.8}$$

$$P_{d,sw} = V_{DC} E_{sw0,d} f_{sw} I_{sw,avg} \tag{3.9}$$

Where:

V_{DC} is the DC-link voltage.

$E_{sw0,x}$ is the temperature dependent sum of the per unit VA turn on and turn off switching energy of the component x.

f_{sw} is the switching frequency.

$I_{sw,avg}$ is the average switched current.

The average switched current of the transistor or the diode is given by an equation that is not independent of the used modulation method. In [45] next equations are derived to evaluate the average switched current using SVM PWM:

$$I_{sw,avg} = \frac{1}{4\pi} \int_0^{2\pi} \tilde{\imath}_{sw}(\theta) d\theta = \frac{\sqrt{2}}{\pi} I_r \tag{3.10}$$

It can be observed that the value of this average switched current only depends on the value of the RMS phase current (I_r).

3.3.1.3 Thermal modeling

As shown in previous sections 3.3.2 and 3.3.3, several semiconductor parameters are temperature dependent. So using thermal modeling of the switches the average temperature can be estimated and correct values for this parameters can be found.

Moreover, using thermal modeling the peak temperature within a fundamental period can be estimated. This is a key parameter to validate a converter design.

But due to time constraints thermal modeling of the switches is not considered. So the parameters of the semiconductor devices are always considered as constants.

3.3.1.4 Phase reactor power losses

In this project is considered that a phase reactor (inductor) is employed in both AC outputs of the VSC-HVDC system for harmonic mitigation. In the case of the back-to-back topology (in DFIG and full-scale SPMSG) is only considered one phase reactor in the AC output of the WF-network side converter.

In the first approach presented in simulations it is considered that the losses in the reactors are included in the static factor μ .

Basically the total power losses of one inductor are equal to the sum of the copper losses, hysteresis losses and eddy current losses.

$$P_L = P_{Cu} + P_{hy} + P_{ed} \tag{3.11}$$

Analytical detailed expressions for each kind of inductor power losses can be found in [45].

3.4 Converter losses [45]

Based on equations presented in sections 3.3.1, 3.3.2 and 3.3.3 the total converter losses can be expressed with the following equation:

$$P_{loss} = P_{conv,1} + P_{conv,2} + P_{L,T} \tag{3.12}$$

Where:

$P_{conv,1}$ represents the total WF-network side HVDC power converter losses (so called machine-side converter for DFIG and full-scale SPMSG):

$P_{conv,2}$ represents the total grid side HVDC converter power losses (so called WF network-side converter for DFIG and full-scale SPMSG)

$P_{L,T}$ represents the total power losses of the inductor filters

For the WF-network side HVDC converter (so called machine-side converter for DFIG and full-scale SPMSG):

$$\begin{aligned} P_{conv,1} &= 6\left(P_{cond,tr} + P_{cond,dr} + P_{sw,tr} + P_{sw,dr}\right) \\ &= 6\left(V_{tr0}(T) \cdot I_{avg,tr} + R_{tr}(T) \cdot I_{tr}^2 + V_{d0}(T) \cdot I_{avg,dr} + R_{dr}(T) \cdot I_{dr}^2\right) + \\ &+6 \cdot V_{DC} \cdot f_{swr} \cdot \left(E_{sw0,tr}(T) + E_{sw0,dr}(T)\right) \cdot I_{swr,avg} \end{aligned} \tag{3.13}$$

For the grid side HVDC converter (so called WF network-side converter for DFIG and full-scale SPMSG):

$$\begin{aligned} P_{conv,2} &= 6\left(P_{cond,tg} + P_{cond,dg} + P_{sw,tg} + P_{sw,dg}\right) \\ &= 6\left(V_{tg0}(T) \cdot I_{avg,tg} + R_{tg}(T) \cdot I_{tg}^2 + V_{d0}(T) \cdot I_{avg,dg} + R_{dg}(T) \cdot I_{dg}^2\right) + \\ &+6 \cdot V_{DC} \cdot f_{swg} \cdot \left(E_{sw0,tg}(T) + E_{sw0,dg}(T)\right) \cdot I_{swg,avg} \end{aligned} \tag{3.14}$$

3.5 Summary

In this chapter two non-ideal models of the PWM two-level three-phase VSC converter were presented. The first one is a very simplified model, which estimates the losses through a static factor μ. This is the model employed in the first method approach. Then a more complex dynamic model which takes into account the switching and conducting losses of switches as well as the reactor losses is presented. This more complex loss-model is based on analytical expressions and verified in [45] through comparison with a non-ideal dynamic model.

Chapter 4 Full-Scale SPMSG Wind Turbine

ABSTRACT

The contents of the next chapter deal with the development of a mathematical model of the full-scale SPMSG WT. Firstly, stress is on development of mathematical model of the SPMSG, which is the basis to tackle the design of the machine model structure. Then, from the study of the power balance equation, an expression for the electromagnetic torque (T_{el}) generated by the SPMSG is obtained. This is the key equation to understand the control strategy chosen for the stator-side PWM converter – Field Oriented Control (FOC). The grid-side converter control strategy – VOC with PLL system – is already explained in Chapter 3. The chapter ends presenting the steady state model of the full-scale SPMSG WT.

4.1 Introduction

The electrical generator employed in the full-scale WT is SPMSG. Three stator windings are directly connected to a back-to-back two level PWM converter.

The stator-side PWM converter behaves as an inverter and is employed to control the torque or the speed of the machine. The grid-side PWM converter behaves as a rectifier, controlling the DC voltage of the DC link and the power factor, while exchanging power with the grid.

The control strategy for the WT grid-side converter (WF network-side converter) is basically the same employed for the HVDC grid-side VSC: VOC with PI controllers and a simple PLL for the estimation of the voltage angle of the WF grid.

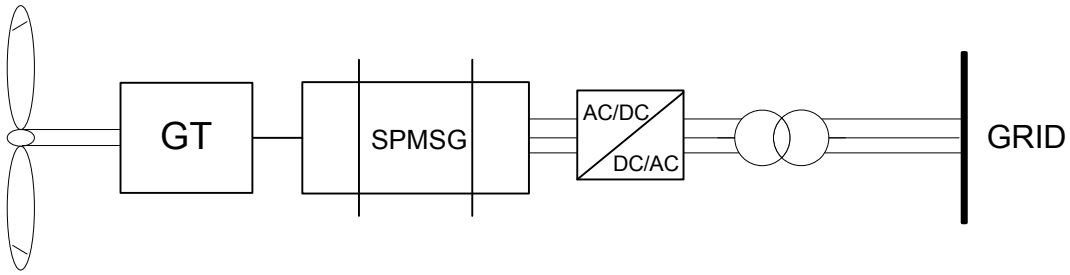

Fig. 4.1 Full-scale WT Topology.

4.2 Permanent magnet ac machines

The Permanent Magnet AC Machines (PMACM) consist of two main parts, an outside stationary stator with armature windings placed in slots, and an inside rotatory rotor with permanent magnets.

Permanent magnets located in the rotor to generate the rotor field results in higher efficiency, since the copper loss in the rotor associated with windings does not exist. Moreover in this design, the commutator and the brushes neither exist: the structure is simpler and some problems are avoided (brushwear, high rotor inertia).

PMACM can be sub-classified into Trapezoidal and Sinusoidal types, depending on the shape of the back-EMF voltage4 waveforms (trapezoidal or sinusoidal) that they induce in each stator phase winding during rotation. To produce torque, the stator of the first ones is excited from rectangular current waveforms, and the stator of the second ones from sinusoidal current waveforms. Despite their simple control the employment of Trapezoidal PMAC machines (also called "Brushless DC Motors" (BLDCM)) is not suitable in all applications due to the presence of non desired torque ripples [66]. Therefore the Sinusoidal PMAC machines (also called "Permanent Magnet Synchronous Machines" (PMSM)) are the most suitable kind of Synchronous Machine (SM) to compete against the Induction machines in wind power applications.

A general comparison between BLDC and PMSM is shown in the next table.

Parameter	3-Phase BLDC Machine	3-Phase PMSM
Winding distribution	Concentrated	Distributed
Energised phase	Two phases on at any time	Three phases on at any time
Stator current	Square/Trapezoidal wave	Sinusoidal wave
Back-EMF	Trapezoidal wave	Sinusoidal wave
Electromagnetic torque	Almost constant	Constant
Torque strength	Stronger	Weaker

Table 4.1 Comparison of BLDC machine and PMSM [67].

The PMSM is constructed with a classic three-phase stator as a conventional IM. If three sinusoidal voltages are applied to the three stator phases a rotating magnetic field is generated and the machine is run as a motor. Sinusoidal currents flow in the coils and generate the rotating stator flux. Then rotation of the rotor shaft is produced by interaction of the permanent rotor flux with the stator flux.

On the other hand, when the machine is run as a generator, the rotation of the rotor shaft is produced by the input mechanical torque, and three sinusoidal currents are induced in the three stator phases.

There are two common setups for the rotor of the PMSM depending on the position of the magnets:

Interior magnets (IPMSM)

Surface mounted magnets (SPMSM)

The IPMSM is built with permanent magnets embedded inside the cylindrical rotor. On the other hand, a SPMSM has arc-shaped permanent magnets on the surface.

General layouts of the two different rotor configurations for an IPMSM four-pole design (45 mechanical degrees) and a SPMSM eight-pole design (22.5 mechanical degrees) are shown in figure below.

[4] *back-EMF voltage: "When a permanent magnet machine rotates, the interaction of the rotor magnetic field with the field generated by the stator currents, generates a voltage on the stator coils (back-EMF voltage) that opposes the voltage of the stator windings. Some control systems use this back-EMF voltage to infer the position of the rotor without using any additional position sensors, in so-called sensorless feedback" Reviewed from [67].*

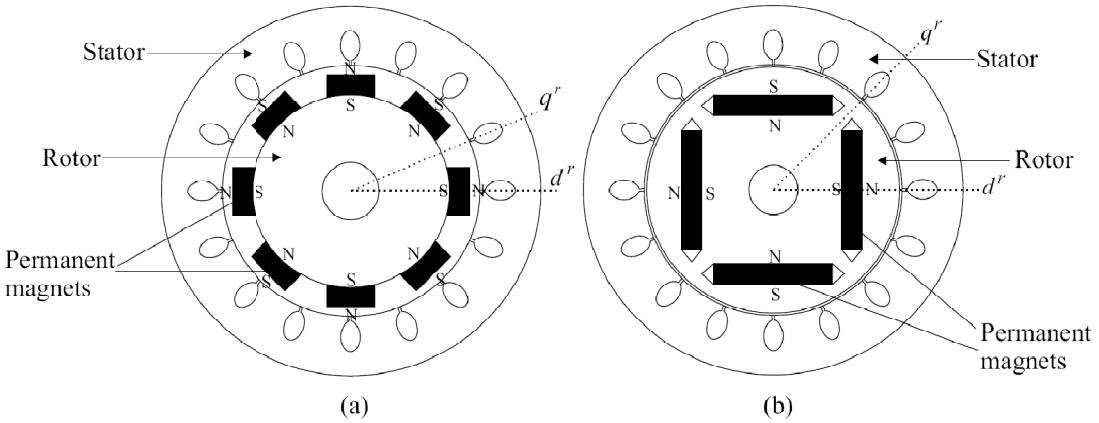

Fig. 4.2 General Layout of SPMSM (a) and IPMSM (b).

"It can be seen that the magnetic flux induced by the magnets defines the rotor direct or dr-axis radially through the centerline of the magnets. The rotor quadrature or qr-axis is orthogonally (90 electrical degrees) placed with rotor dr-axis. Since the permeability of permanent-magnets is almost same as the air, in interior magnets type configuration the effective airgap of dr-axis is increased compared to the qr-axis. Therefore, the dr-axis reluctance is higher than the qr-axis reluctance. This results in the qr-axis inductance is higher than the dr-axis inductance, i.e. Lq > Ld, in IPMSMs" [66].

"The interior magnets type rotor configuration brings saliency characteristics to the machines which are not present in a machine with surface magnets type rotor" [66].

It means that an IPMSM is a salient pole machine. On one hand this is an advantage, because an IPMSM can utilize magnetic and reluctance torque (torque generated by the natural tendency of its rotor to move to a position where the excited winding inductance is maximized), but on the other hand this is a disadvantage, since salient pole machines have higher cogging torque. Cogging torque is always an undesired effect especially prominent at lower speeds, which contributes to the output ripple, vibration, and noise in the machine [68]. Figure 3.2 explains the effect of the cogging torque through a mechanical analogy. Changes in magnetic field density take place around the rotor's PM when is rotating closed the non-uniform slot surface of the stator. This results on a pulsating speed which affects negatively to the machine performance.

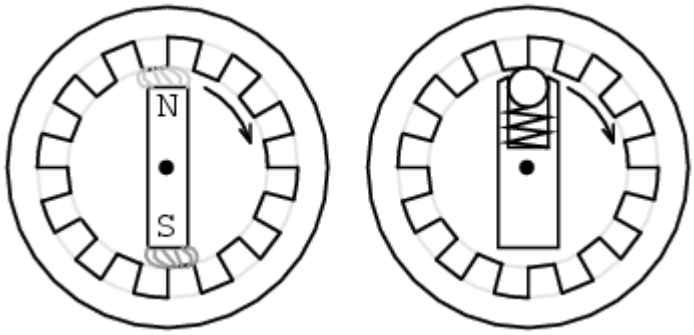

Fig. 4.3 Mechanical analogy of cogging torque [69]

Because of that a SPMSM is a non-salient pole machine and only utilize magnetic torque. Therefore SPMSM control strategies are easier to implement since, as explained in followings, the electromagnetic torque is only proportional to the q component of the stator current in rotor reference frame ( ), the number of poles ( ) and the permanent magnet flux ( ).

$$T_e = \frac{3}{2} \cdot \frac{p}{2} (\Psi_m \cdot i_q) \tag{4.1}$$

Because of that in this project a SPMSG have been employed in the full-scale WT configuration.

4.3 SPMSG model in dq synchronous reference frame [15,17]

In order to design the control system a mathematical model of the SPMSG is needed. Next assumptions are used to simplify the development of the machine model:

Assumptions

1. The spatial stator phase winding distribution in the air gap is sinusoidal.
2. No thermal effect for stator resistance and the permanent-magnet flux.
3. No saturation effect for the inductances.
4. No core loss in the machine.
5. The three stator windings are equal.
6. The machine is considered an ideal non-salient pole machine.
7. The air gap is considered uniform.
8. The voltages are balanced and the motor is star-connected (the sum of phase currents is equal to zero). This assumption is equivalent to assumption (5).

4.3.1 Dynamic model

Applying Clarke and Parke transformations the voltage equations based on the d, q synchronous rotating reference frame are derived from the equations of the three phase stationary a, b, c reference frame.

$$v_d = L_s \cdot \frac{di_d}{dt} + R_s \cdot i_d - w_s \cdot \Psi_q \tag{4.2}$$

$$v_q = L_s \cdot \frac{di_q}{dt} + R_s \cdot i_q + w_s \cdot \Psi_d \tag{4.3}$$

This can be also written in vector form as:

$$\bar{v_s} = R_s \cdot \bar{i_s} + L_s \cdot \frac{d\bar{i_s}}{dt} + j \cdot w_s \cdot \Psi_s \tag{4.4}$$

Where three stator windings are considered equal:

$$R_s = R_a = R_b = R_c \tag{4.5}$$

Consequently, the equivalent circuits for the d, q reference frame are:

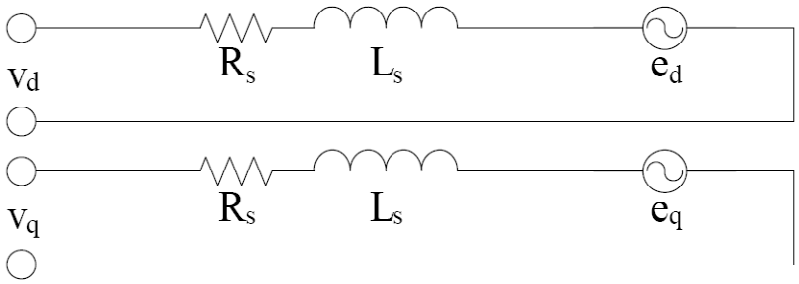

Fig. 4.4 Equivalent circuits for the *d, q* reference frame [70].

Then the magnetic flux linkages in the direct and quadratic directions are defined:

$$\Psi_d = \Psi_m + i_d \cdot L_s \tag{4.6}$$
$$\Psi_q = i_q \cdot L_s \tag{4.7}$$

Where considering an ideal non-salient pole machine:

$$L_s = L_d = L_q = L_a = L_b = L_c \tag{4.8}$$

Employing these previous relationships the most common scalar form of the voltage equations in the rotating d, q reference is derived:

$$v_d = L_s \frac{di_d}{dt} + R_s i_d - \omega_s L_s i_q \tag{4.9}$$
$$v_q = L_s \frac{di_q}{dt} + R_s i_q + \omega_s L_s i_d + \omega_s \Psi_m \tag{4.10}$$

Then the main equations used to model the machine in matrix notation are [18]:

$$\frac{d}{dt}\begin{bmatrix} i_d \\ i_q \end{bmatrix} = \frac{1}{L_s}\left\{\begin{bmatrix} -R_s & \omega_s L_s \\ -\omega_s L_s & -R_s \end{bmatrix}\begin{bmatrix} i_d \\ i_q \end{bmatrix} - \omega_s \Psi_m \begin{bmatrix} 0 \\ 1 \end{bmatrix} + \begin{bmatrix} v_d \\ v_q \end{bmatrix}\right\} \tag{4.11}$$

and the next dynamic equation:

$$\frac{d\omega_s}{dt} = \frac{p}{2}\frac{1}{J}\left(T_{el} - T_{mec} - T_{df} - \frac{B\omega_s}{p/2}\right) \tag{4.12}$$

Where:

- p is the number of poles.
- T_e is the electromagnetic torque generated by the SPMSM [Nm].
- T_m is the mechanical input torque [Nm].
- T_{df} is the dry friction torque [Nm].
- B is the mechanical coefficient due to friction [Nms/rad].
- J is the moment of inertia [kg m2].

4.3.2 Steady-state model

Neglecting electrical transient equations (4.11) and (4.12) can be written as:

$$\begin{bmatrix}0\\0\end{bmatrix} = \frac{1}{L_s}\left\{\begin{bmatrix}-R_s & \omega_s L_s\\ -\omega_s L_s & -R_s\end{bmatrix}\begin{bmatrix}i_d\\ i_q\end{bmatrix} - \omega_s \Psi_m \begin{bmatrix}0\\1\end{bmatrix} + \begin{bmatrix}v_d\\ v_q\end{bmatrix}\right\} \quad (4.13)$$

$$0 = \frac{p}{2}\frac{1}{J}\left(T_e - T_m - T_{df} - \frac{B\omega_s}{p/2}\right) \quad (4.14)$$

4.3.3 The electromagnetic torque

The expression of the electromagnetic torque (T_{el}) generated by the SPMSM can be obtained employing power balance equation.

The power balance equation for generator mode can be written as:

$$P_{mech} = P_{loss} + P_{stored} + P_{out} \quad (4.15)$$

Where:

Power loss in conductors:

$$P_{loss} = \frac{3}{2}\left(i_d^2 \cdot R_s + i_q^2 \cdot R_s\right) \quad (4.16)$$

Rate of change of stored energy in magnetic fields:

$$P_{stored} = \frac{3}{2}\left(L_s \cdot \frac{d}{dt}\frac{i_d^2}{2} + L_s \cdot \frac{d}{dt}\frac{i_q^2}{2}\right) \quad (4.17)$$

It can be seen that this power is zero in steady state operation.

Instantaneous power flowing out the machine:

$$P_{out} = \frac{3}{2}\left(i_d \cdot v_d + i_q \cdot v_q\right) \quad (4.18)$$

Mechanical power (for energy conversion)

$$P_m = T_m \cdot \Omega_r \quad (4.19)$$

From the previous equation and equation (4.14) we can derive in steady-state the value of the electromagnetic torque T_{el} since the electromechanical power P_e is just equal to the power output from the motor shaft P_m if the mechanical losses of the machine are neglected ($T_{df} = 0$ and $B = 0$).

This means that the electromechanical power P_{el} is equal to the product of the electromagnetic torque T_{el} by the mechanical angular speed:

$$P_m = T_m \cdot \Omega_r \approx P_e = T_e \cdot \Omega_r \quad (4.20)$$

$$P_e = \frac{3}{2}\left(i_q \cdot \omega_s \cdot \Psi_d - i_d \cdot \omega_s \cdot \Psi_q\right) \quad (4.21)$$

On the other side, taking into account that a complete turn of the magnetic field is equivalent to a mechanical turn of the rotor by two poles, the relationship between mechanical speed of the rotor and the electrical speed is:

$$\Omega_r = \frac{2}{p} \cdot \omega_s \tag{4.22}$$

Then the electromagnetic torque T_e can be expressed as:

$$T_e = \frac{3}{2} \cdot \frac{p}{2}\left(\Psi_d \cdot i_q - \Psi_q \cdot i_d\right) = \frac{3}{2} \cdot \frac{p}{2}\left((\Psi_m + i_d \cdot L_s) \cdot i_q - i_q \cdot L_s \cdot i_d\right) == \frac{3}{2} \cdot \frac{p}{2}\left(\Psi_m \cdot i_q\right) \tag{4.23}$$

From the equation above it can be stated that the electromagnetic torque is directly proportional to the q component of the stator current in rotor reference frame. In a control sense fast response in current will mean fast torque response – higher dynamic response of the system. Also it can be stated that the d component of the stator current in rotor reference frame should be always zero, since this does not produce electromagnetic torque.

In SPMSM, the electromagnetic torque is only proportional to the q component of the stator current in rotor reference frame.

$$T_e = \frac{3}{2} \cdot \frac{p}{2}\left(\Psi_m \cdot i_q\right) \tag{4.24}$$

4.4 Full-scale spmsg stator side converter control [66] [71]

FOC is the chosen control strategy for the stator side converter in the full-scale SPMSG WT.

The purpose of Field Oriented Control (FOC) strategy is "to perform real-time control of torque variations demand, to control the rotor mechanical speed and to regulate phase currents in order to avoid current spikes during transient phases"[72].

This control strategy employs mathematical reference frame transformations (Clarke and Park) in order to simplify the electrical equations – time and position dependences are removed.

The block diagram of the FOC with torque and speed controller is shown below.

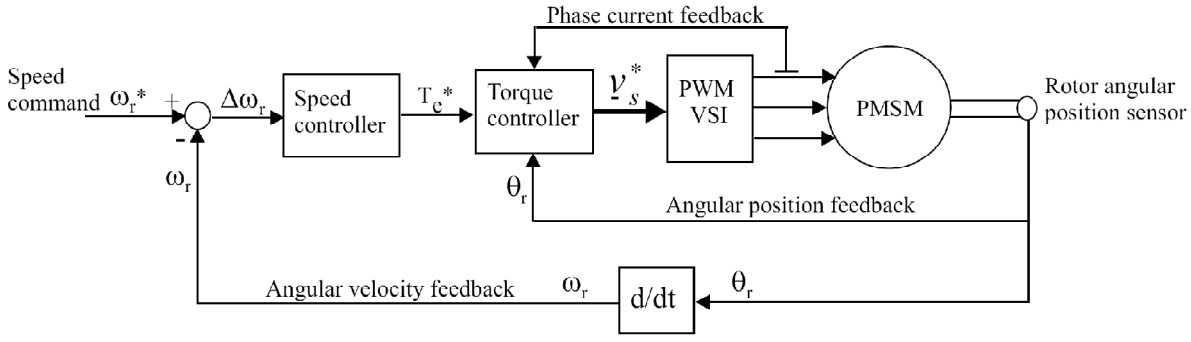

Fig. 4.5 The block d

iagram of the FOC with torque and speed controller.

Feedback of the stator currents to the torque controller is necessary since the electromagnetic torque characteristic is related to them. Furthermore, to ensure self-synchronization rotor angular position feedback is also necessary.

As the current control inside the torque controller is made in field-oriented frame, this control strategy is called Field-Oriented-Control.

Rotor speed control is done through an external feedback speed loop (cascade control structure). The rotor angular speed is obtained from the same rotor position sensor.

A more detailed block diagram of the FOC is shown in next figure, where the transformations in the reference frame can be observed, as well as the control property block:

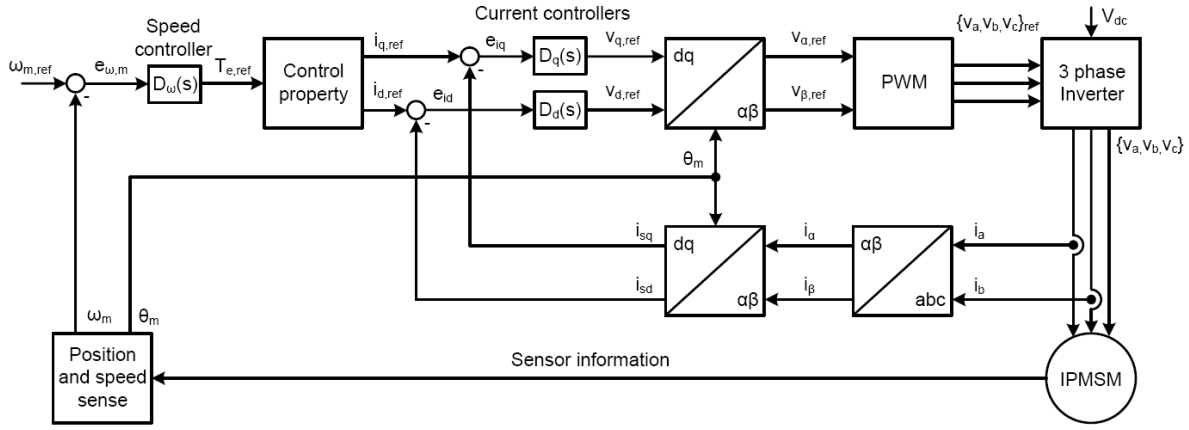

Fig. 4.6 diagram for the FOC of a PMSM.

The FOC strategy allows accurate real-time control of torque and speed in every state of operation (steady state or transient), full torque at zero speed and constant control of stator currents. On the other hand FOC requires more computational time (many transformations, PWM...) than other simpler strategies.

4.4.1 Control property

Several control properties have been developed for the SPMSM during last decades. Some of the most important are listed below and described next.

- Unity power factor control
- Constant torque angle control
- Maximum torque per ampere control

Unity power factor control

The advantage of this method is to maintain the power factor at unity, which minimizes the volt-ampere rating required. This is made keeping the power factor angle $\varphi = 0$ (Fig. 4.7).

But as a consequence the efficiency and the maximum torque are lower with this method.

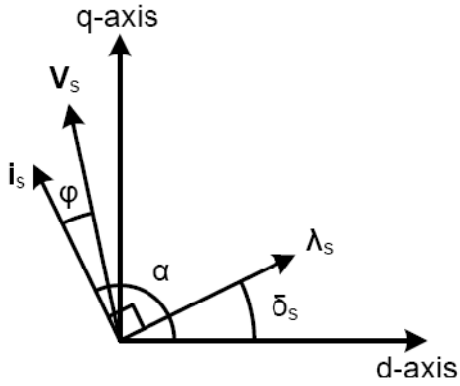

Fig. 4.7 Current and voltage vector, power factor angle φ, stator flux linkage angle δ_s and torque angle α.

Constant torque angle

The torque angle α is defined as the angle between the rotor d-axis and the stator current space vector i_s (Fig. 4.7). In this method the torque angle is kept constant $= {}^{\pi}/_{2}$. This is easily reached making the d-axis current zero:

$$i_d = 0 \Rightarrow |i_s| = i_q \tag{4.25}$$

Then the relationship between torque and current is expressed as:

$$T_e = \frac{3}{2} \cdot \frac{p}{2} (\Psi_m \cdot i_q) \tag{4.26}$$

This method is not recommended for IPMSM since the reluctance torque is not used. But is highly recommended for SPMSM, since is very simple to implement and linearizes the relation torque-current.

Maximum torque per ampere

This control property is characterized by keeping the minimum current amplitude for a certain electromagnetic torque. This means that the copper losses are minimized, so the PMSM is operating at higher efficiency.

For the SPMSM the maximum torque per ampere property (MTPAC) is equal to the constant torque angle property (CTAC).

4.5 Full-scale spmsg model structure

Full-scale SPMSG simulation system is made up of three different subsystems. The first one models the behavior of the SPMSG controlled with FOC strategy by the stator-side converter. The second one models the behavior of the WF network-side converter controlled by VOC strategy taking into account the whole losses in the converter. Finally, the third one models the three-phase two winding transformer.

Since in this project the WF is considered always in steady-state with a perfect track of the reference values by the control system[5], the reference signals represent directly steady-states in the machine models.

As well, a perfect estimation of stator angular speed is assumed –so there is no need to include PLL systems in the WF models.

[5] *See general assumptions – Chapter 1, section 1.7.*

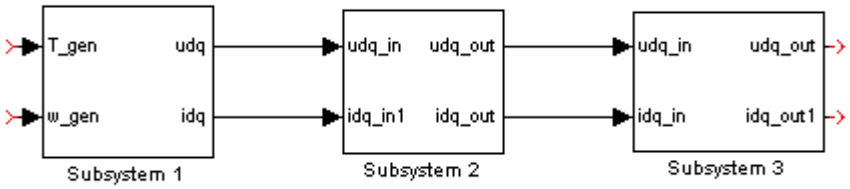

Fig. 4.8 Block diagram of the full-scale SPMSG WT model

In next section the modeling of the first subsystem is presented.

For the second subsystem the performance of the WF network-side converter controlled with VOC strategy is modeled as explained previously in Chapter 3. Next equations summarize its modeling:

$$\begin{aligned} P_{out} &= \mu P_{in} \\ v_{qout} i_{qout} &= \mu v_{qin} i_{qin} \\ Q_{out} &= 0 \Rightarrow i_{dout} = 0 \end{aligned} \tag{4.27}$$

As first approach the whole losses in the back-to-back converter are just modeled by a static factor of $\mu = 0.95$ included in this second subsystem.

On the other hand, the model of the transformer is included in Chapter 8. If no losses in the transformer are considered in first approach next simple equations can be employed in steady-state simulation:

$$\begin{aligned} \frac{v_{out}}{N_{out}} &= \frac{v_{in}}{N_{in}} \\ i_{out} N_{out} &= i_{in} N_{in} \end{aligned} \tag{4.28}$$

4.5.1 Steady-state model of SPMSG controlled with FOC strategy by stator-side converter

Based on a simplified steady-state FOC strategy and the steady state SPMSG equations, the core of the full-scale SPMSG WT model implemented in MATLAB/SIMULINK is developed.

The already presented equations for the SPMSG are modified according to the characteristics of the FOC ($i_d = 0$ and $i_q = f(T_e)$). The outputs of the system are currents and voltages in the stator (i_d , i_q , v_d and v_q). The inputs of the system, as it can be seen in Fig. 4.8, are the electromagnetic torque and electrical angular speed (T_e and ω_s).

Therefore, the model equations are the next:

$$\begin{aligned} i_q &= T_e \frac{2}{3} \cdot \frac{2}{p} \cdot \frac{1}{\Psi_m} \\ v_d &= R_s i_d - \omega_s L_s i_q \\ v_q &= R_s i_q + \omega_s L_s i_d + \omega_s \Psi_m \end{aligned} \tag{4.29}$$

4.6 Conclusion

Next, the main goals achieved in this chapter are summarized:

Development of a mathematical model of the SPMSG.

Obtaining of the electromagnetic torque equation.

Fundamentals of generator model structure.

Presentation of a control strategy for stator-side converter.

Development of a steady-state model for full-scale SPMSG WT.

At the beginning of the chapter the differences between several PM AC machines were commented. Specially the differences between the IPMSM and the SPMSM, which can be summarized in next statement: "the interior magnets type rotor configuration brings saliency characteristics to the machines which are not present in a machine with surface magnets type rotor". This results in that the SPMSM is a non-salient pole machine and only uses magnetic torque (does not employ reluctance torque).

It has been stated that for SPMSM, the electromagnetic torque is only proportional to the q component of the stator current in d-q reference frame.

The employment of reference frame transformations allows great simplification on system equations, since the values of parameters are non-dependent on the rotor rotating angle. Thanks to that, sinusoidal signals can be treated as constant signals by the control system.

Taking into account previous statements a whole steady-state model for full-scale SPMSG WT was developed. As first approach the whole losses in the back-to-back converter were just modeled by a static factor of $\mu = 0.95$ and a lossless transformer was considered.

Chapter 5 DFIG WIND TURBINE

ABSTRACT

The following chapter deals with the development of a mathematical model of the DFIG WT. Firstly, a mathematical model of the general IM is derived, which is the basis to understand the DFIG performance. Then the DFIG rotor-side converter control estrategy is explained. The grid-side converter control strategy – VOC with PLL system – is already explained in chapter 3. Finally the steady state model of the DFIG WT is presented

5.1 Introduction

The electrical generator employed in the DFIG-WT is a wound rotor induction generator (WRIG). A WRIG with short-circuit rotor terminals is similar to SCIG and presents fixed speed behaviour when is running at constant stator frequency. Using DFIG a variation of the rotor speed from -40% to +30% of the synchronous speed is allowed.[9]

In DFIG-WT configuration the generator presents three stator windings directly connected to the supply network while rotor windings are connected through a back-to-back two level PWM converter (Fig. 5.1).

The rotor-side PWM converter behaves as an inverter and is employed to control the torque or the speed of the machine as well as the power factor at the stator terminals. The grid-side PWM converter behaves as a rectifier, controlling the DC voltage of the DC link, while exchanging power with the grid. [9][49]

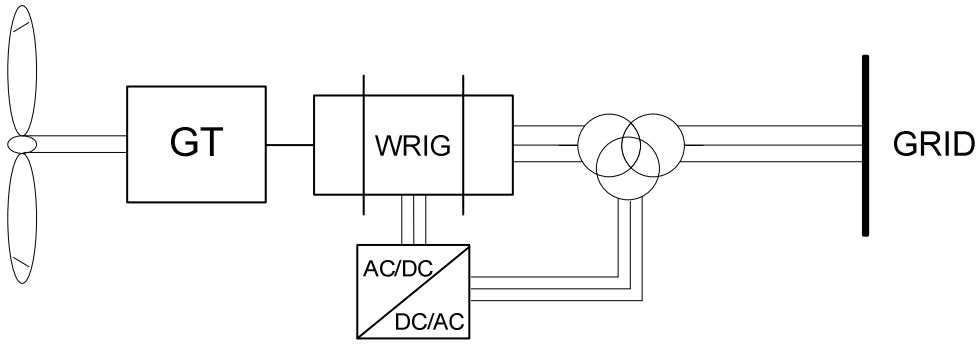

Fig. 5.1 Typical DFIG Topology

The control strategy for the WT grid-side converter (WF-network side converter) is mainly the same employed for the HVDC grid-side VSC: VOC with PI controllers and a simple PLL for the estimation of the voltage angle of the WF grid.

The converter attached to the rotor terminals of the DFIG generator can deliver or absorb power from or to the grid through the rotor terminals, while a permanent injection of power into the grid is done through the stator windings. When the generator is operated at sub synchronous speed power is injected into the grid by the stator. Some of this power is self-consumed y the machine in the rotor windings. For over synchronous both the stator and the rotor inject power into the grid. Fig. 5.2

$$P_M = \omega_r T_e \tag{5.1}$$

$$P_M = P_s - P_r \tag{5.2}$$

$$P_s = sP_r \tag{5.3}$$

$$P_s = \frac{P_M}{1-s} \tag{5.4}$$

$$s = \frac{\omega_s - \omega_r}{\omega_r} \tag{5.5}$$

Where:		
	P_M	Mechanical power through the shaft of the generator
	P_s	Power through the stator
	P_r	Power through the stator
	ω_r	rotor angular speed [rad/s]
	ω_s	synchronous speed [rad/s]
	s	slip (s>0 sub synchronous operation, s<0 over synchronous operation)

The ideal power distribution in steady state through the rotor and stator windings is dependent on the slip of the generator.

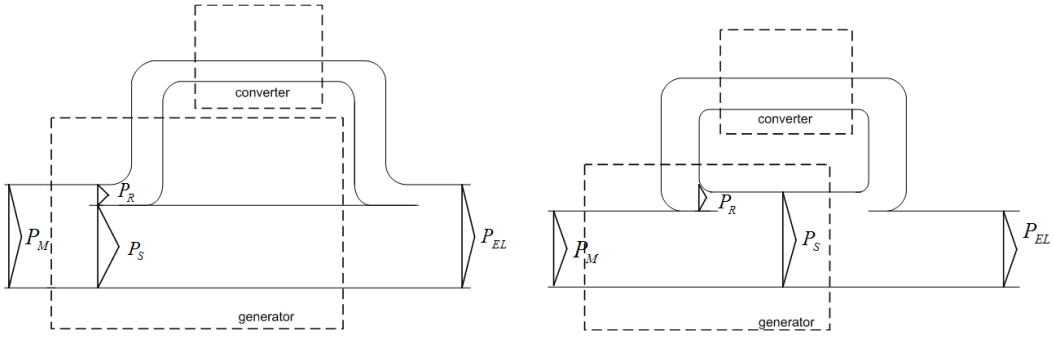

Fig. 5.2 Power flow of an ideal DFIG at over synchronous speed and sub synchronous speed [9].

From the figure Fig. 5.3 it can be observed that under synchronous speed the stator is providing power (Ps) and the rotor is subtracting (Pr=-s*Ps), while over synchronous speed at both are injecting (Pr=s*Ps).

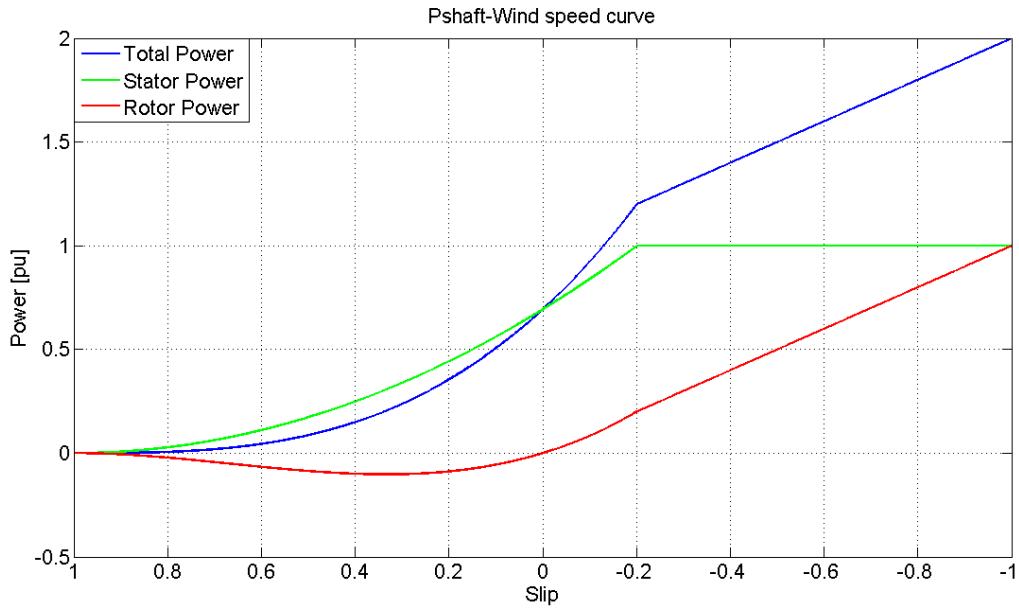

Fig. 5.3 Power flow in the 2MW DFIG

5.2 IM general model in dq-arbitrary reference frame

The Induction Machine (IM) ABC/abc model is well known and described in [1][9][23]. In this section the dynamic and the steady-state models in dq-arbitrary reference frame are described. The generation convention is considered, setting the currents as outputs and providing positive sign for the active and reactive power when they are injecting into the grid.[24]

Next assumptions are used to simplify the development of the machine model:

Assumptions

9. The spatial stator phase winding distribution in the air gap is sinusoidal.
10. No thermal effect for stator and rotor resistance.
11. No saturation effect for the inductances.
12. No core loss in the machine.
13. The air gap is considered uniform.
14. The voltages are balanced and the motor is star-connected (the sum of phase currents is equal to zero).

5.2.1 Dynamic model

Voltage equations in the arbitrary reference frame can be written as [25].

$$[V] = -[R][I] + \frac{d}{dt}[\Psi] + [\Omega][\Psi] \tag{5.6}$$

$$\begin{bmatrix} v_{sd} \\ v_{sq} \\ v_{rd} \\ v_{rq} \end{bmatrix} = \begin{bmatrix} R_s & 0 & 0 & 0 \\ 0 & R_s & 0 & 0 \\ 0 & 0 & R_r & 0 \\ 0 & 0 & 0 & R_r \end{bmatrix} \begin{bmatrix} i_{sd} \\ i_{sq} \\ i_{rd} \\ i_{rq} \end{bmatrix} + \frac{d}{dt} \begin{bmatrix} \Psi_{sd} \\ \Psi_{sq} \\ \Psi_{rd} \\ \Psi_{rq} \end{bmatrix} + \begin{bmatrix} 0 & -\omega_d & 0 & 0 \\ \omega_d & 0 & 0 & 0 \\ 0 & 0 & 0 & -\omega_{da} \\ 0 & 0 & \omega_{da} & 0 \end{bmatrix} \begin{bmatrix} \Psi_{sd} \\ \Psi_{sq} \\ \Psi_{rd} \\ \Psi_{rq} \end{bmatrix} \tag{5.7}$$

Where ωd is the reference frame speed and $\omega_{da} = \omega_d - \omega_r$. With $\omega_r = p\Omega_r$ the electrical speed of the machine and Ω_r is the mechanical speed of the rotor.

The mechanical angel is set as $\frac{d\vartheta_m}{dt} = \Omega_r$.

Relation between the linkage fluxes and currents is given by:

$$[\Psi] = [L][I] \tag{5.8}$$

$$\begin{bmatrix} \Psi_{sd} \\ \Psi_{sq} \\ \Psi_{rd} \\ \Psi_{rq} \end{bmatrix} = \begin{bmatrix} L_s & 0 & L_m & 0 \\ 0 & L_s & 0 & L_m \\ L_m & 0 & L_r & 0 \\ 0 & L_m & 0 & L_r \end{bmatrix} \begin{bmatrix} i_{sd} \\ i_{sq} \\ i_{rd} \\ i_{rq} \end{bmatrix} \tag{5.9}$$

Where $L_s = L_{\sigma s} + L_m$ is the stator self inductance, $L_r = L_{\sigma r} + L_m$ is the rotor self inductance and L_m is the mutual inductance I the general reference frame.

In this description the fluxes are selected as state variables, but it could be selected currents as well. For this the currents can be expressed by:

$$[I] = [L]^{-1}[\Psi] \tag{5.10}$$

$$[L]^{-1} = \frac{1}{G} \begin{bmatrix} L_r & 0 & -L_m & 0 \\ 0 & L_r & 0 & -L_m \\ -L_m & 0 & L_s & 0 \\ 0 & -L_m & 0 & L_s \end{bmatrix} \tag{5.11}$$

Where $G = L_s L_r - L_m^2$ and resulting by some mathematical transformations:

$$\frac{d}{dt}[\Psi] = [V] - \left[[\Omega] - [R][L]^{-1}\right][\Psi] \tag{5.12}$$

$$\frac{d}{dt} \begin{bmatrix} \Psi_{sd} \\ \Psi_{sq} \\ \Psi_{rd} \\ \Psi_{rq} \end{bmatrix} = \begin{bmatrix} v_{sd} \\ v_{sq} \\ v_{rd} \\ v_{rq} \end{bmatrix} - \frac{1}{G} \begin{bmatrix} R_s L_r & -\omega_d G & -R_s L_m & 0 \\ \omega_d G & R_s L_r & 0 & -R_s L_m \\ -R_s L_m & 0 & R_r L_s & -\omega_{da} G \\ 0 & -R_s L_m & \omega_{da} G & R_r L_s \end{bmatrix} \begin{bmatrix} \Psi_{sd} \\ \Psi_{sq} \\ \Psi_{rd} \\ \Psi_{rq} \end{bmatrix} \tag{5.13}$$

Power and Electromagnetic torque

Stator and rotor active and reactive power can be written in terms of:

$$P_s = \frac{3}{2}\left(v_{sd}i_{sd} + v_{sq}i_{sq}\right) \tag{5.14}$$

$$P_r = \frac{3}{2}\left(v_{rd}i_{rd} + v_{rq}i_{rq}\right) \tag{5.15}$$

$$Q_s = \frac{3}{2}\left(v_{sq}i_{sd} - v_{sd}i_{sq}\right) \tag{5.16}$$

$$Q_r = \frac{3}{2}\left(v_{rq}i_{rd} - v_{rd}i_{rq}\right) \tag{5.17}$$

In this model only copper losses are taken into account, these losses are modeled by:

$$P_{cu} = \frac{3}{2}\left(\mathrm{R}_s i_{sd} + \mathrm{R}_s i_{sq} + \mathrm{R}_r i_{rd} + \mathrm{R}_r i_{rq}\right) \tag{5.18}$$

The electromagnetic torque is:

$$T_e = \frac{P_m}{\Omega_r} = \frac{3}{2}p\left(\Psi_{sd}i_{sq} - \Psi_{sq}i_{sd}\right) \tag{5.19}$$

Where p is the number of pole pairs and Ω_r is the mechanical speed of the rotor.

The electromagnetic torque of an induction machine also can be expressed in different ways as:

$$T_e = \frac{3}{2}p\left(\Psi_{rq}i_{rd} - \Psi_{rd}i_{rq}\right) \tag{5.20}$$

$$T_e = \frac{3}{2}pL_m\left(\mathrm{i}_{sq}i_{rd} - i_{sd}i_{rq}\right) \tag{5.21}$$

$$T_e = \frac{3}{2}p\frac{L_m}{G}\left(\Psi_{sq}\Psi_{rd} - \Psi_{sd}\Psi_{rq}\right) \tag{5.22}$$

And the relation between mechanical torque (T_m) and electrical torque (T_e) for a one mass model neglecting mechanical losses is:

$$T_e - T_m = J\frac{d\Omega_r}{dt} \tag{5.23}$$

Where, J is the inertia of the machine.

In the next figure (Fig. 5.4) the Simulink model based on (5.13), (5.19) and (5.22) is shown

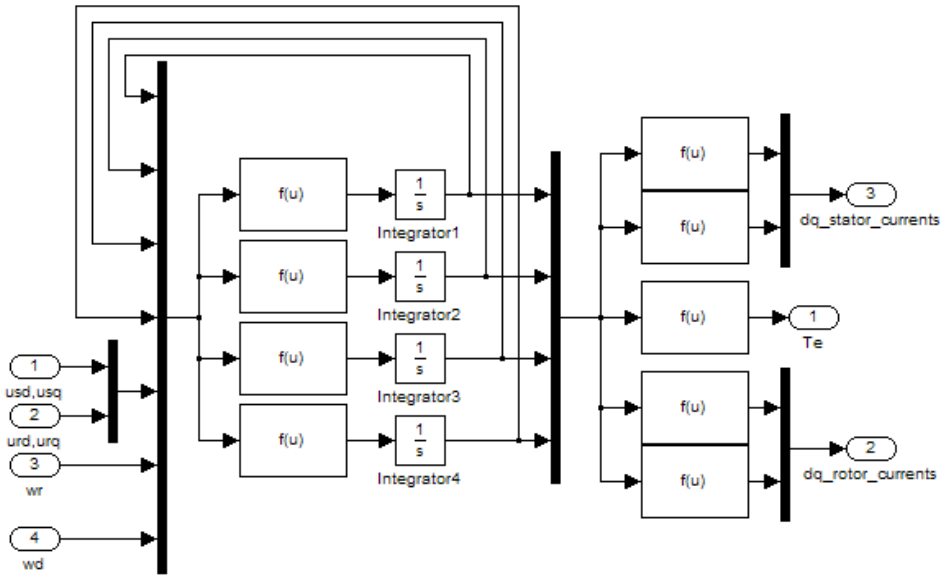

Fig. 5.4 Simulink Implementation of the Dynamic model for the Induction Machine

5.2.2 Steady-State model

In the Steady State model the electric transients are neglecting [23] meaning that $\frac{\mathrm{d}}{\mathrm{dt}}[\Psi] = 0$ obtaining from equation (3.6):

$$[V] = [R][I] + [\Omega][\mathrm{L}][I] \tag{5.24}$$

In order to avoid computational problems due to algebraic loops currents should be written depending only on voltages. Equation (5.24) should be written as:

$$[I] = \left[[R] + [\Omega][\mathrm{L}]\right]^{-1}[V] \tag{5.25}$$

Where

$$[A]^{-1} = \left[[R] + [\Omega][\mathrm{L}]\right]^{-1} \tag{5.26}$$

$$[A]^{-1} = \begin{bmatrix} -R_s & \omega_d L_s & 0 & \omega_d L_m \\ -\omega_d L_s & -R_s & -\omega_d L_m & 0 \\ 0 & \omega_{da} L_m & -R_r & \omega_{da} L_r \\ -\omega_{da} L_m & 0 & -\omega_{da} L_r & -R_r \end{bmatrix}^{-1} = \frac{1}{|A|} \begin{bmatrix} b_{11} & b_{12} & b_{13} & b_{14} \\ b_{21} & b_{22} & b_{23} & b_{24} \\ b_{31} & b_{32} & b_{33} & b_{34} \\ b_{41} & b_{42} & b_{43} & b_{44} \end{bmatrix} \tag{5.27}$$

The terms of the inverse matrix $[\mathrm{A}]^{-1}$ are:

$$b_{11} = b_{22} = -(R_s R_r^2 + R_s(\omega_{da} L_r)^2 + \omega_d \omega_{da} L_m^2 R_r) \tag{5.28}$$

$$b_{12} = -b_{21} = -\omega_d \left(L_s R_r^2 + \omega_{da}^2 L_r (L_s L_r - L_m^2)\right) \tag{5.29}$$

$$b_{13} = b_{24} = \omega_d L_m (\omega_d L_s R_r + \omega_{da} L_r R_s) \tag{5.30}$$

$$b_{14} = -b_{23} = -\omega_d L_m \left(R_s R_r - \omega_d \omega_{da} (L_s L_r - L_m^2)\right) \tag{5.31}$$

$$b_{31} = b_{42} = \omega_{da} L_m (\omega_d L_s R_r + \omega_{da} L_r R_s) \tag{5.32}$$

$$b_{32} = -b_{41} = -\omega_{da} L_m \left(R_s R_r - \omega_d \omega_{da} (L_s L_r - L_m^2)\right) \tag{5.33}$$

$$b_{33} = b_{44} = -R_r R_s^2 + R_r(\omega_d L_s)^2 + \omega_d \omega_{da} L_m^2 R_s \tag{5.34}$$

$$b_{34} = -b_{43} = -\omega_{da} \left(L_r R_s^2 + \omega_d^2 L_s (L_s L_r - L_m^2)\right) \tag{5.35}$$

$$|A| = (R_s R_r + \omega_d \omega_{da} L_m^2)^2 + \omega_{da}^2 L_r^2 (\omega_d^2 L_s^2 + R_s^2) + \omega_d^2 L_s (R_r^2 L_s - 2\omega_{da}^2 L_r L_m^2) \tag{5.36}$$

The Steady State Simulink model of the Induction Machine, in dq-arbitrary reference frame, is based on (5.25) and minus (5.21) as shown in figure Fig. 5.5

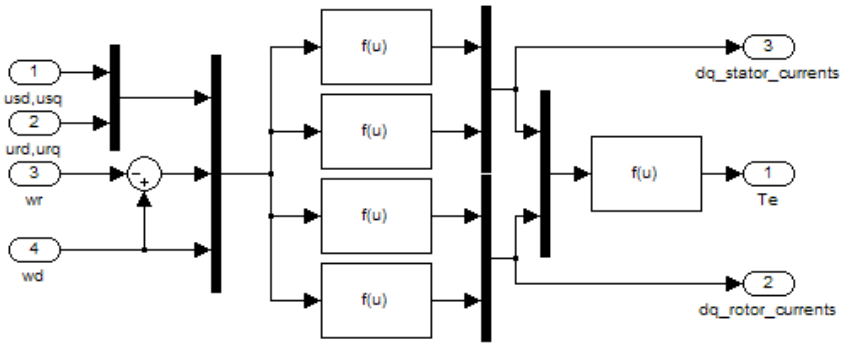

Fig. 5.5 Simulink Implementation of the Steady State model for the Induction Machine

In the next figures the comparison between the dynamic and the steady state models, when a change in the torque is applied, are shown.

In Fig. 5.6 it can be observed the step change in the torque from -40 to -50 (N*m^2) for both steady state and dynamic models.

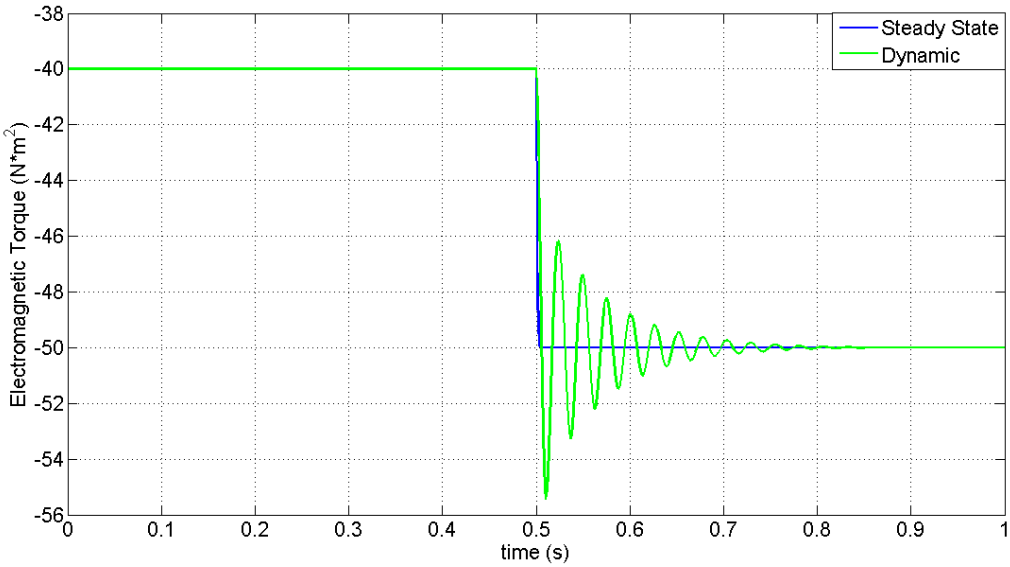

Fig. 5.6 Step change in the Electromagnetic Torque in Steady State and Dynamic models of an IM

In the next figures it can be seen how this torque step-change affects in the mechanical speed (Fig. 5.7) and in the dq-stator currents (Fig. 5.8, Fig. 5.9).

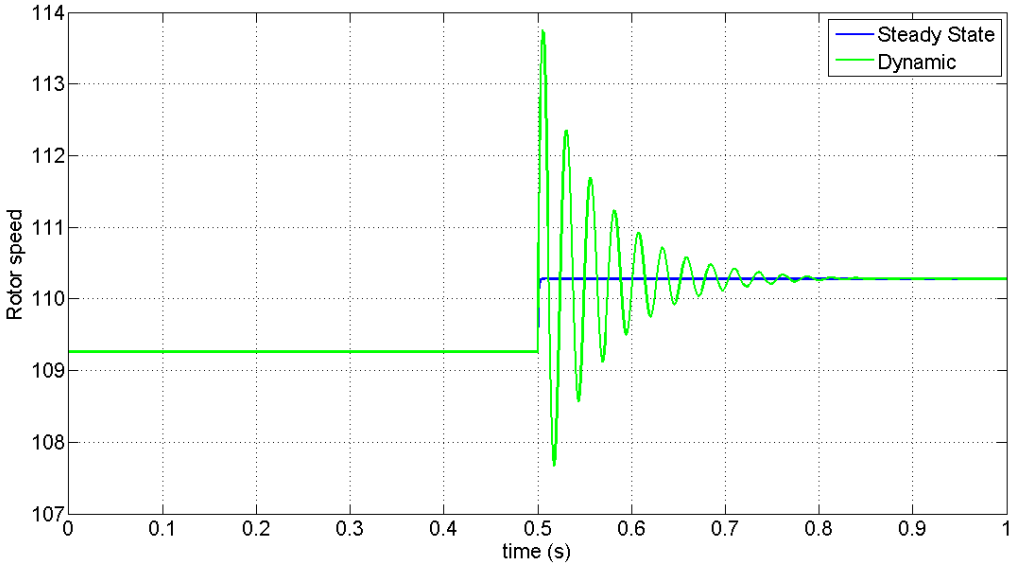

Fig. 5.7 Speed during step change in the Electromagnetic Torque in Steady State and Dynamic models of a IM

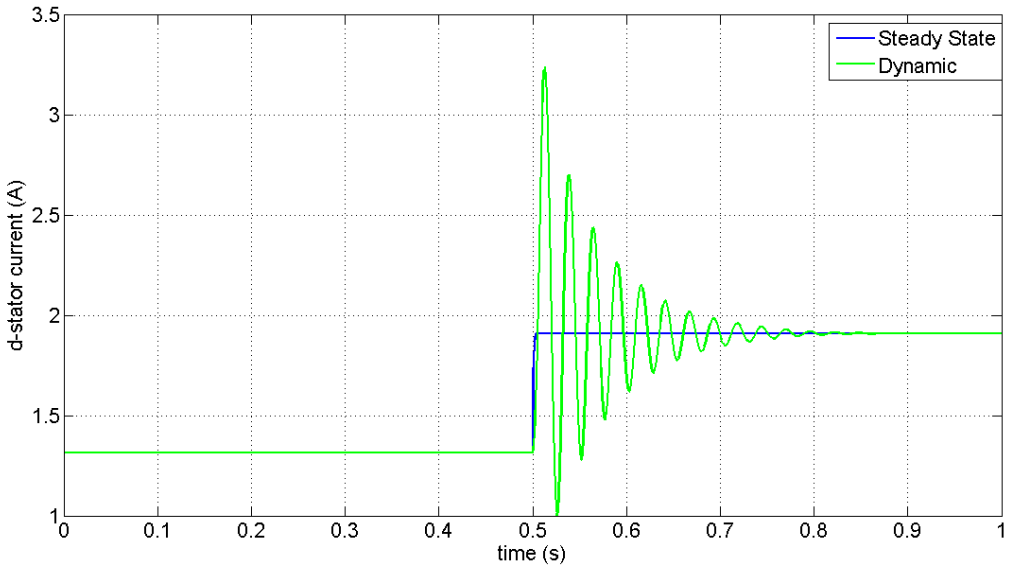

Fig. 5.8 d-stator current during step change in the Electromagnetic Torque in Steady State and Dynamic models of a IM

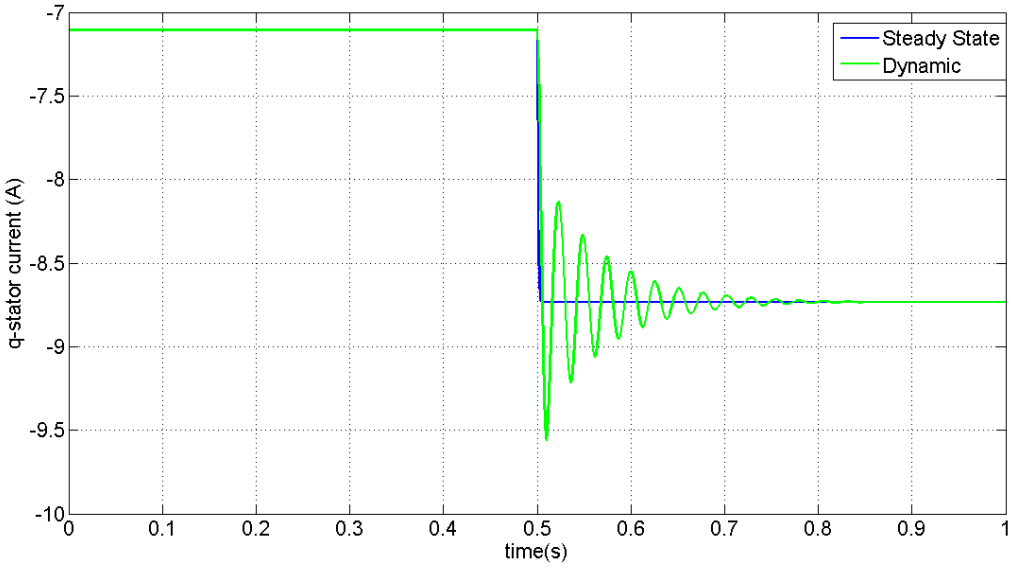

Fig. 5.9 q-stator current during step change in the Electromagnetic Torque in Steady State and Dynamic models of a IM

It can be observed in the previous figures that the difference between the dynamic model and the steady state model is only when the change in the torque occurs; The dynamic model present an oscillation at this moment due to the electric transients while the steady state model does not.

5.3 DFIG rotor-side converter control

The control strategy chosen for the rotor-side converter is Direct Power Control (DPC). This control strategy employs mathematical reference frame transformations (Clarke and Park) in order to simplify the electrical equations – time and position dependences are removed.

In Fig. 5.10 a schematic block diagram for a rotor-side DPC can be seen.

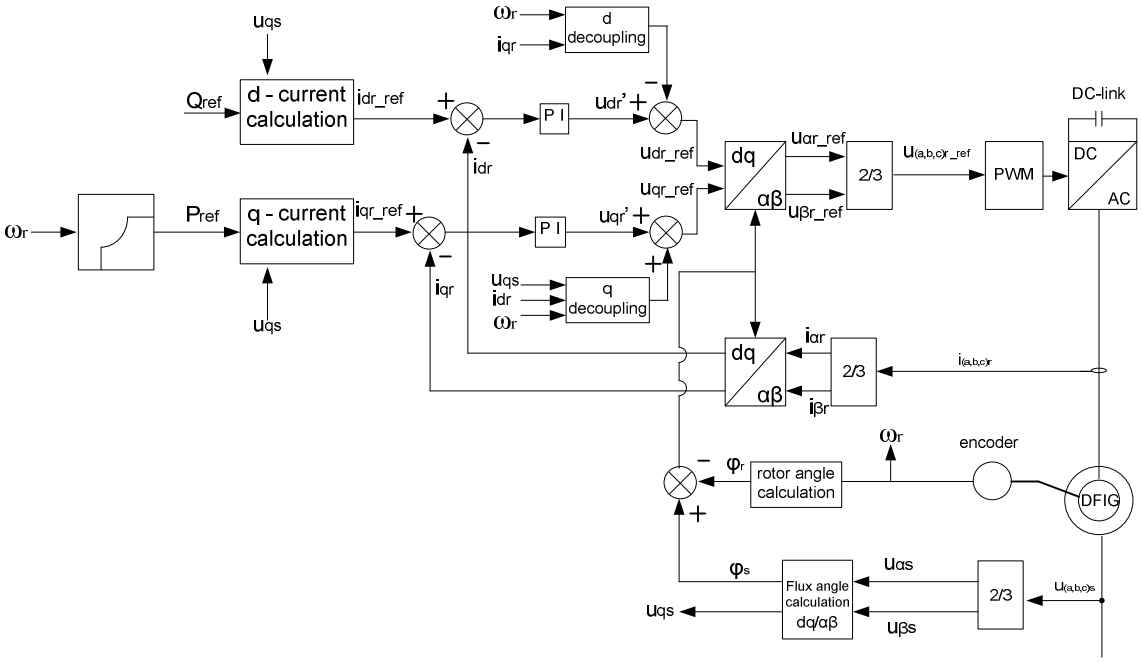

Fig. 5.10 Block diagram for the rotor side DPC.

By controlling the current in the rotor side of the DFIG, active and reactive power of the wind turbine can be controlled. A vector-control approach is used, orientating the d-axis along the stator-flux vector position. In this way the current, voltage and flux of the stator and rotor become DC values that are easily to control, and also a decoupled control of the active and reactive power is obtained.[9][50][51]

Aligning the d-axis of the reference frame through the stator flux space vector, the q component of the stator flux is zero (Ψs=Ψqs=0). As it can be seen in the Fig. 5.11 the voltage and the flux are moving in quadrature, so the d axes of the stator voltage us=uds=0.[52]

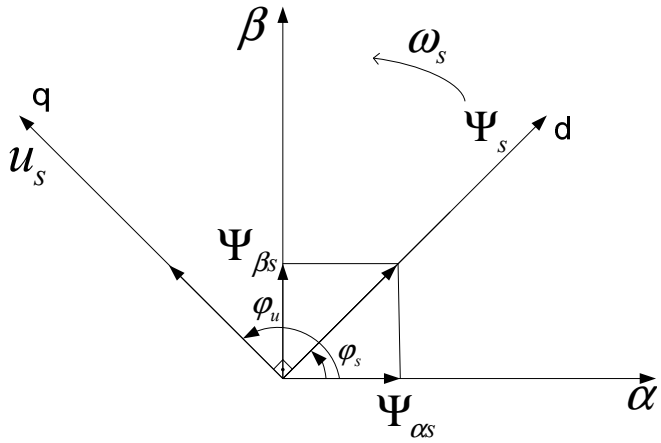

Fig. 5.11 Vector diagram of the dq reference frame aligned to the stator flux, with stator voltage in quadrature

Feedback of the rotor currents and stator voltages is necessary. Furthermore, to measure rotor angular position, a sensor is employed. From this measurement rotor angular speed is derived. Typically stator angular speed is obtained from a PLL system.

5.4 DFIG model structure

DFIG simulation system is made up of three different subsystems. The first one models the behaviour of the WRIG controlled with DPC strategy by the rotor-side converter. The second one models the behaviour of the WF network-side converter controlled by VOC strategy taking into account the whole losses in the converter. Finally, the third one models the three-phase three winding transformer.

As stated in previous chapter, since in this project the WF is considered always in steady-state with a perfect track of the reference values by the control system, the reference signals represent directly steady-states in the machine models.

As well, a perfect estimation of stator angular speed is assumed –so there is no need to include PLL systems in the WF models.

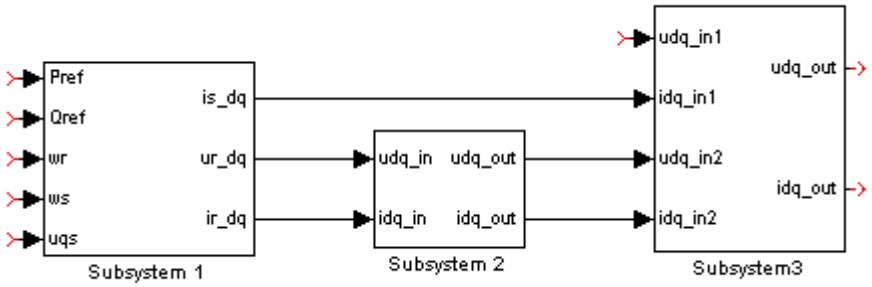

Fig. 5.12 Block diagram of the DFIG WT model

In next section the modelling of the first subsystem is presented.

For the second subsystem the performance of the WF network-side converter controlled with VOC strategy is modelled as explained previously in Chapter 3. Next equations summarize its modelling:

$$\begin{aligned} P_{out} &= \mu P_{in} \\ v_{qout} i_{qout} &= \mu v_{qin} i_{qin} \\ Q_{out} &= 0 \Rightarrow i_{dout} = 0 \end{aligned} \tag{5.37}$$

As first approach the whole losses in the back-to-back converter are just modelled by a static factor of $\mu = 0.95$ included in this second subsystem.

On the other hand, the model of the transformer is included in Chapter 8. If no losses in the transformer are considered in first approach next simple equations can be employed in steady-state simulation:

$$\begin{aligned} \frac{v_{out}}{N_{out}} &= \frac{v_1}{N_1} = \frac{v_2}{N_2} \\ i_{out} N_{out} &= i_1 N_1 + i_2 N_2 \end{aligned} \tag{5.38}$$

5.4.1 Steady-state model of WRIG controlled with DPC strategy by rotor-side converter

Based on a simplified steady-state DPC strategy and the steady state WRIG equations, the core of the DFIG WT model implemented in MATLAB/SIMULINK is developed.

The already presented equations for the WRIG are modified according to the characteristics of the DPC (Ψqs=0 and uds=0). The outputs of the system are currents in the stator (i_{sd} and i_{sq}) and currents and voltages in the rotor (i_{rd} and i_{rq}, v_{rd} and v_{rq}). The inputs of the system, as it can be seen in Fig. 5.12, are the active (Pref) and reactive (Qref) stator power references, the electrical rotor speed (ωr) and the stator voltage (usq) and frequency (ωs). Qref is considered always zero (unity power factor condition). Therefore, the model equations are the next:

$$i_{sq} = \frac{2}{3}\frac{P_{s\_ref}}{u_{sq}} \tag{5.39}$$

$$i_{sd} = \frac{2}{3}\frac{Q_{s\_ref}}{u_{sq}} \tag{5.40}$$

$$i_{rq} = -\frac{L_s}{L_m} i_{sq} \tag{5.41}$$

$$i_{rd} = \frac{u_{sq} - R_s i_{sq}}{\omega_s} - \frac{L_s}{L_m} i_{sd} \tag{5.42}$$

$$u_{rd} = R_r i_{rd} - (\omega_s - \omega_r)\left(L_r i_{rq} + L_m i_{sq}\right) \tag{5.43}$$

$$u_{rq} = R_r i_{rq} + (\omega_s - \omega_r)(L_r i_{rd} + L_m i_{sd}) \tag{5.44}$$

These equations allow modeling of the WRIG controlled with DPC by the rotor-side converter as a unique system.

5.5 SUMMARY

The following main goals were reached in this chapter:

- Development of a mathematical model of the IM.
- Fundamentals of generator model structure.
- Presentation of a control strategy for rotor-side converter.
- Development of a steady-state model for DFIG WT.

It should be stressed that the employment of reference frame transformations allows great simplification on system equations, since the values of parameters are non-dependent on the rotor rotating angle. Thanks to that, sinusoidal signals can be treated as constant signals by the control system.

In the DFIG WT, as first approach, the whole losses in the back-to-back converter are just modeled by a static factor of $\mu = 0.95$ and a lossless transformer is considered

Chapter 6 RCC-IG WT FOR VSC-HVDC WF

ABSTRACT

In this chapter the RCC-IG WT is presented. As the DFIG the RCC-IG mathematical model is also based on a general IM. Firstly, the steady-state model of the RCC-IG is presented. Then the torque-slip characteristic is studied based on equivalent circuits. The derived equations from previous study together with the aerodynamic power conversion equations are the core of a developed program which calculates the RCC-IG reference signals for any simulation conditions.

6.1 Introduction

The machine proposed for the WF in this topology is a wound rotor induction generator (WRIG) with external variable rotor resistors.

The effect of changing rotor resistance on the rotor terminals is obtained controlling the rotor current through the external resistors. In Vestas this is called Vestas Rotor Current Control (VRCC) and is made up of the external rotor resistors, a diode-bridge, an IGBT semiconductor switch, current sensors and a microprocessor controller. To avoid ring brushes all the hardware rotates together with the rotor - communication and control signals are sent through an optical link. Vestas called this generator principle OptiSlip® [9][18][19].

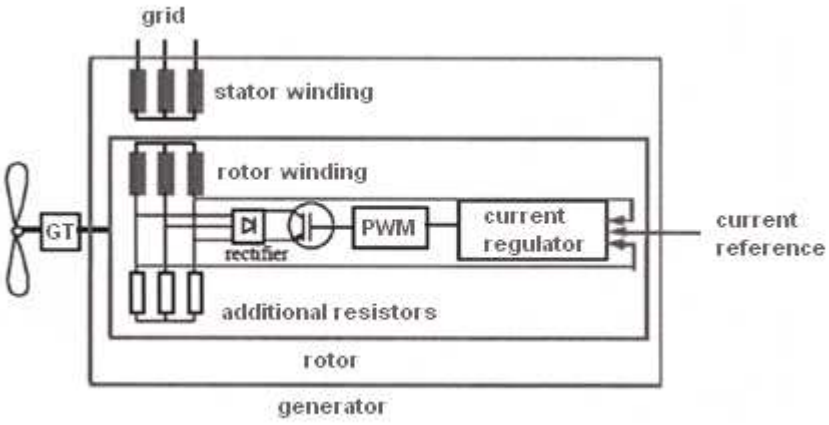

Fig. 6.1 OptiSlip® VRCC.

The virtual variation of the rotor resistance results in a group of torque-speed characteristic (Fig. 6.2). This is so called dynamic slip control and VESTAS has achieved a speed range up to 10% applying this technology in so called VRCC.

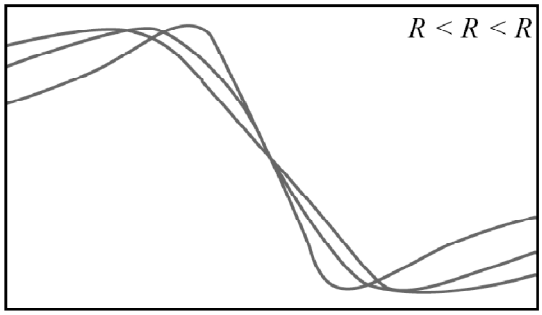

Fig. 6.2 Torque and speed characteristics of DSC WRIG system [5].

By now, the RCC-IG configuration only has been employed (mainly) to avoid output power pulsations due to strong wind gusts in WT directly connected to the grid, improving quality of delivered power in comparison with fixed speed systems.

However, in HVDC-WFs the rotor resistance variation could be employed to achieve certain range of speed variation in order to improve the aerodynamic conversion of each WT. This range of speed variation is improved further if the WF network voltage and frequency are controlled depending on the average incoming wind of the WF turbines.

Next figure Fig. 6.3 shows the configuration of the RCC-IG with WF Vf-control:

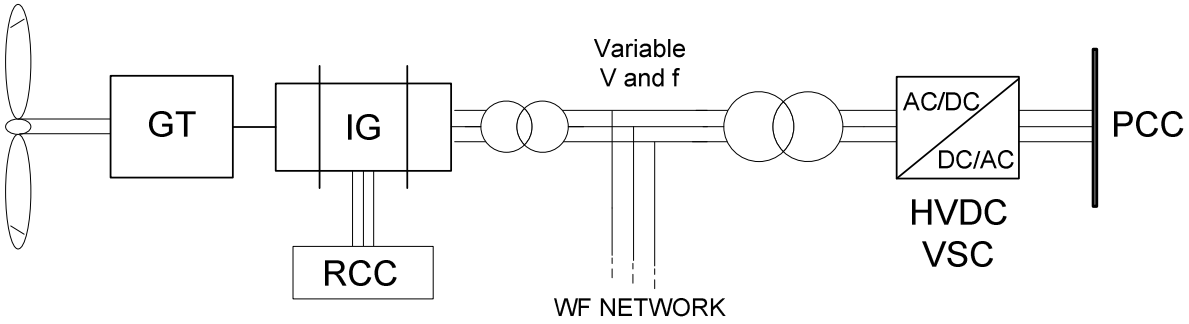

Fig. 6.3 RCC-IG WT in Vf-controlled WF

6.2 IM general model in dq-arbitrary reference frame

The Induction Machine (IM) ABC/abc model is well known and described in [1][9][23]. In chapter 5 the dynamic and the steady-state models in dq-arbitrary reference frame are already described.

For the RCC-IG these equations referred to synchronous reference frame ($\omega_d = \omega_s$, $\omega_{da} = \omega_s - \omega_r$) are used. Aligning the d-axis of the reference frame through the stator flux space vector, since the flux and voltage of the stator are in quadrature, the q component of the stator flux is zero (Ψs=Ψsq=0) as well as the d-axes of the stator voltage (us=usq=0).

Mathematical equations for modeling the RCC-IG are the same as for an IG configuration but considering that the resistance in the rotor of the generator can be changed ($R_r = R_{cc} + R_{r0}$).

Next equations are obtained for the steady-state model:

$$i_{sq} = \frac{2P_s}{3u_{sq}} \tag{6.1}$$

$$i_{rd} = \frac{-(\omega_s - \omega_r)(L_r L_s - L_m^2) i_{sq}}{R_{r0} + R_{cc}} \tag{6.2}$$

$$i_{sd} = \frac{u_{sq} - R_s i_{sq}}{\omega_s L_s} - \frac{L_m}{L_s} i_{rd} \tag{6.3}$$

$$i_{rq} = -\frac{L_s}{L_m} i_{sq} \tag{6.4}$$

These four equations define the model of the generator.

Fig. 6.4 represents the simulink steady-state model of the RCC-IG.

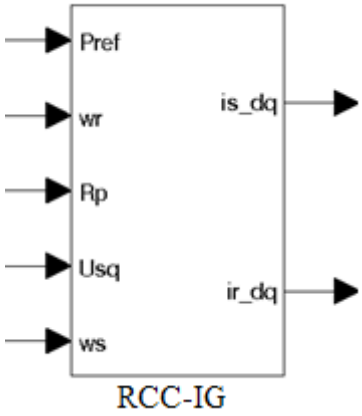

Fig. 6.4 Simulink model of the RCC-IG

The variable inputs of this model are stator active power (Pref), rotor angular speed (ωr), rotor resistance (Rr), stator voltage (Usd=0, Usq) and stator angular speed (ωs).

6.3 Torque-slip characteristic of RCC-IG [54]

A large amount of authors derive in literature the next equivalent circuit of the IM.

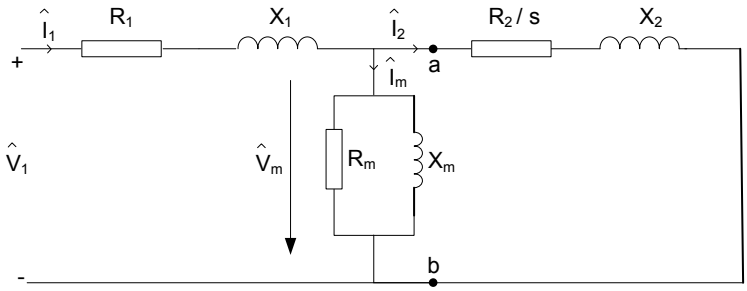

Fig. 6.5 Single-phase equivalent circuit of IM.

Analysis of the IM equivalent circuit is simplified by omitting the core-loss resistance. By applying the Thevenin's network theorem on this circuit, important simplifications for the study the torque-slip characteristic are achieved. The next equivalent circuit is obtained transforming the network to the left of a-b using Thevenin's theorem.

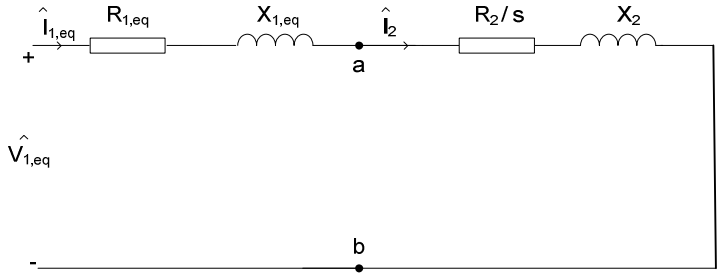

Fig. 6.6 Single-phase equivalent circuit of IM simplified according Thevenin's theorem.

Following Thevenin's theorem, an equivalent voltage source $\hat{V}_{1,eq}$ in series with an equivalent impedance $\hat{Z}_{1,eq}$ are calculated with next equations:

$$\hat{V}_{1,eq} = \hat{V}_1 \left(\frac{jX_m}{R_1 + j(X_1 + X_m)} \right) \tag{6.5}$$

$$Z_{1,eq} = \frac{jX_m(R_1 + jX_1)}{R_1 + j(X_1 + X_m)} \tag{6.6}$$

And the equivalent rotor current according Thevenin's equivalent circuit is:

$$\hat{I}_2 = \frac{\hat{V}_{1,eq}}{\hat{Z}_{1,eq} + jX_2' + R_2/s} \tag{6.7}$$

Then, from the single-phase equivalent circuit of IM, it can be stated that the total power transferred through the air gap to the stator is:

$$P_{gap} = P_s = n_{ph} I_2^2 (R_2/s) \tag{6.8}$$

Where n_{ph} represents the number of phases.

The total rotor copper losses are:

$$P_{r,loss} = n_{ph} I_2^2 R_2 \tag{6.9}$$

Now the power balance equation can be written as:

$$P_m = P_{gap} - P_{r,loss} = n_{ph} I_2^2 R_2 \left(\frac{1-s}{s}\right) = (1-s) P_{gap} \tag{6.10}$$

Therefore, from the torque expression:

$$T_m = \frac{P_m}{\Omega_m} = \frac{P_{gap}}{\omega_s / p} = \frac{p}{\omega_s} \left[\frac{n_{ph} \hat{V}_{1,eq} (R_2/s)}{(R_{1,eq} + (R_2/s))^2 + (X_{1,eq} + X_2)^2} \right] \tag{6.11}$$

Next plot shows the torque-slip characteristic and the equivalent rotor current of the modeled RCC-IG. The maximum and the minimum virtual values of the rotor resistance are used. The program written to plot this curves is included in APPENDIX.

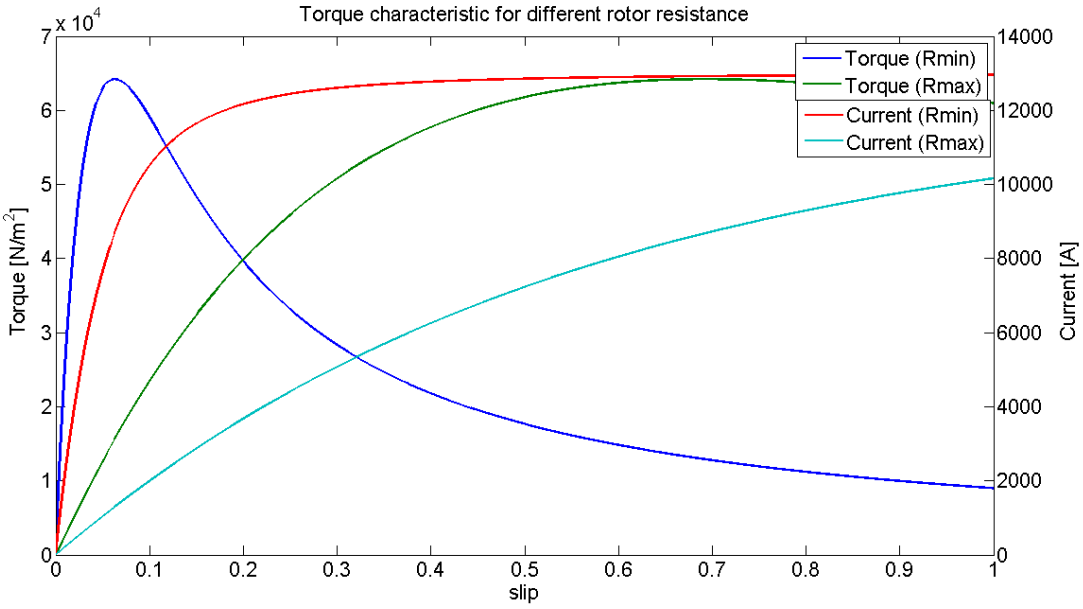

Fig. 6.7 Torque-slip characteristic and rotor equivalent current of RCC-IG for different virtual values of the rotor resistance.

The minimum value of the rotor resistance is equal to the rotor windings resistance. The maximum virtual value has been chosen equal to the rotor resistance which results in rotor copper losses of 5% of total delivered electric power at nominal operation.

Another program, also included in APPENDIX, has been written in MATLAB script in order to estimate this value.

6.4 Reference signals for the rcc-ig

To generate the inputs of the RCC-IG Simulink block model (

Fig. 6.4) a program has been written on MATLAB scrip. The generated code is included in APPENDIX.

The basic structure of the program is shown in following block diagrams.

First the main system is shown (SYSTEM 1). Local wind speed, stator angular speed and stator voltages are the inputs of the system. As outputs the references signals for the RCC-IG model are obtained – rotor angular speed (ωr'), rotor resistance (Rr') and mechanical torque (Tm').

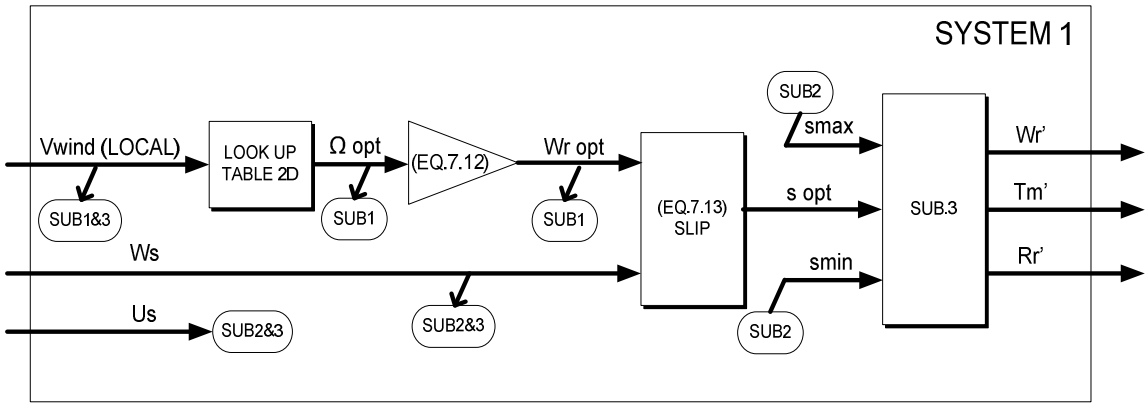

Fig. 6.8 Block diagram of main system.

From the local wind, using a look up table, an optimum mechanical angular speed is calculated (Ωopt). Then using the gear box ratio and the number of pole pairs an optimum rotor angular speed is calculated (ωropt).

$$\omega_{r\,opt} = \Omega_{opt} \cdot G_{box} \cdot p \qquad (6.12)$$

From stator angular speed (ωs) and optimum rotor angular speed (ωropt) the optimum slip is calculated using next equation:

$$s_{opt} = \frac{w_s - w_r}{w_s} \qquad (6.13)$$

The optimum slip of a WT is defined as the slip which results in optimum aerodynamic conversion of this WT under certain operating conditions of the WF.

Next in SUBSYSTEM 2 the limits of the allowable slip variation (smax and smin) are calculated according to maximum and minimum allowable rotor resistance values. Variable inputs of this block are stator voltage (Us), stator angular speed (ωs) and optimum rotor electromagnetic torque (Tropt).

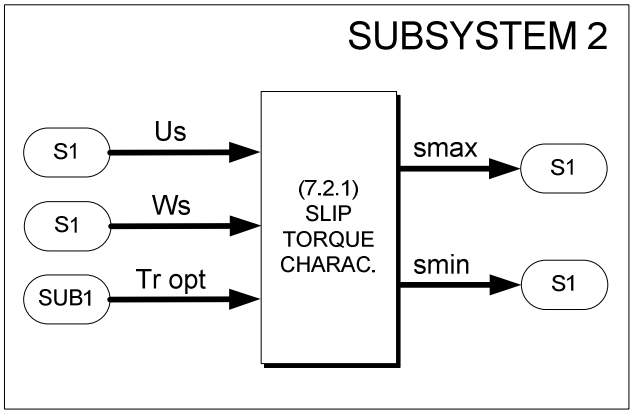

Fig. 6.9 Block diagram of subsystem 2.

Calculations in SUBSYSTEM 2 are based on torque-slip characteristic equations explained in previous section (6.3).

Optimum rotor electromagnetic torque (Tropt) is calculated previously in SUBSYSTEM 1, based on aerodynamic power equations (from Chapter 2) and torque-power equation. Then, if no mechanical losses are considered in the gear train and the generator next equations can be employed.

$$\mathrm{Pwt} = \frac{1}{2}\rho A_v (V_{wind})^3 Cp(\lambda, \theta) \tag{6.14}$$

$$\mathrm{Tr\ opt} \approx \frac{\mathrm{Pwt}}{\Omega_{opt}} = \frac{\mathrm{Pwt} \cdot G_{box} \cdot p}{\omega_{r\ opt}} \tag{6.15}$$

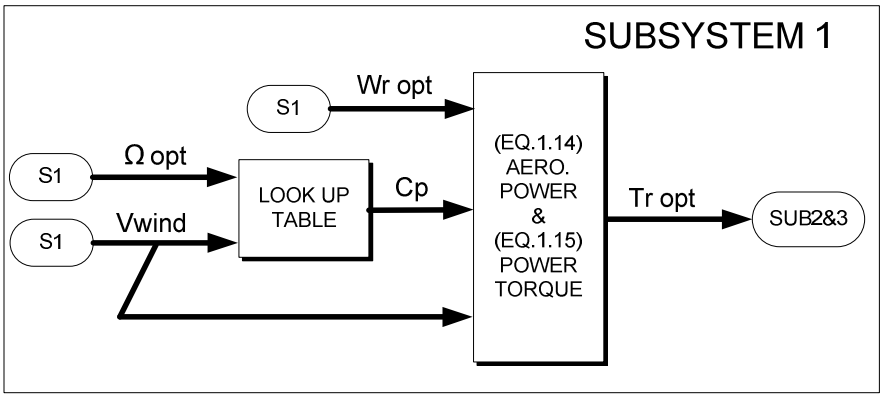

Fig. 6.10 Block diagram of subsystem 1.

Finally in SUBSYSTEM 3 the references signals for the RCC-IG model are obtained – rotor angular speed (ωr'), rotor resistance (Rr') and mechanical torque (Tm').

If the optimum slip (Sopt) satisfies next condition (6.16) the reference values are directly the optimum values (OUT1).

$$S_{min} \leq S_{opt} \leq S_{max} \tag{6.16}$$

It should be noted that Sopt, Smax and Smin are absolute values.

Next simulink plot shows the slip characteristics (Smax, Sopt, Smin) of a RCC-IG WT whose optimum slip is almost always between the upper and lower limits under certain simulation conditions.

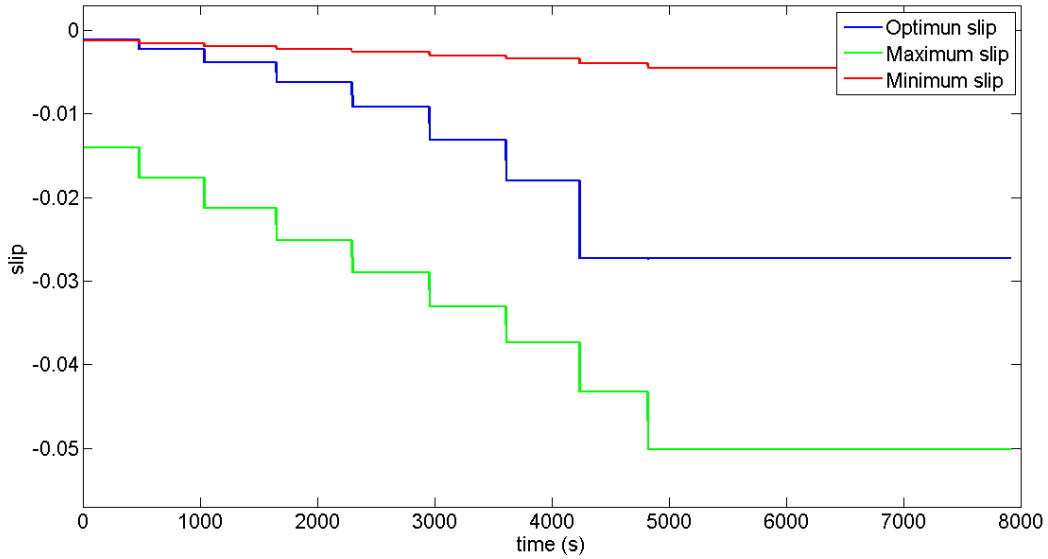

Fig. 6.11Slip characteristics of a RCC-IG WT whose optimum slip is almost always between the upper and lower limits under certain simulation conditions.

If the condition (6.16) is not satisfied a new operating point different from optimum must be found for the generator, since the slip which results in optimum aerodynamic conversion of the WT cannot be achieved.

If $S_{opt} < S_{min}$ the rotor resistance value is set to minimum rotor resistance and if $S_{opt} > S_{max}$ the rotor resistance value is set to maximum virtual rotor resistance.

Then a non-linear system of equations must be solved in order to find the new operating point and therefore the new reference values (OUT2).

The non-linear system of equations is made up of the torque-slip characteristic equations (from section 6.3) and the aeromechanical torque equations (from section 2.1).

The programs written in MATLAB script to solve these non-linear systems of equations are included in APPENDIX.

Next simulink plots show the slip characteristics (Smax, Sopt, Smin) of a RCC-IG WT whose optimum slips are during certain time outside of the optimum range under certain simulation conditions.

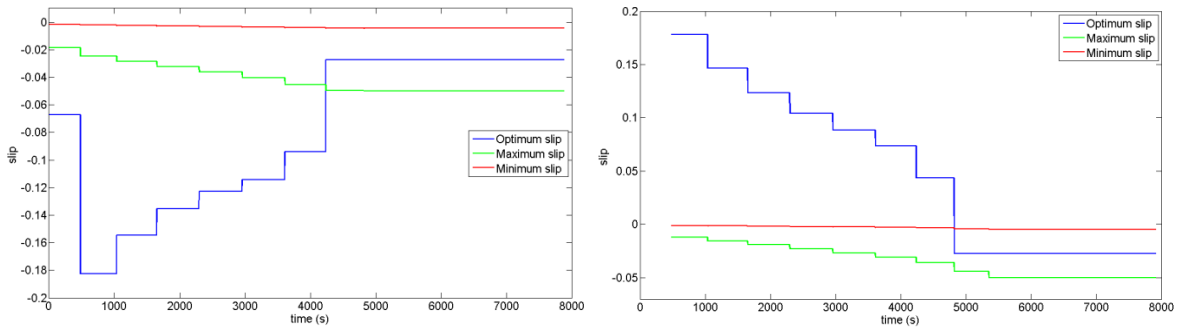

Fig. 6.12 Slip characteristics of a RCC-IG WT whose optimum slips are during certain time outside of the optimum range under certain simulation conditions.

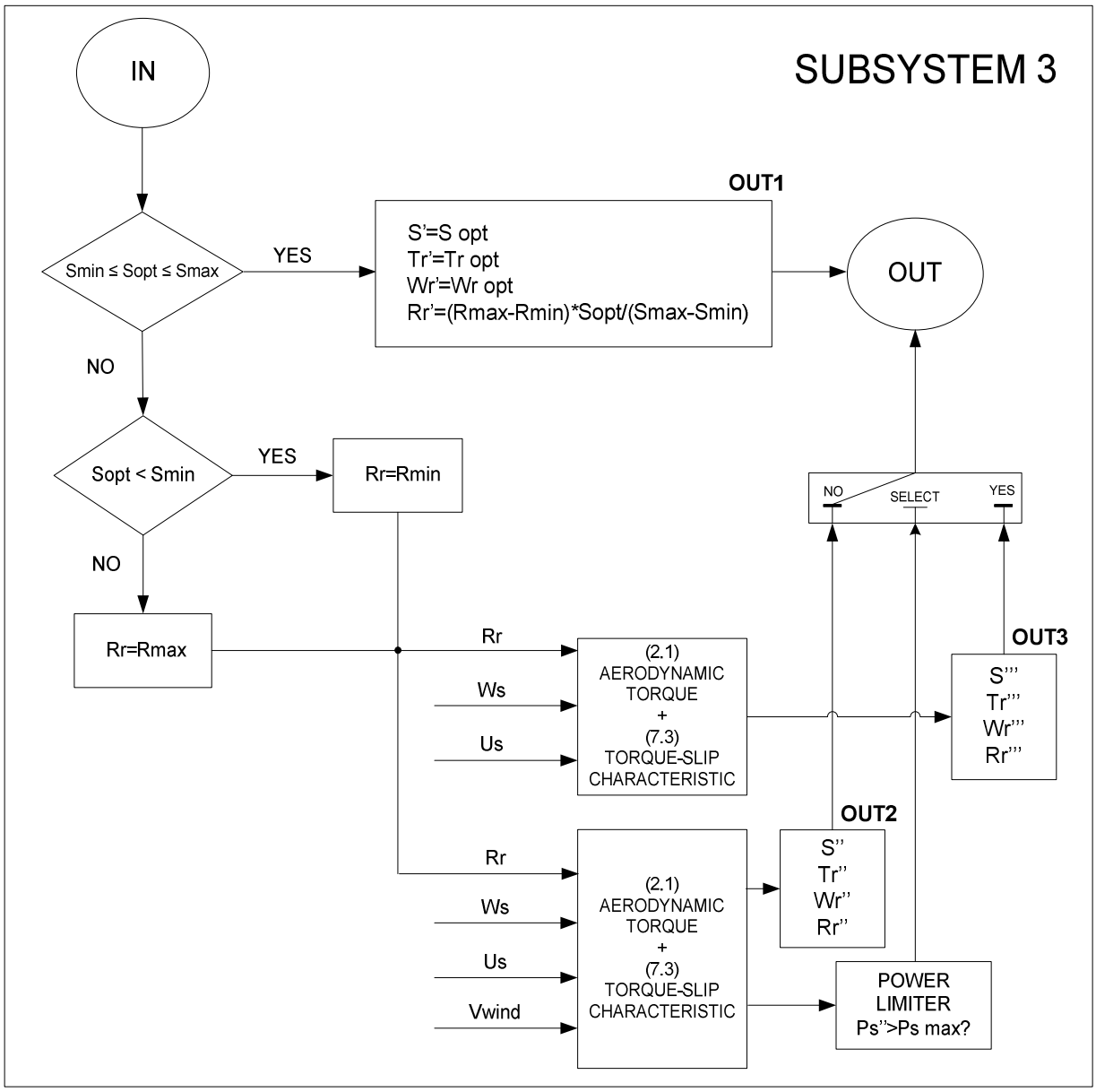

Fig. 6.13 Block diagram of subsystem 3.

If the new generating point defined in OUT2 gives a mechanical input power bigger than the maximum allowable power a limitation block actuates switching a selector block. In this case the new output reference values are defined in OUT3.

Values of OUT3 are estimated solving another non-linear system of equations. This system is made up of the torque-slip characteristic equations (from section 7.2.1) considering maximum mechanical input power.

The program written in MATLAB script to solve this non-linear system of equations is also included in APPENDIX.

6.5 SUMMARY

The next main objectives were reached in this chapter:

- Development of a mathematical model of the RCC-IG.
- Fundamentals of generator model structure.
- Study of the torque-slip characteristics.
- Presentation of a self-developed program to estimate reference signals for the RCC-IG model .
- Development of a steady-state model for RCC-IG WT.

It should be emphasized again that the employment of reference frame transformations allows great simplification on system equations.

Chapter 7 SCIG Vf-control

ABSTRACT

In this chapter a mathematical model of the SCIG WT is developed. A certain variable speed performance is reached through wind farm network Vf control. It should be noted that input reference signals for the SCIG model are generated with already presented equations of the IM torque-slip characteristic and aerodynamic power conversion (Chapter 6).

7.1 Introduction

The induction generator is the most common generator used in wind turbines, several advantages such as robustness, mechanical simplicity and low price makes this kind of generator attractive to the costumers [56]. A large amount of installed wind turbines are fixed speed stall-regulated turbines with Squirrel-Cage Induction Generators (SCIGs), due to its simplicity, high efficiency and low maintenance requirements.

By using a DC connection to this kind of wind farm, variable speed operation can be achieved. The voltage and frequency of the WF-network can be modified in the WF-side HVDC-converter, producing a variation in the operating speed of the SCIG generator.

7.2 SCIG model and control

Next figure Fig. 6.3 shows how the configuration of the IM Vf-control is:

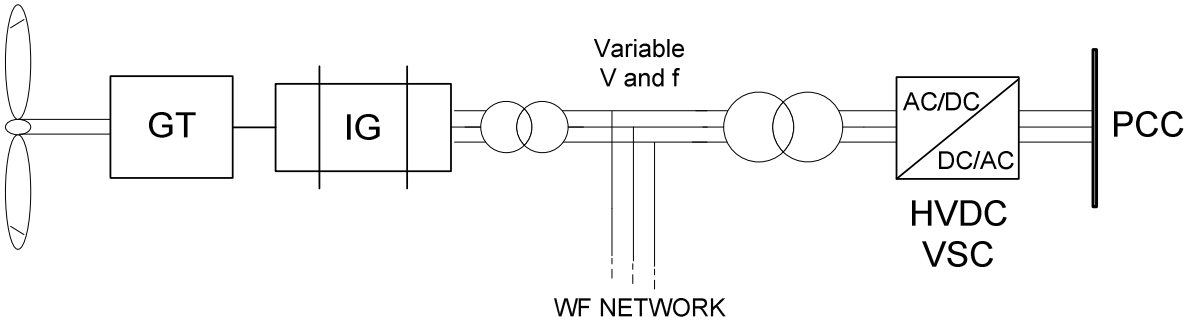

Fig. 7.1 IM Vf-control WF configuration

In this configuration a Squirrel-Cage Induction Generator (SCIG) is used. For modeling this machine equations describe in chapter 5 are used referred to the synchronous reference frame ($\omega_d = \omega_s$, $\omega_{da} = \omega_s - \omega_r$). Voltages in the rotor are equal to zero , also by aligning the d-axis of the reference frame through the stator flux space vector, the q component of the stator flux is zero (Ψs=Ψsq=0) and the d axes of the stator voltage us=usq=0, because off the flux and voltage of the stator are in quadrature:

Next equations are obtained for a steady-state model:

$$i_{sq} = \frac{2P_s}{3u_{sq}} \tag{7.1}$$

$$i_{rd} = \frac{-(\omega_s - \omega_r)(L_r L_s - L_m^2) i_{sq}}{R_r} \tag{7.2}$$

$$i_{sd} = \frac{u_{sq} - R_s i_{sq}}{\omega_s L_s} - \frac{L_m}{L_s} i_{rd} \tag{7.3}$$

$$i_{rq} = -\frac{L_s}{L_m} i_{sq} \tag{7.4}$$

These four equations are used to define the model of the generator.

Fig. 6.4 represents the simulink steady-state model of the SCIG.

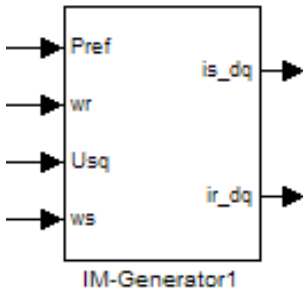

Fig. 7.2 Simulink model of the IM

This WF-configuration is controlled to have variable speed wind turbines, but this control is done by a general Vf-control (chapter) in the WF-side HVDC-converter. All the turbines will have a variable stator voltage and frequency, although it will be the same for all of them, set by the average incoming wind speed of the WF turbines; this make that some turbines do not work exactly at the MPP, set by the Vf-control.

7.3 Summary

The following main goals were reached in this chapter:

- Development of a mathematical model of the SCIG.
- Fundamentals of generator model structure.
- Development of a steady-state model for SCIG WT.

Once again it should be stressed that the employment of reference frame transformations allows great simplification on system equations.

Chapter 8 Wind farm models

ABSTRACT

In followings the aggregated WF models implemented in Matlab/Simulink are briefly presented. Next, models of the AC transmission line and the transformers in dq-reference frame are presented. The AC transmission line models are derived for dynamic and steady-state, while ideal and real models of the transformers in steady-state are described.

8.1 Aggregated Wind farm models

The overall dynamic performance of a WF can be described by detailed models of each WT receiving certain incoming wind and the WF electrical network. But when the number of WTs is very large this detailed approximation presents a high order model, resulting in too low simulation speed (even detailed models could be impossible to simulate).

In this case is possible to simplify the WF model employing aggregated WT models – WTs experiencing identical or similar incoming wind speed can be aggregated into an equivalent WT model (EWTM). In this way an equivalent WF model (EWFM) is obtained based on an equivalent WF electrical network of aggregated WTs [27, 34-37]. This equivalent model of the WF is made up of as many EWTMs as WTs groups experiencing identical or similar winds.

This is a very reasonable approach for off-shore WFs due to the topology of the parks. In off-shore WFs the WTs are distributed in several rows at certain angles according to prevailing wind direction, with a minimum distance between turbines of the same row (3-5 times rotor diameter) and turbines of consecutive rows (5-9 times rotor diameter) [34]. This topology leads to a performance where WTs of the same row experience similar incoming winds, whereas WTs of different rows experience different winds due to park effect (shadowing).

In this thesis a EWFM is used to model the off-shore WFs made up of 100 WTs proposed by VESTAS. The turbines are located in 10 rows with 10 turbines each and fulfill minimum distance requirements. So it can be stated that each row of 10 turbines presents similar incoming winds.

The EWTM size is n-times the size of one single WT, so its rated power is n-times the rated power of one turbine, where n represents the number of WTs of each row (aggregated in the EWTM). Due to the non linear relation between mechanical power (or torque) and wind speed the equivalent incoming wind of a EWTM is not equal to the sum of the incoming winds of each turbine. This equivalent wind is calculated averaging the incoming wind for those n-turbines of a row.

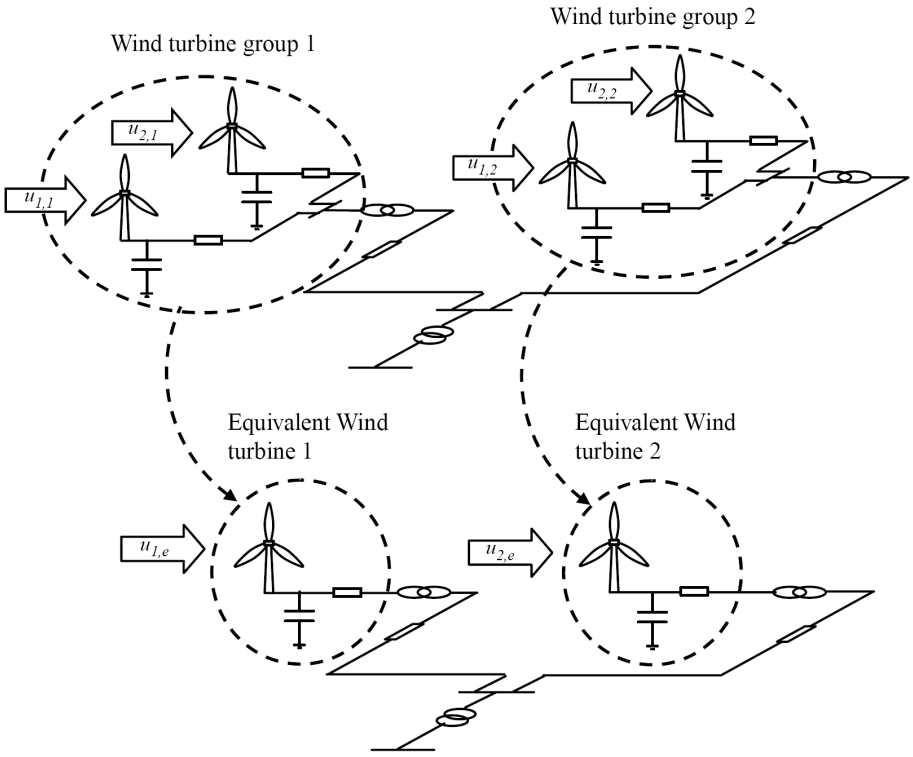

Fig. 8.1 EWFM employing EWTM for aggregated WT with similar winds [34]

This equivalent incoming wind, u_e, is used as input for a WT rotor model equal to that of one individual WT (same rotor diameter and power coefficient). From the mechanical torque of this individual model the torque of the EWTM can be derived as:

$$P_{w,e} = nT_{w,i} \quad (8.1)$$

Where, e subindex corresponds to equivalent WT and i subindex to individual WT.

Then this equivalent aerodynamic torque is used as input for a model of the drive train and the generator system also equal to that of one individual WT - with equal electrical and mechanical parameters per unit. This generator system model must include all the devices related with electrical performance (generator machine, converters, control system, etc). Next the EWTM is connected to an equivalent WF network model (EWFNM).

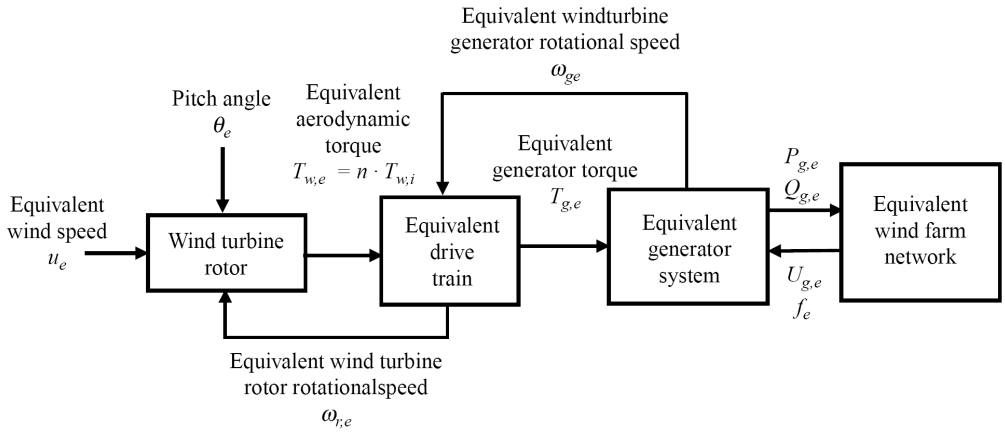

Fig. 8.2 EWTM with equivalent incoming wind connected to EWFNM [34]

8.2 Simulink aggregated Wind Farm Models

Next figures show the implemented simulink WF models, made up of 10 aggregated wind turbines models composed each one of 10 turbines, so a WF of 100 is modeled. From the average annual wind speed, the annual wind speed of each row is obtained. The WF voltage and frequency of the DFIG and full-scale SPMSG WF topologies is set to a constant value (30kV, 50Hz). In the IM and RCC-IG configurations the V/f control, that establishes the voltage and frequency of the wind farm, is set by the calculated average wind speed of all the aggregated WT as explained in chapter 3. Output electrical and mechanical power values are sent to scopes since they are the interest of this project.

8.2.1 Full-scale SPMSG wind farm

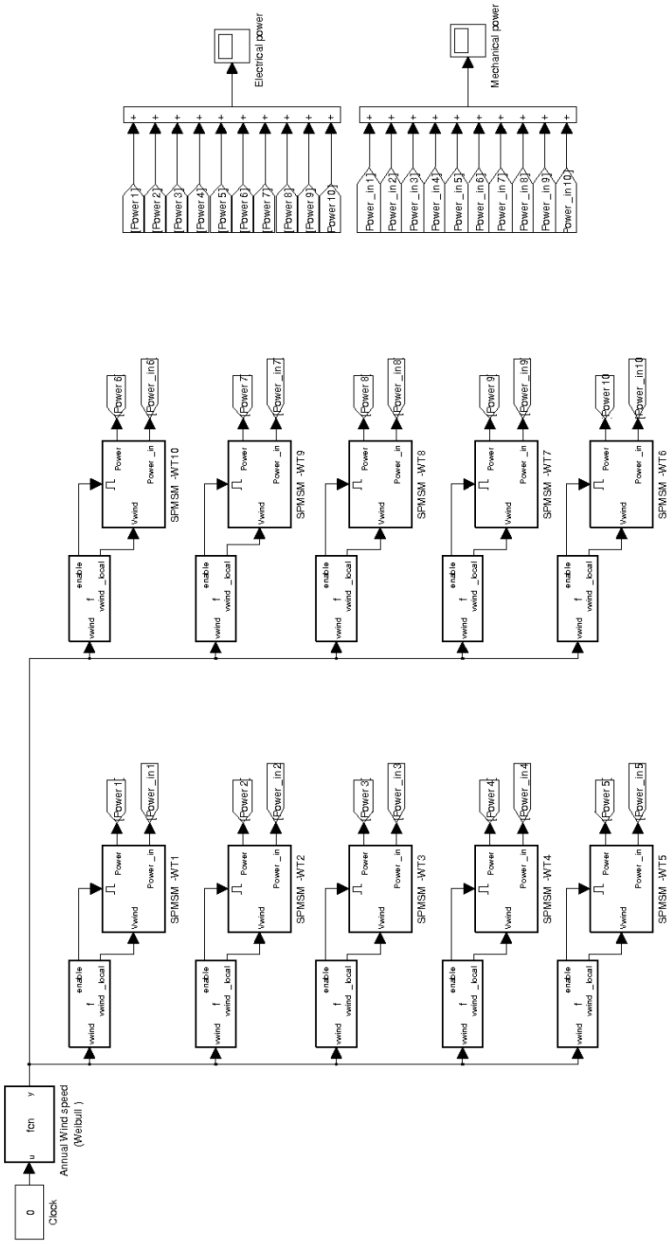

Fig. 8.3 Full-scale SPMSG aggregated WF simulink model

8.2.2 DFIG wind farm

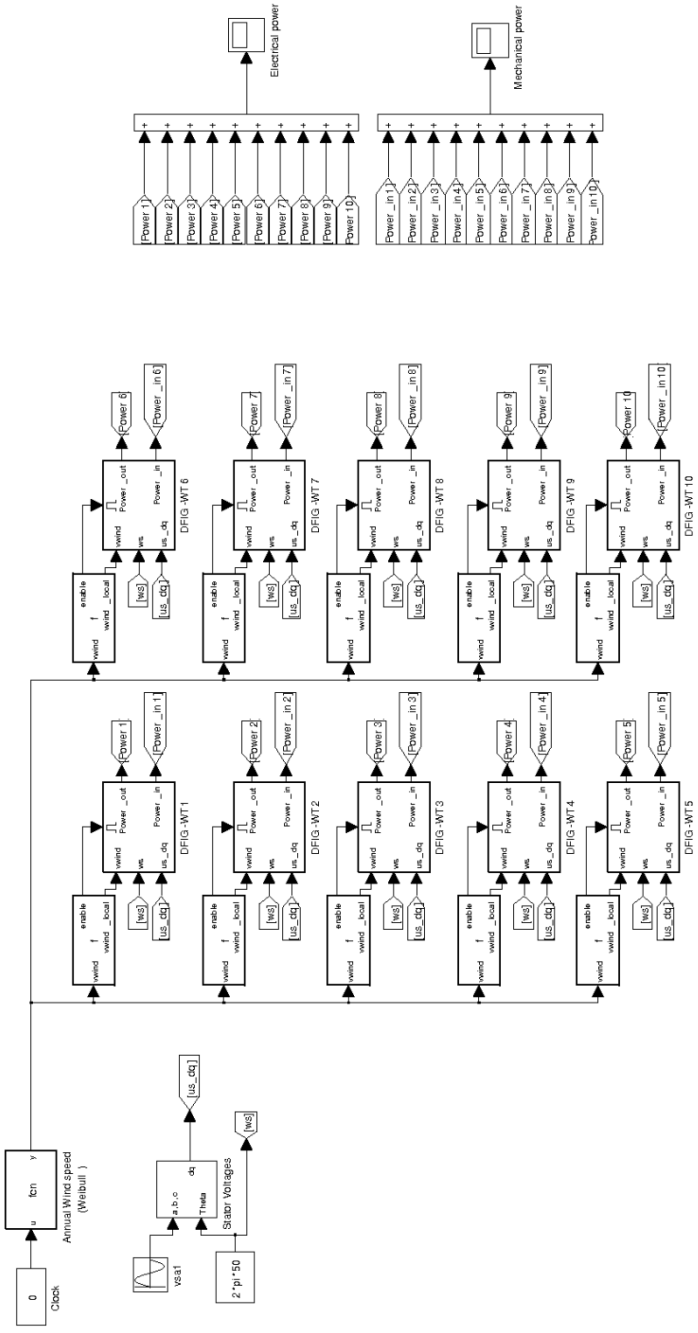

Fig. 8.4 DFIG aggregated WF simulink model

8.2.3 IM wind farm

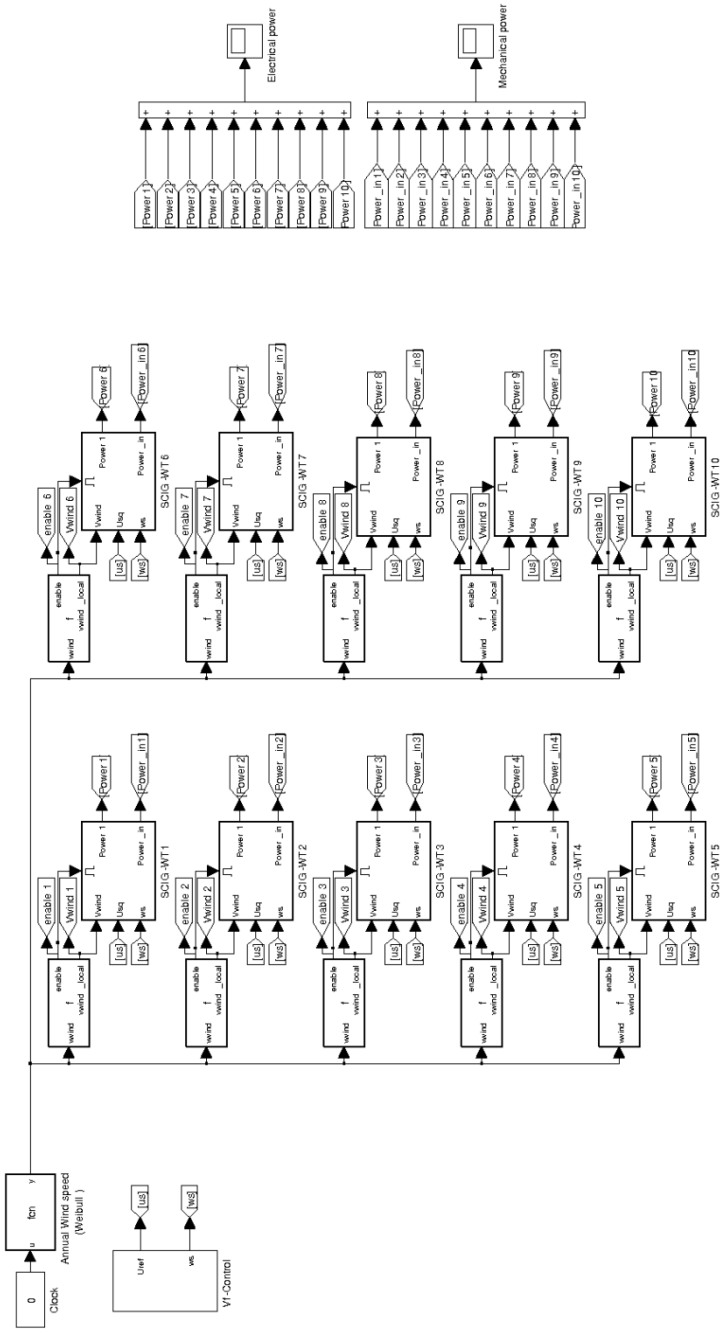

Fig. 8.5 IM aggregated WF simulink model

8.2.4 RCC-IG wind farm

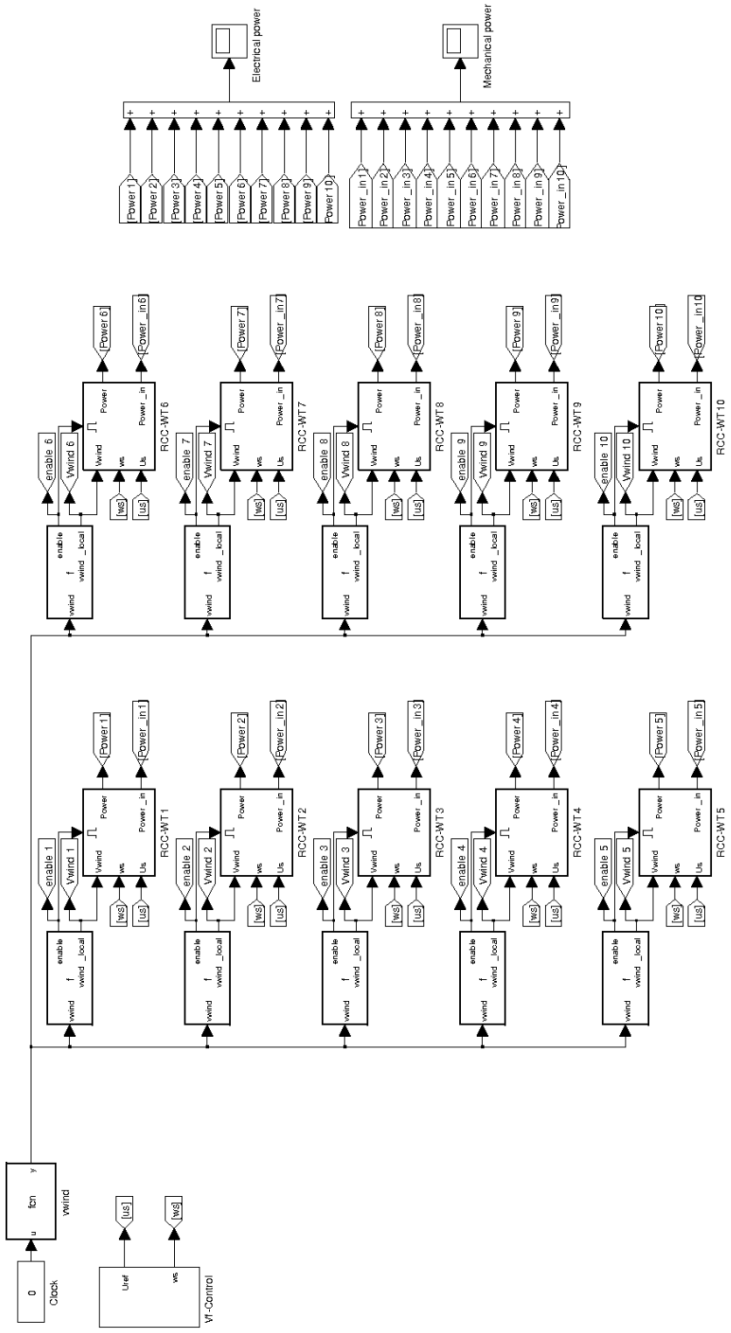

Fig. 8.6 RCC-IG aggregated WF simulink model

8.3 Models of transformers and wf-network

8.3.1 Series RL [24]

In this section the dq-model of a three-phase series RL line is presented. The ground return is not taken into account because the circuit is supposed to be balanced. The derivation of the dq-equations can be obtained considering the inductive and resistive drops of the a-phase equations.

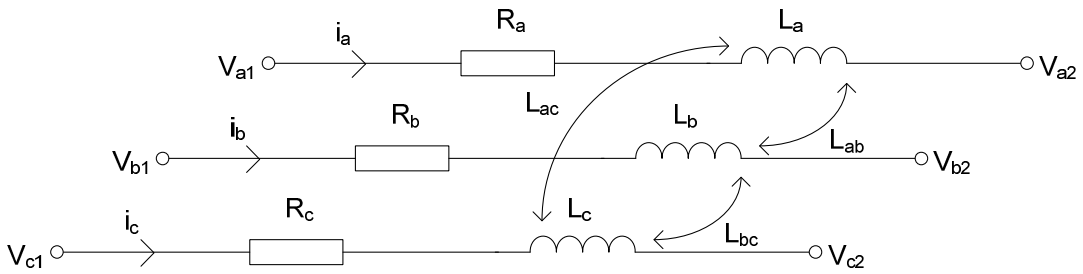

Fig. 8.7 Three-phase RL line

$$v_{a1} = R_a i_a + L_a \frac{di_a}{dt} + L_{ab} \frac{di_b}{dt} + L_{ac} \frac{di_c}{dt} + v_{a2} \tag{8.2}$$

$$[v_{1,abc}] - [v_{2,abc}] = [R][i_{abc}] + \frac{d}{dt}[\mathrm{L}][i_{abc}] \tag{8.3}$$

Where

$$[v_{1,abc}] = \begin{bmatrix} v_{a1} \\ v_{b1} \\ v_{c1} \end{bmatrix} \quad [v_{2,abc}] = \begin{bmatrix} v_{a2} \\ v_{b2} \\ v_{c2} \end{bmatrix} \tag{8.4}$$

And for a uniformly line where Ra=Rb=Rc=Rs, La=Lb=Lc=Ls, and Lab= Lbc= Lca= Lm the resistance [R] and inductance [L] matrices are simplified to:

$$[R] = \begin{bmatrix} R_s & 0 & 0 \\ 0 & R_s & 0 \\ 0 & 0 & R_s \end{bmatrix} \tag{8.5}$$

$$[L] = \frac{1}{G} \begin{bmatrix} L_s & L_m & L_m \\ L_m & L_s & L_m \\ L_m & L_m & L_s \end{bmatrix} \tag{8.6}$$

For the calculation of the dq-equations the resistive and inductive drops of the a-phase are considered. The resistive drop is given by:

$$R_a i_a + R_m(i_b + i_c) \tag{8.7}$$

Knowing that 0=ia+ib+ic and replacing in (8.7), it is obtained:

$$(R_s - R_m)i_a \tag{8.8}$$

And by expressing ia in dq-terms, the resistive drop is:

$$(R_s - R_m)(i_d cos\theta_d - i_q sin\theta_d) \tag{8.9}$$

For de inductive drop is in similar way:

$$L_s \frac{di_a}{dt} + L_m \frac{d(i_b + i_c)}{dt} \tag{8.10}$$

$$(L_s - L_m)\frac{di_a}{dt} \tag{8.11}$$

And by expressing ia in dq-terms, the inductive drop becomes:

$$(L_s - L_m)\frac{d}{dt}(i_d cos\theta_d - i_q sin\theta_d) \tag{8.12}$$

and, knowing that:

$$\frac{d}{dt}cosx = -sinx\frac{dx}{dt} \tag{8.13}$$

and

$$\frac{d}{dt}sinx = cosx\frac{dx}{dt} \tag{8.14}$$

Equation (8.12) can be written as

$$(L_s - L_m)\left[-i_d sin\theta_d \frac{d\theta_d}{dt} + cos\theta_d \frac{di_d}{dt} - i_q cos\theta_d \frac{d\theta_d}{dt} - sin\theta_d \frac{di_q}{dt}\right] \tag{8.15}$$

Applying the dq-transform also to the voltage difference $\Delta v_a = v_{a1} - v_{a2}$, results in:

$$\Delta v_d cos\theta_d - \Delta v_q sin\theta_d \tag{8.16}$$

By building the equation of the a-phase with the resistive and inductive drops and the voltage difference, it is obtained:

$$\Delta v_d cos\theta_d - \Delta v_q sin\theta_d = (R_s - R_m)(i_d cos\theta_d - i_q sin\theta_d) + (L_s - L_m)\left[-i_d sin\theta_d \frac{d\theta_d}{dt} + cos\theta_d \frac{di_d}{dt} - i_q cos\theta_d \frac{d\theta_d}{dt} - sin\theta_d \frac{di_q}{dt}\right] \quad (8.17)$$

Equating the coefficients of the $\cos\theta_d$, $\sin\theta_d$, and constant terms, it is obtained:

$$\Delta v_d = (R_s - R_m)i_d + (L_s - L_m)\frac{di_d}{dt} - (L_s - L_m)i_q \frac{d\theta_d}{dt}$$
$$\Delta v_q = (R_s - R_m)i_q + (L_s - L_m)\frac{di_q}{dt} + (L_s - L_m)i_d \frac{d\theta_d}{dt} \quad (8.18)$$

When mutual inductances are zero Lm=0 and with $\omega_d = \frac{d\theta_d}{dt}$ final equations are:

$$\Delta v_d = R_s i_d + L_s \frac{di_d}{dt} - L_s i_q \omega_d$$
$$\Delta v_q = R_s i_q + L_s \frac{di_q}{dt} + L_s i_d \omega_d \quad (8.19)$$

The equivalent dq-circuits are shown in Fig. 8.8.

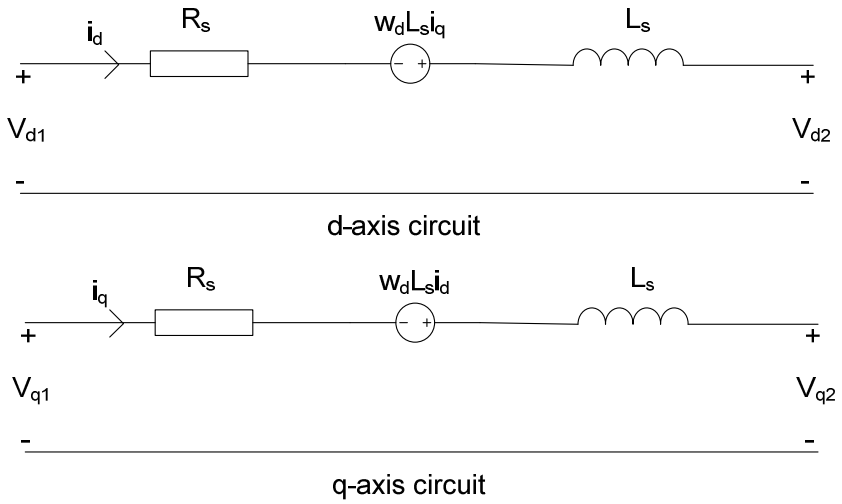

Fig. 8.8 Equivalent dq-circuit of a series RL line

8.3.2 Shunt C [24]

Here the dq-equations for the voltage drops across the shunt capacitances of a three-phase line Fig. 8.9 are derived.

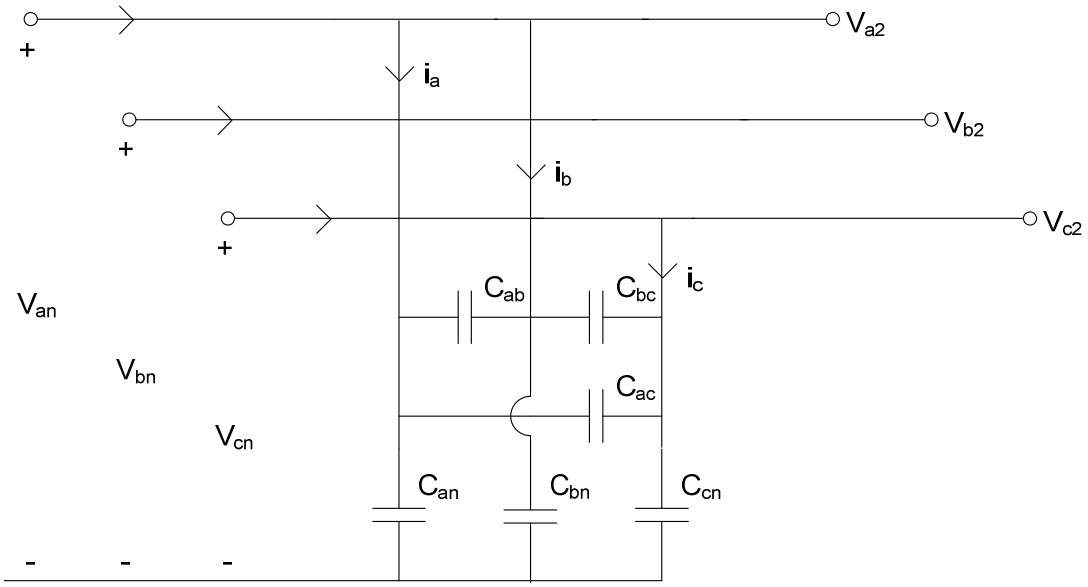

Fig. 8.9 Shunt capacitances of a three-phase line

Where the expression of the a-phase current is:

$$i_a = C_{an}\frac{dv_{an}}{dt} + C_{ab}\frac{d}{dt}(v_{an} - v_{bn}) + C_{ac}\frac{d}{dt}(v_{an} - v_{cn}) \tag{8.20}$$

Assuming that Cab=Cbc=Cac=Cm, Can=Cbn=Ccn, and Cs=Can+2Cab, equation (5.25) becomes:

$$i_a = C_s\frac{dv_{an}}{dt} - C_m\frac{dv_{bn}}{dt} - C_m\frac{dv_{cn}}{dt} \tag{8.21}$$

Introducing $0 = (v_{an} + v_{bn}v_{cn})$ into (8.21) gives:

$$i_a = (C_s + C_m)\frac{dv_{an}}{dt} \tag{8.22}$$

Applying the dq-transformation to the voltage and current in equation (8.22) it is obtained:

$$i_d cos\theta_d - i_q sin\theta_d = (C_s + C_m)\frac{d}{dt}(v_d cos\theta_d - v_q sin\theta_d)v_{an} \tag{8.23}$$

Transforming equation (8.23) in similar way as in (8.12) to (8.18), the following set of equations is obtained:

$$\begin{aligned} i_d &= (C_s + C_m)\frac{dv_d}{dt} - (C_s + C_m)v_q\frac{d\theta_d}{dt} \\ i_q &= (C_s + C_m)\frac{dv_q}{dt} + (C_s + C_m)v_d\frac{d\theta_d}{dt} \end{aligned} \tag{8.24}$$

When mutual capacitances between phases are considered zero then Cm=0 and with $\omega_d = \frac{d\theta_d}{dt}$ equation (8.24) results in:

$$i_d = C_s \frac{dv_d}{dt} - C_s v_q \omega_d$$
$$i_q = C_s \frac{dv_q}{dt} + C_s v_d \omega_d \quad (8.25)$$

8.3.3 Transformer [1][54]

The transformer is a significant component of AC power systems. Its fundamental operation is to increase or decrease the voltage or the current in an AC system. Also it can isolate circuits from each other and furthermore it can increase or decrease the apparent value of a capacitor, an inductor or a resistor. Essentially it consists in two or more windings coupled by a mutual magnetic flux. If one of these windings – primary winding – is connected to an AC voltage source, it will produce an alternating flux whose amplitude will depend on the frequency and amplitude of the applied voltage and by the number of turns. The mutual flux will induce an AC voltage into the other winding – secondary winding – whose value will depend on the frequency, magnitude of the mutual flux and the number of turns in the secondary winding.

Both windings can be coupled through air, but complying through high permeability ferromagnetic materials is much more effective. Typically this ferromagnetic material is iron. Transformers build in this way are so called iron-core transformers.

To reduce the eddy-currents losses the iron core is typically made up of a stack of thin laminations.

In the transformer most of the flux is confined into the iron-core coupling both windings, but some of the flux links only one winding without linking the other – leakage flux. This leakage flux also results in losses in the transformer.

Two kinds of three phase iron-core transformers are studied in this section. The three windings transformer used in DFIG-WT configuration and the two windings transformer used in the other configurations. The models are presented as the ideal ones and the real ones in the d-q reference frame.

8.3.3.1 Three-phase two-windings transformer

This kind of transformer is used in all the configurations studied in this project. The ideal and the real model are presented next. An especial situation appears for the RCC and IM topology due to the variation of the voltage and frequency produce by the Vf-control in the HVDC converter. But since the variation of the voltage is proportional to the frequency, normal transformers can be used. Equation shows that since the voltage and frequency varies in a proportional way the value of the maximum flux ϕ_{max} keeps constant.

$$\frac{V_1}{f} = \frac{2\pi}{\sqrt{2}} N_1 \phi_{max} \quad (8.26)$$

Where, V1 is the rms value of the voltage in the primary winding.

Ideal

The ideal transformer is considered as a no losses transformer where the voltages and the currents in the primary windings are related to the secondary windings by the turns ratio of the transformer. For the dq-model only the transformer of one phase is considered. Fig. 8.10 represents the circuit of the ideal transformer of one of the phases.

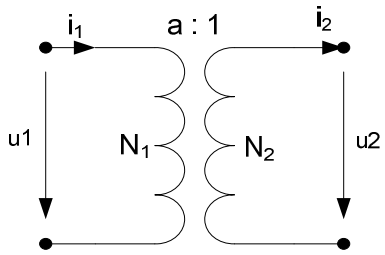

Fig. 8.10 Ideal two-winding transformer of one phase

In the figure, a represents the turns ratio of the transformer, where a=N1/N2, where N1 is the number of turns in the primary winding and N2 the number of turns in the secondary winding. From this model, simple equations relating voltages and currents in the primary and secondary winding are obtained:

$$\frac{v_1}{v_2} = \frac{N_1}{N_2} = a$$
$$\frac{i_1}{i_2} = \frac{N_2}{N_1} = \frac{1}{a} \tag{8.27}$$

Real

The equivalent circuit for a real single phase of a two-winding transformer is shown in Fig. 8.11

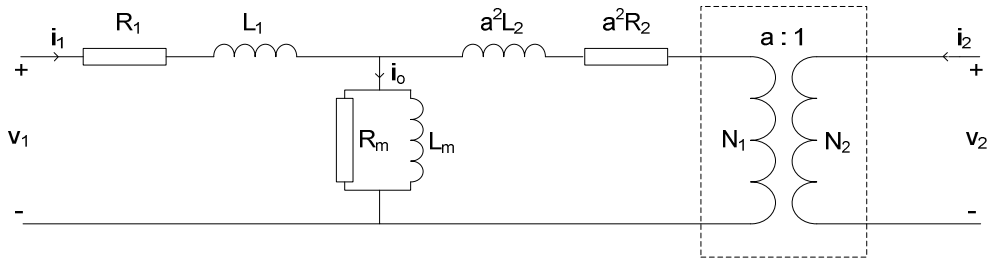

Fig. 8.11 Single-phase equivalent circuit of a three-phase two-winding transformer

Typically the magnetization circuit is modeled placing the resistor Rm in parallel with Lm , but it can be also placed in series with Lm. For most applications, the two models – series or parallel – only manage to calculate equal losses for a certain working point – certain voltage and frequency – but in some other applications results are different. [46]

The equivalent dq-circuit of the transformer Fig. 8.11 is shown in the next figure:

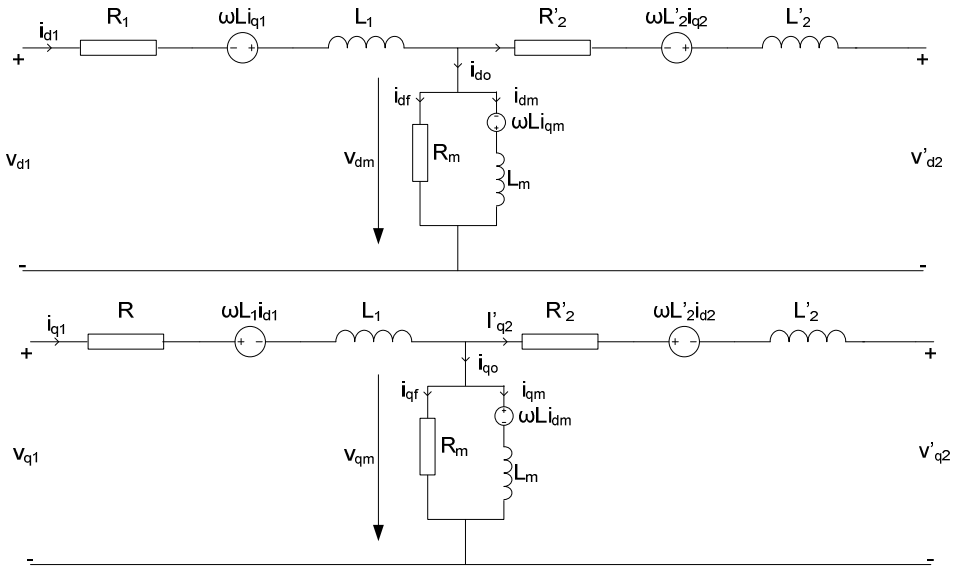

Fig. 8.12 Equivalent dq-model of a three-phase two-winding transformer

From the equivalent dq-circuit next equations are obtained:

$$\begin{aligned} v_{1d} &= R_1 i_{1d} + L_1 \frac{di_{1d}}{dt} - L_1 i_{1q}\omega + v_{md} \\ v_{1q} &= R_1 i_{1q} + L_1 \frac{di_{1q}}{dt} + L_1 i_{1d}\omega + v_{mq} \\ v_{2d} &= -R_2 i_{2d} - \frac{di_{2d}}{dt} + L_2 i_{2q}\omega + v_{md} \\ v_{2q} &= -R_2 i_{2q} - L_2 \frac{di_{2q}}{dt} - L_2 i_{2d}\omega + v_{mq} \end{aligned} \tag{8.28}$$

The voltage v_m in the magnetization circuit is obtained by the next equations:

$$\begin{aligned} v_{md} &= R_m i_{fd} = L_m \frac{di_{md}}{dt} - L_m i_{mq}\omega \\ v_{md} &= R_m i_{fq} = L_m \frac{di_{md}}{dt} - L_m i_{md}\omega \end{aligned} \tag{8.29}$$

and by knowing that:

$$i_o = i_1 - i_2 = i_f + i_m \tag{8.30}$$

Equations in steady-state for the transformer depend only in the primary and secondary currents:

$$\begin{bmatrix} v_{1d} \\ v_{2d} \\ v_{1q} \\ v_{2q} \end{bmatrix} = \begin{bmatrix} R_1 + \frac{A}{B}\omega L_m & -\frac{A}{B}\omega L_m & -\omega L_1 - \frac{\omega L_m}{B} & \frac{\omega L_m}{B} \\ \frac{A}{B}\omega L_m & -R_2 - \frac{A}{B}\omega L_m & -\frac{\omega L_m}{B} & \omega L_2 + \frac{\omega L_m}{B} \\ \omega L_1 + \frac{\omega L_m}{B} & -\frac{\omega L_m}{B} & R_1 - \frac{A}{B}\omega L_m & \frac{A}{B}\omega L_m \\ \frac{\omega L_m}{B} & -\omega L_2 - \frac{\omega L_m}{B} & -\frac{A}{B}\omega L_m & -R_2 + \frac{A}{B}\omega L_m \end{bmatrix} \begin{bmatrix} i_{1d} \\ i_{2d} \\ i_{1q} \\ i_{2q} \end{bmatrix} \tag{8.31}$$

Where $A = \frac{\omega L_m}{R_m}$ and $B = 1 + A^2$.

And by these equations, dq-currents of the primary winding are obtained:

$$\begin{aligned} i_{1d} &= \frac{i_{2d}\left(\omega L_2 - AR_2 + \frac{\omega L_m}{B}(1 - A^2)\right) + i_{2q}(R_2 + A\omega L_2) - Av_{2d} + v_{2q}}{\frac{\omega L_m (1 - A^2)}{B}} \\ i_{1q} &= \frac{i_{2q}\left(\omega L_2 + AR_2 + \frac{\omega L_m}{B}(1 - A^2)\right) + i_{2d}(-R_2 + A\omega L_2) + Av_{2q} - v_{2d}}{\frac{\omega L_m (1 - A^2)}{B}} \end{aligned} \tag{8.32}$$

By these equations the steady-state dq-model of a three-phase two-winding transformer is described.

The considered losses are: copper losses and iron losses.

The copper losses for this transformer are modeled by:

$$P_{cu,trafo} = \frac{3}{2}\left(R_1 i_{1d}^2 + R_1 i_{1q}^2 + R_2 i_{2d}^2 + R_2 i_{2d}^2\right) \tag{8.33}$$

The transformer iron losses are:

$$\begin{aligned} P_{fe,trafo} &= \frac{3}{2}\left(R_m i_{fd}^2 + R_m i_{fq}^2\right) = \\ &= \frac{3}{2}\left(R_m \left(\frac{i_{1d} - i_{2d} - \frac{R_m}{\omega L_m}(i_{1q} - i_{2q})}{1 + \left(\frac{R_m}{\omega L_m}\right)^2}\right)^2 + R_m \left(\frac{i_{1q} - i_{2q} + \frac{R_m}{\omega L_m}(i_{1d} - i_{2d})}{1 + \left(\frac{R_m}{\omega L_m}\right)^2}\right)^2\right) \end{aligned} \tag{8.34}$$

8.3.3.2 Three-phase three-windings transformer

This kind of transformer is only used in the DFIG configuration. The ideal and the real model are presented next.

Ideal

As for the two-winding transformer ideal transformer is considered as a no losses transformer. For the dq-model only the transformer of one phase is considered. Fig. 8.10 represents the circuit of the ideal transformer of one of the phases.

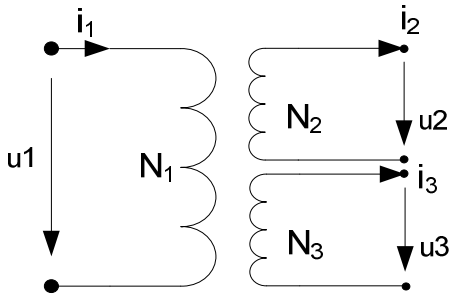

Fig. 8.13 Ideal three-winding transformer of one phase

From this model simple equations relating voltages and currents in the windings are obtained:

$$\frac{v_1}{N_1} = \frac{v_2}{N_2} = \frac{v_3}{N_3}$$
$$i_1 N_1 = i_2 N_2 + i_3 N_3 \tag{8.35}$$

Where, N_1 is the number of turns in the primary winding, N_2 the number of turns in the secondary winding and N_3 the number of turns in the tertiary winding.

Real

Next figure shows the real equivalent circuit of a three-phase three-winding transformer.

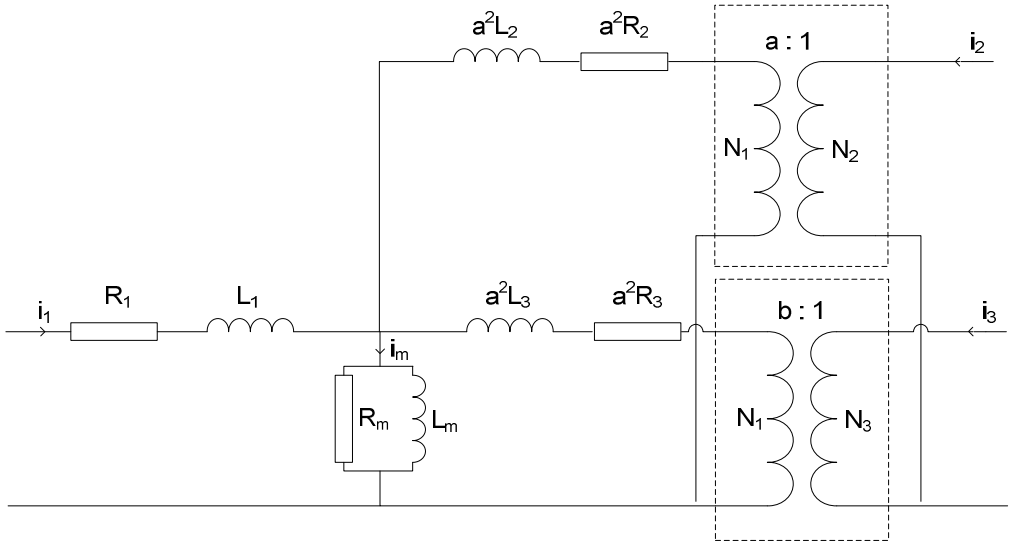

Fig. 8.14 Single-phase equivalent circuit of a three-phase three-winding transformer

From the previous figure Fig. 8.14 the dq-circuit of the transformer can be obtained, as shows Fig. 8.15.

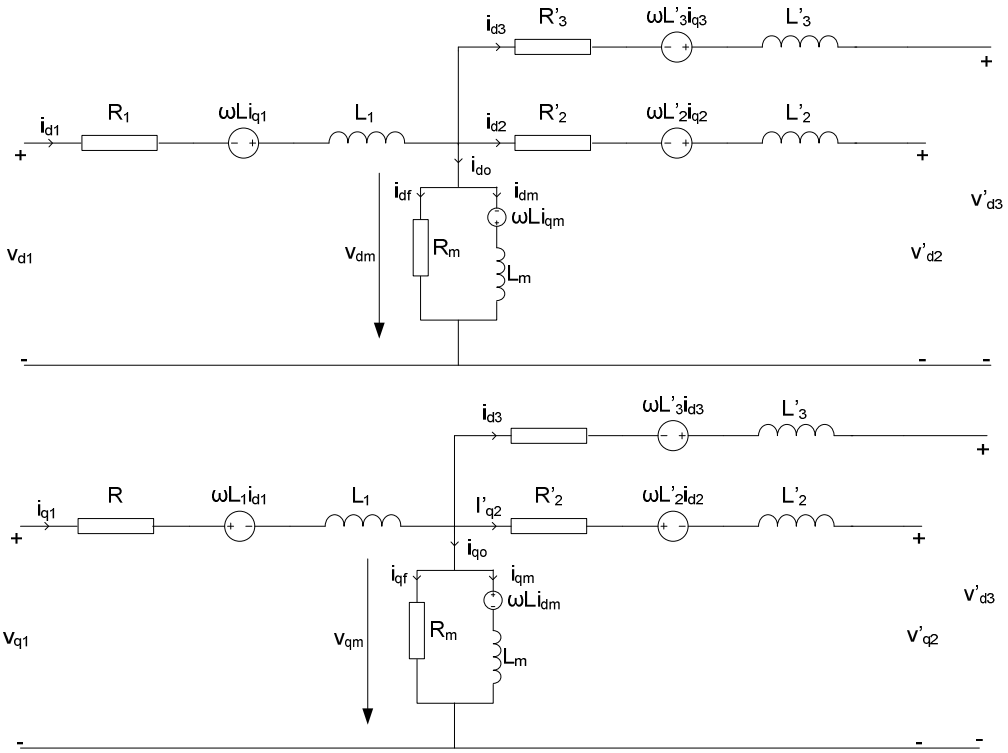

Fig. 8.15 Equivalent dq-model of a three-phase three-winding transformer

The dynamic voltage dq-equations are obtained from the previous figure:

$$
\begin{aligned}
v_{1d} &= R_1 i_{1d} + L_1 \frac{di_{1d}}{dt} - L_1 i_{1q}\omega + v_{md} \\
v_{1q} &= R_1 i_{1q} + L_1 \frac{di_{1q}}{dt} + L_1 i_{1d}\omega + v_{mq} \\
v_{2d} &= -R_2 i_{2d} - \frac{di_{2d}}{dt} + L_2 i_{2q}\omega + v_{md} \\
v_{2q} &= -R_2 i_{2q} - L_2 \frac{di_{2q}}{dt} - L_2 i_{2d}\omega + v_{mq} \\
v_{3d} &= -R_3 i_{3d} - \frac{di_{3d}}{dt} + L_3 i_{3q}\omega + v_{md} \\
v_{3q} &= -R_3 i_{3q} - L_3 \frac{di_{3q}}{dt} - L_3 i_{3d}\omega + v_{mq}
\end{aligned}
\tag{8.36}
$$

Voltage equations for the magnetization circuit are the same as for the two-winding transformer, equation (8.29).

Relation between winding currents and currents in the magnetization circuit is:

$$
i_o = i_1 - i_2 - i_3 = i_f + i_m \tag{8.37}
$$

By using the previous equations, equations in steady-state for the transformer, dependent only in the primary, secondary and tertiary winding currents, are:

$$\begin{bmatrix} v_{1d} \\ v_{2d} \\ v_{3d} \\ v_{1q} \\ v_{2q} \\ v_{3q} \end{bmatrix} = [Z] \begin{bmatrix} i_{1d} \\ i_{2d} \\ i_{3d} \\ i_{1q} \\ i_{2q} \\ i_{3q} \end{bmatrix} \tag{8.38}$$

$$[Z] = \begin{bmatrix} R_1 + \frac{A}{B}\omega L_m & -\frac{A}{B}\omega L_m & -\frac{A}{B}\omega L_m & -\omega L_1 - \frac{\omega L_m}{B} & \frac{\omega L_m}{B} & \frac{\omega L_m}{B} \\ \frac{A}{B}\omega L_m & -R_2 - \frac{A}{B}\omega L_m & -\frac{A}{B}\omega L_m & -\frac{\omega L_m}{B} & \omega L_2 + \frac{\omega L_m}{B} & \frac{\omega L_m}{B} \\ \frac{A}{B}\omega L_m & -\frac{A}{B}\omega L_m & -R_3 - \frac{A}{B}\omega L_m & -\frac{\omega L_m}{B} & \frac{\omega L_m}{B} & \omega L_3 + \frac{\omega L_m}{B} \\ \omega L_1 + \frac{\omega L_m}{B} & -\frac{\omega L_m}{B} & -\frac{\omega L_m}{B} & R_1 - \frac{A}{B}\omega L_m & \frac{A}{B}\omega L_m & \frac{A}{B}\omega L_m \\ \frac{\omega L_m}{B} & -\omega L_2 - \frac{\omega L_m}{B} & -\frac{\omega L_m}{B} & -\frac{A}{B}\omega L_m & -R_2 + \frac{A}{B}\omega L_m & \frac{A}{B}\omega L_m \\ \frac{\omega L_m}{B} & -\frac{\omega L_m}{B} & -\omega L_3 - \frac{\omega L_m}{B} & -\frac{A}{B}\omega L_m & \frac{A}{B}\omega L_m & -R_3 + \frac{A}{B}\omega L_m \end{bmatrix} \tag{8.39}$$

And by these equations, dq-currents of the primary winding are obtained:

$$\begin{aligned} i_{1d} &= \frac{i_{2d}\left(\omega L_2 - AR_2 + \frac{\omega L_m}{B}(1-A^2)\right) + i_{2q}(R_2 + A\omega L_2) + i_{3d}\frac{\omega L_m}{B}(1-A^2) - Av_{2d} + v_{2q}}{\frac{\omega L_m(1-A^2)}{B}} \\ i_{1q} &= \frac{i_{2q}\left(\omega L_2 + AR_2 + \frac{\omega L_m}{B}(1-A^2)\right) + i_{2d}(-R_2 + A\omega L_2) + i_{3q}\frac{\omega L_m}{B}(1-A^2) + Av_{2q} - v_{2d}}{\frac{\omega L_m(1-A^2)}{B}} \end{aligned} \tag{8.40}$$

By these equations the steady-state dq-model of a three-phase three-winding transformer is described.

The copper losses for this transformer are modeled by:

$$P_{cu,trafo} = \frac{3}{2}\left(R_1 i_{1d}^2 + R_1 i_{1q}^2 + R_2 i_{2d}^2 + R_2 i_{2d}^2 + R_3 i_{3d}^2 + R_3 i_{3d}^2\right) \tag{8.41}$$

The transformer iron losses are:

$$\begin{aligned} P_{fe,trafo} &= \frac{3}{2}\left(R_m i_{fd}^2 + R_m i_{fq}^2\right) = \\ &= \frac{3}{2}\left(R_m\left(\frac{i_{1d} - i_{2d} - i_{3d} - \frac{R_m}{\omega L_m}\left(i_{1q} - i_{2q} - i_{3q}\right)}{1 + \left(\frac{R_m}{\omega L_m}\right)^2}\right)^2\right. \\ &\quad \left. + R_m\left(\frac{i_{1q} - i_{2q} - i_{3q}\frac{R_m}{\omega L_m}\left(i_{1d} - i_{2d} - i_{3q}\right)}{1 + \left(\frac{R_m}{\omega L_m}\right)^2}\right)^2\right) \end{aligned} \tag{8.42}$$

8.3.4 AC transmission line

Next figure shows the equivalent circuit of an AC transmission line – RLC circuit.

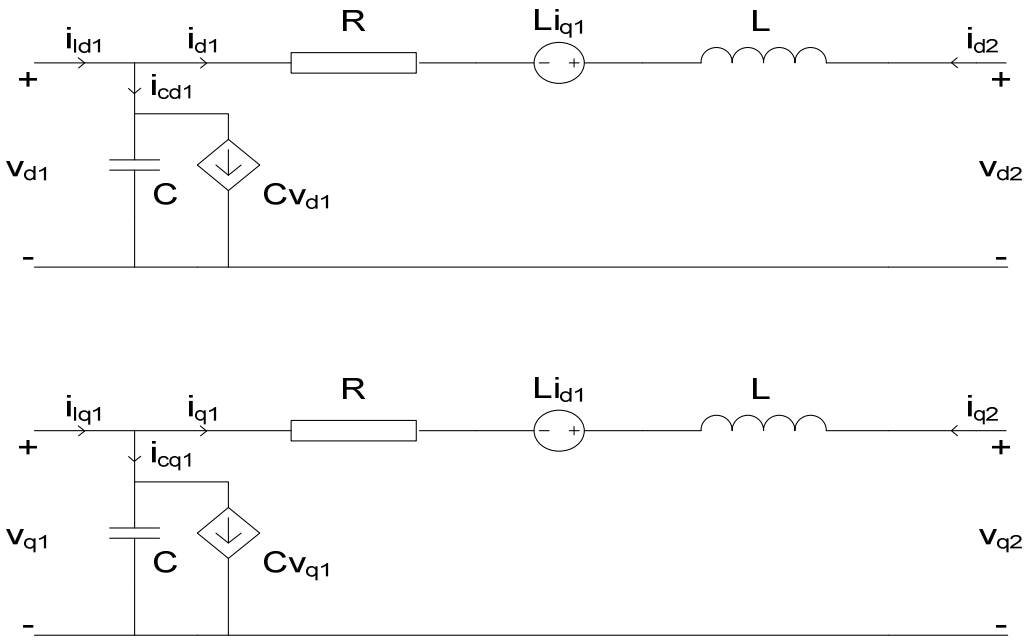

Fig. 8.16 AC-Transmission line in dq-components

To obtain equations for the dynamic model of an AC-transmission line in dq-components, showed in Fig. 8.16, the circuit is divided into the RL circuit and the Shunt C circuit.

By taking into account the equations of the series RL circuit:

$$\begin{bmatrix} v_{d1} \\ v_{q1} \end{bmatrix} - \begin{bmatrix} v_{d2} \\ v_{q2} \end{bmatrix} = \begin{bmatrix} R & -\omega_d L \\ \omega_d L & R \end{bmatrix} \begin{bmatrix} i_{d1} \\ i_{q1} \end{bmatrix} + L_s \frac{d}{dt} \begin{bmatrix} i_{d1} \\ i_{q1} \end{bmatrix} \tag{8.43}$$

$$\frac{d}{dt} \begin{bmatrix} i_{d1} \\ i_{q1} \end{bmatrix} = \frac{1}{L} \left[\begin{bmatrix} v_{d1} \\ v_{q1} \end{bmatrix} - \begin{bmatrix} v_{d2} \\ v_{q2} \end{bmatrix} - \begin{bmatrix} R & -\omega_d L \\ \omega_d L & R \end{bmatrix} \begin{bmatrix} i_{d1} \\ i_{q1} \end{bmatrix} \right] \tag{8.44}$$

Applying the equations from the Shunt C circuit:

$$\frac{d}{dt} \begin{bmatrix} v_{d1} \\ v_{q1} \end{bmatrix} = \frac{1}{C} \left[\begin{bmatrix} i_{dc1} \\ i_{qc1} \end{bmatrix} + \omega_d C \begin{bmatrix} 0 & 1 \\ -1 & 0 \end{bmatrix} \begin{bmatrix} v_{d1} \\ v_{q1} \end{bmatrix} \right] \tag{8.45}$$

In the steady state model the derivative terms of the equation (8.43) are equal to zero, obtaining:

$$\begin{bmatrix} v_{d1} \\ v_{q1} \end{bmatrix} - \begin{bmatrix} v_{d2} \\ v_{q2} \end{bmatrix} = \begin{bmatrix} R & -\omega_d L \\ \omega_d L & R \end{bmatrix} R_s \begin{bmatrix} i_{d1} \\ i_{q1} \end{bmatrix} \tag{8.46}$$

$$\begin{bmatrix} i_{d1} \\ i_{q1} \end{bmatrix} = \frac{1}{R^2 + (\omega_d L)^2} \begin{bmatrix} R & \omega_d L \\ -\omega_d L & R \end{bmatrix} \left[\begin{bmatrix} v_{d1} \\ v_{q1} \end{bmatrix} - \begin{bmatrix} v_{d2} \\ v_{q2} \end{bmatrix} \right] \tag{8.47}$$

and for the shunt C circuit:

$$\begin{bmatrix} v_{d1} \\ v_{q1} \end{bmatrix} = \frac{1}{\omega_d C} \begin{bmatrix} 0 & 1 \\ -1 & 0 \end{bmatrix} \begin{bmatrix} i_{dc1} \\ i_{qc1} \end{bmatrix} \tag{8.48}$$

By using equations (8.47), (8.48) and knowing that $i_{l\_dq1} = i_{dq1} + i_{c\_dq1}$ the steady state model of the transformer is obtained.

Chapter 9 Comparison and evaluation

ABSTRACT

In this chapter the first approach of the developed method is employed to evaluate annual energy production of the four proposed off-shore VSC-HVDC WF configurations (full scale SPMSG, DFIG, RCC-WRIG, SCIG). Results from simulations are evaluated and compared. A new variable speed wind turbine concept based on RCC-WRIG is also evaluated, showing promising features under certain wind conditions. It should be noted that the main purpose of this chapter is to present the general performance of the developed method – the presentation of specific results from the simulation is a secondary task.

9.1 Introduction

The same WF distribution is considered for all WFs: 100 parallel turbines distributed on ten rows of ten turbines. As explained in Chapter 8, WF models are based on aggregated WT models.

The same annual wind speed distribution model is employed for all WFs. As explained in Chapter 2, this wind model is based on Weibull distribution.

It should be noted that next simplifications have been done in this first modeling approach:

- No mechanical losses are considered in the WT gear train and generator.
- The converter power losses are modeled through a static factor μ.
- Ideal transformers are employed.
- The power is measured after the transformer of each WT, so the WF network is not modeled.

Next figure shows where is the power measuring point (PMP) for this first modeling approach:

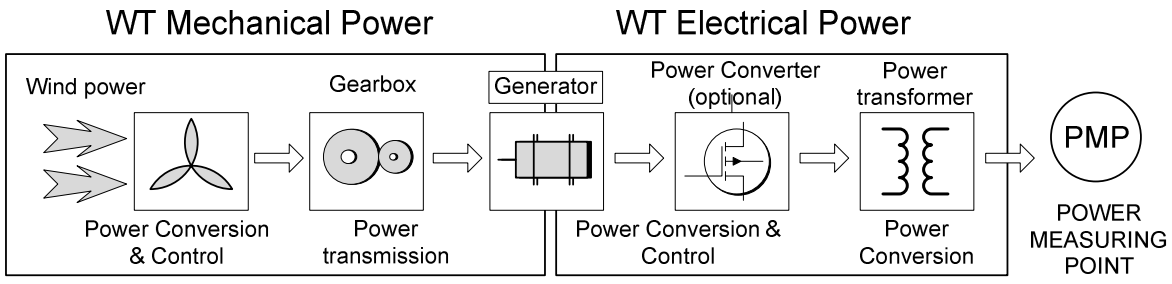

Fig. 9.1 PMP chosen in first modeling approach.

More complex models of the gear train, the transformers, the WF network and the converter power losses are presented in this project, but due to time constraints are not implemented in the WF models.

The DC-transmission line cable is not modeled, but since the scope of this project is to develop a fast method to evaluate and compare annual energy production the WF analysis could be reduced if the power measuring point is placed in the DC side of HVDC off-shore terminal station:

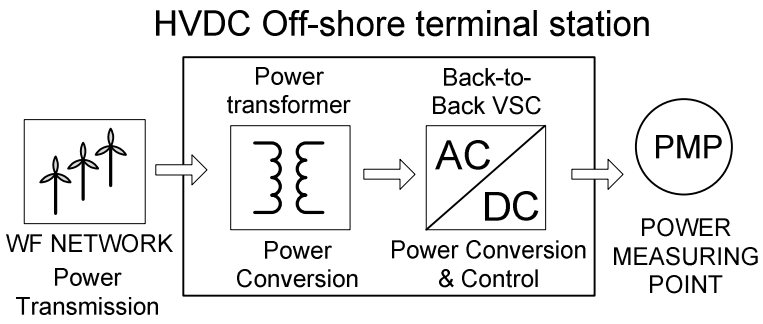

Fig. 9.2 PMP proposed for next modeling approach.

9.2 Simulations

It is assumed that WTs of the same row experience similar incoming wind and the incoming wind speed difference between two consecutive rows is constant. The maximum deviation from the average WF wind speed that a single WT of a row can experience is described by a parameter so called wind factor. Following these assumptions, three different symmetric wind speed distributions across the WF are considered:

WF row \ Wind factor	±0.9 m/s	±1.8 m/s	±2.7 m/s
1	$V_{wind,WFavg} - 0.9$	$V_{wind,WFavg} - 1.8$	$V_{wind,WFavg} - 2.7$
2	$V_{wind,WFavg} - 0.7$	$V_{wind,WFavg} - 1.4$	$V_{wind,WFavg} - 2.1$
3	$V_{wind,WFavg} - 0.5$	$V_{wind,WFavg} - 1$	$V_{wind,WFavg} - 1.5$
4	$V_{wind,WFavg} - 0.3$	$V_{wind,WFavg} - 0.6$	$V_{wind,WFavg} - 0.9$
5	$V_{wind,WFavg} - 0.1$	$V_{wind,WFavg} - 0.2$	$V_{wind,WFavg} - 0.3$
6	$V_{wind,WFavg} + 0.1$	$V_{wind,WFavg} + 0.2$	$V_{wind,WFavg} + 0.3$
7	$V_{wind,WFavg} + 0.3$	$V_{wind,WFavg} + 0.6$	$V_{wind,WFavg} + 0.9$
8	$V_{wind,WFavg} + 0.5$	$V_{wind,WFavg} + 1$	$V_{wind,WFavg} + 1.5$
9	$V_{wind,WFavg} + 0.7$	$V_{wind,WFavg} + 1.4$	$V_{wind,WFavg} + 2.1$
10	$V_{wind,WFavg} + 0.9$	$V_{wind,WFavg} + 1.8$	$V_{wind,WFavg} + 2.7$

Table 9.1 The three symmetric wind speed distributions across the WF considered in simulation[6].

Firstly, to help the reader, the shape of the average WF wind speed distribution is plotted here again (from Chapter 2).

[6] $V_{wind,WFavg}$ stands for the average wind speed of the WF.

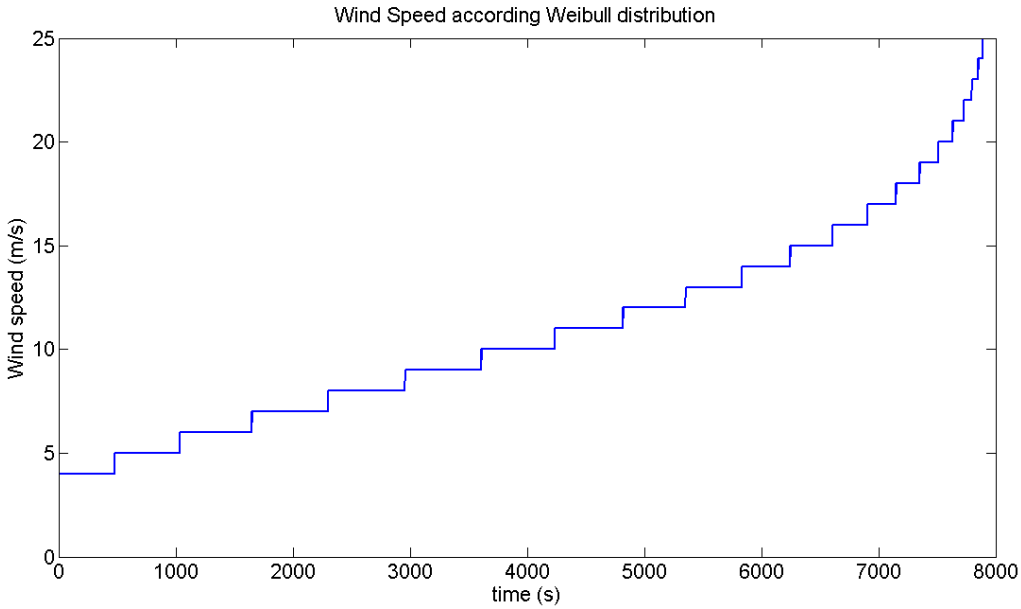

Fig. 9.3 Average wind Speed distribution used in the WF simulation

Next plot shows electrical power delivered by each WF for a ±0.9 m/s factor.

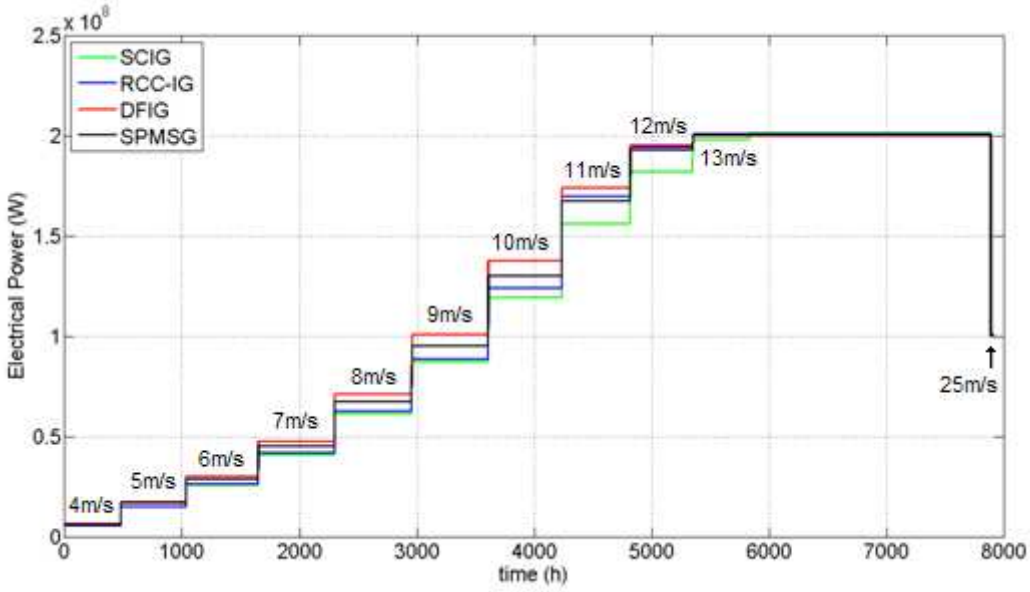

Fig. 9.4 Electrical power delivered by each WF for ±0.9 m/s wind factor.

On this first figure (only), again in order to help the reader, the average wind speed of the WF ($V_{wind,WFavg}$) is plotted for each step. According to the ±0.9 m/s factor the maximum and minimum incoming wind speeds that a group of WT experiences at each step are given by: $V_{wind,WFavg}$ ±0.9 m/s.

It can be seen that all WFs apart from SCIG reach nominal power (100x2MW) at an average wind speed of the WF of 13 m/s. SCIG achieves nominal speed at 14 m/s. Also it can be observed that at 25 m/s half of the WTs of all the WFs are disconnected, since this is the rated cut-off wind speed.

It can be observed that the DFIG WT shows the best performance (respect to energy production), followed by the full-scale SPMSG and the RCC-IG. The SCIG WT shows the worse performance.

The RCC-IG shows an improvement respect to SCIG mainly at average wind speeds in the range of 10-13 m/s.

Looking at the next plot, mechanical power delivered by each WF for ±0.9 m/s factor, the reasons behind those differences can be explained better.

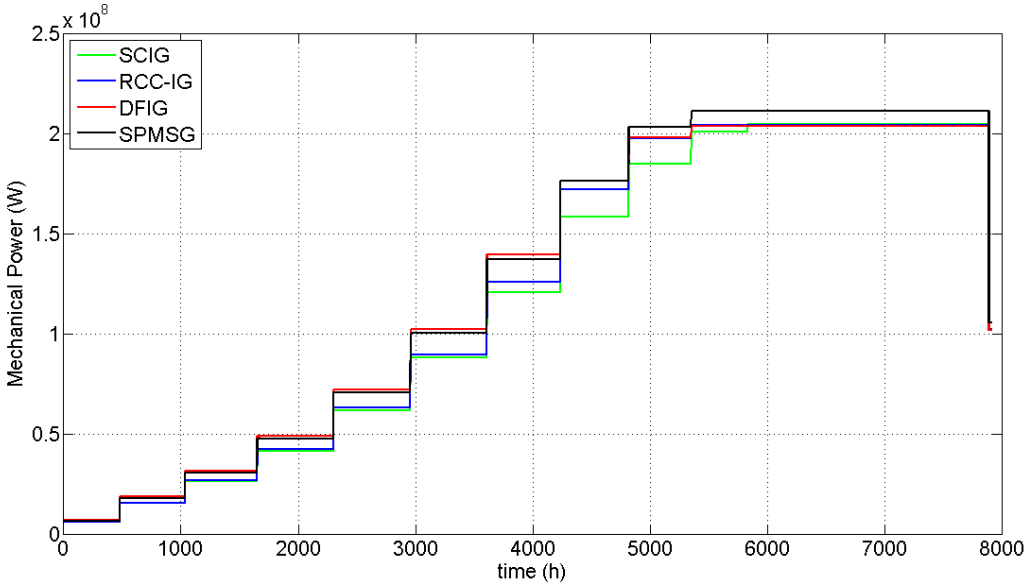

Fig. 9.5 Mechanical power[7]* delivered by each WF for ±0.9 m/s wind factor.

From Fig. 9.5 it can be stated that DFIG and full-scale SPMSG WTs present higher effectiveness of power generation, since the rotor speed can be adjusted accurately to wind speed in order to follow maximum values of Cp curve. Also RCC-IG shows certain improvement over SCIG.

Moreover it can be observed that the full-scale SPMSG is the WT topology which requires higher mechanical input power to deliver nominal power. This is because of the considered static losses of the back-to-back converter (μ=0.95). This can also explain the electrical power generation differences between the DFIG and the full-scale SPMSG, since in the DFIG configuration only the power delivered from (or injected to) the rotor is affected by these converter losses.

Slight differences of generated mechanical power are observed between DFIG and full-scale SPMSG in the range of average wind speeds from 4-11 m/s. This is due to certain assumptions on DFIG stator power reference generation (Chapter 5).

The performance of the WFs can be explained in an analog way for higher values of the wind factor. In followings, plots of electrical and mechanical power of each WF are shown for ±1.8 m/s and ±2.7 m/s wind factors.

[7] Total mechanical power is calculated from power balance equation

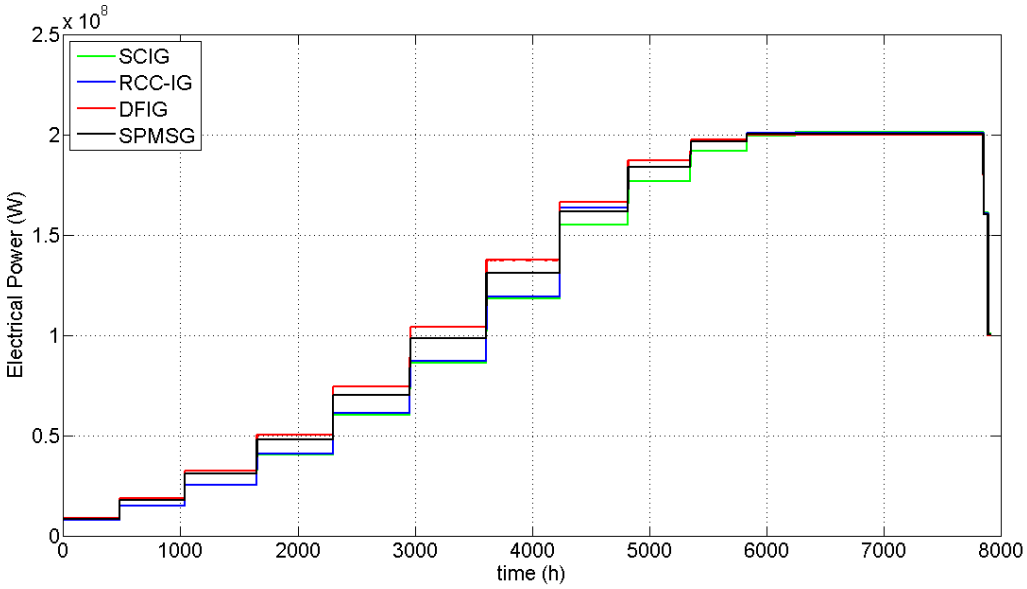

Fig. 9.6 Electrical power delivered by each WF for ±1.8 m/s wind factor.

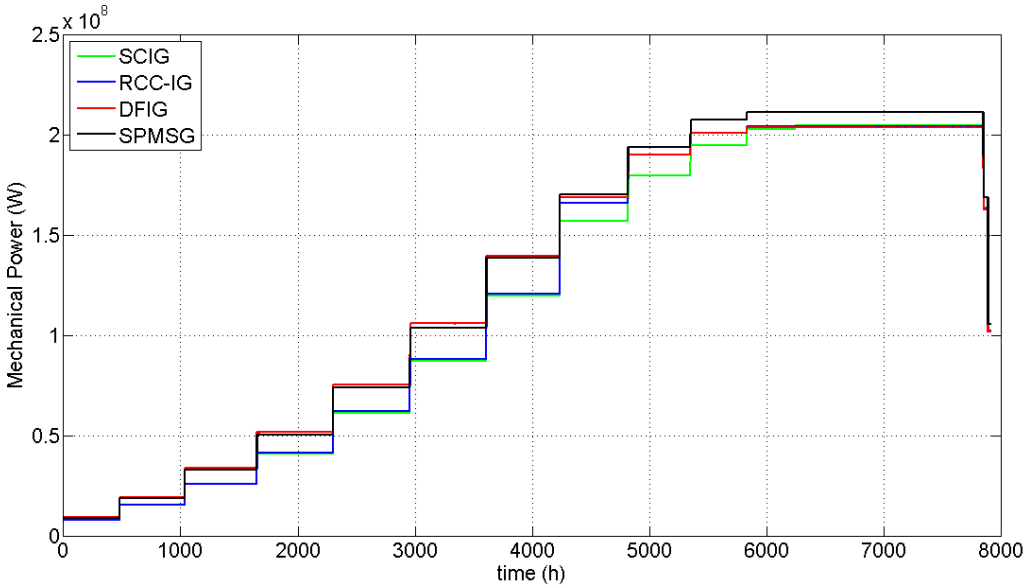

Fig. 9.7 Mechanical power delivered by each WF for ±1.8 m/s wind factor.

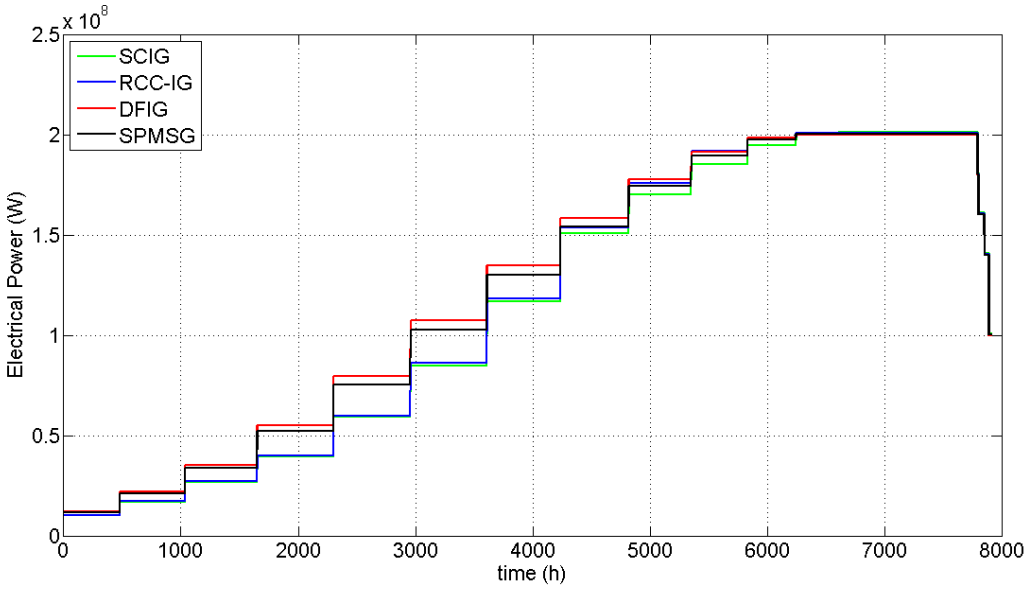

Fig. 9.8 Electrical power delivered by each WF for ±2.7 m/s wind factor

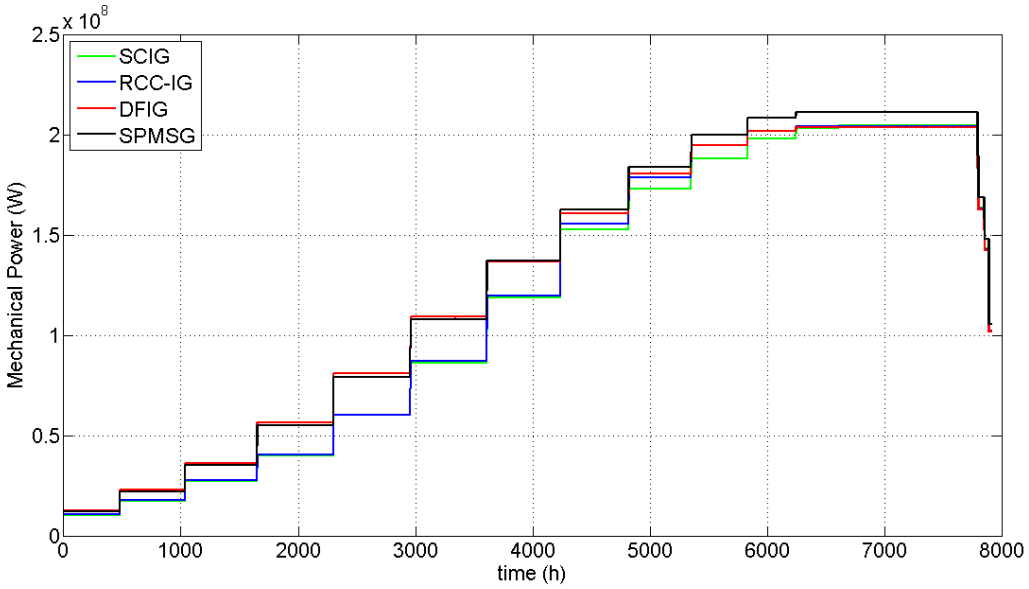

Fig. 9.9 Mechanical power delivered by each WF for ±2.7 m/s wind factor

It can be observed that the performance of the RCC-IG is more similar to the SCIG when the incoming wind speed difference between two consecutive rows is higher.

It should be also noted that at an average wind speed of the WF below 25 m/s some WTs are disconnected. This is just because the incoming wind speed of some WTs rows is higher than 25 m/s (cut-off speed) before due to employment of higher wind factors (±1.8 m/s and ±2.7 m/s).

Next Table 9.2 summarizes the numerical results obtained from previous simulations.

Electrical Power [W]									
wind difference of ±0.9m/s			wind difference of ±1.8m/s			wind difference of ±2.7m/s			
Generator	Annual power production	Power per hour	Generator	Annual power production	Power per hour	Generator	Annual power production	Power per hour
SCIG	9,24E+11	105449774,3	SCIG	9,14E+11	104319754,7	SCIG	9,00E+11	102721611,5
RCC-IG	9,44E+11	107812052,3	RCC-IG	9,29E+11	106036066,2	RCC-IG	9,11E+11	104018403,2
DFIG	9,76E+11	111371622,2	DFIG	9,74E+11	111147049,3	DFIG	9,70E+11	110690645,6
SPMSG	9,57E+11	109195132,7	SPMSG	9,55E+11	109009887,3	SPMSG	9,51E+11	108595910,8
Mechanical Power [W]								
Generator	Annual power production	Power per hour	Generator	Annual power production	Power per hour	Generator	Annual power production	Power per hour
SCIG	9,38E+11	107031397,5	SCIG	9,28E+11	105887726,7	SCIG	9,13E+11	104267557,6
RCC-IG	9,59E+11	109445950,3	RCC-IG	9,43E+11	107642324,8	RCC-IG	9,25E+11	105592418,2
DFIG	9,93E+11	113314387,2	DFIG	9,91E+11	113077425,5	DFIG	9,86E+11	112600504,2
SPMSG	1,01E+12	115163447	SPMSG	1,01E+12	114968556,7	SPMSG	1,00E+12	114532720,1
Ratios								
Ratio (Electrical Power)/(Aerodynamic Power)			Ratio (Electrical Power)/(Aerodynamic Power)			Ratio (Electrical Power)/(Aerodynamic Power)		
SCIG		18,89%	SCIG		18,69%	SCIG		18,40%
RCC-IG		19,31%	RCC-IG		19,00%	RCC		18,63%
DFIG		19,95%	DFIG		19,91%	DFIG		19,83%
SPMSG		19,56%	SPMSG		19,53%	SPMSG		19,45%
Ratio (Electrical Power)/(Mechanical Power)			Ratio (Electrical Power)/(Mechanical Power)			Ratio (Electrical Power)/(Mechanical Power)		
SCIG		98,52%	SCIG		98,52%	SCIG		98,52%
RCC-IG		98,51%	RCC-IG		98,51%	RCC-IG		98,51%
DFIG		98,29%	DFIG		98,29%	DFIG		98,29%
SPMSG		94,82%	SPMSG		94,82%	SPMSG		94,82%

Table 9.2 Electrical and Mechanical power of the 4 WFs for different wind speeds[8]

[8] *The Total Average Aerodynamic Power is calculated from the Weibull distribution and the general equation Paero=4,89E+12[Appendix]*

Electrical power / Mechanical power ratio

The ratio Electrical power / Mechanical power represents the average electrical efficiency of each WT concept. The highest one is found for the SCIG (98,52%), followed by the RCC-IG (98,51%), the DFIG (98,29%) and the full-scale SPMSG (94,82%).

The lower electrical efficiency of DFIG and full-scale SPMSG is due to the considered static losses of the back-to-back converter. Similar efficiency is found for the SCIG and the RCC-IG since the average virtual rotor resistance for all the RCC-IG WTs (under simulation conditions) is similar to the rotor resistance of the SCIG WTs.

It can be seen that the average value of the electrical efficiency is independent of the considered wind factor.

Electrical power / Aerodynamic power ratio

Looking at the ratio Electrical power / Aerodynamic power it can be stated that the DFIG WT is the most efficient from an aerodynamic point of view, followed by the full-scale SPMSG, the RCC-IG and the SCIG. It should be noted that the value of this average aerodynamic efficiency is not independent of the considered wind factor.

For higher wind factors the average aerodynamic efficiency is lower for all WT concepts.

For DFIG and full-scale SPMSG the average aerodynamic efficiency is just lower because more WTs are disconnected – more WTs experiences incoming wind speed higher than the cut-off speed (25 m/s).

In the case of the SCIG and RCC-IG the average aerodynamic efficiency is lower because more WTs are disconnected and also because the aerodynamic power conversion is worse – many WTs are working far from the maximum power conversion point.

9.3 Simulation time

One of the main requirements of this report is to develop a fast method. Table shows the simulation times for each WF topology when the simulink models are run with the specified computer and solver options:

Computer details: Intel Core2 Duo, 2.66Ghz, 2,95GB RAM.

Solver options:

- Type: *fixed speed*
- Solver: *discrete*
- Fixed-step size: *1*

	Time 1 (s)	Time 2 (s)	Time 3 (s)	Time 4 (s)	Average (s)
SCIG	562.9713	563.8969	563.9498	564.2281	563.761525
RCC-IG	1380.1591	1381.3351	1382.9451	1382.3893	1381.70715
DFIG	1.4082	1.4044	1.4052	1.4065	1.406075
SPMSG	1.0762	1.111	1.115	1.1024	1.10115

Table 9.3 Simulation times.

It can be observed that the DFIG and the full-scale SPMSG WF simulations run extremely fast – 7916 virtual seconds are simulated in less than 1.5 seconds of real time. But the SCIG and RCC-IG WF models run slower since several systems of non-linear equations have to be solved systematically. Since the amount of non-linear systems is higher in RCC-IG its real simulation time (1381.7s) is even larger that the simulation time of the SCIG WF (563.76s). In any case it could be considered that this simulation times are relatively low, so it could be considered that the method is fast enough.

Further improvements on simulation time could be achieved if the non-linear systems solving processes are optimized in some way (changing the solver, improving the initial guess value, increasing the tolerance…).

9.4 Conclussions

In this chapter many results and conclusions regarding annual energy production evaluation were presented for specific WFs configurations employing a first approach of the developed method.

A turbine size of 2 MW was used for a WF made up of 100 WTs distributed in ten rows of 10 WTs. Aggregated WTs models were employed in each row. The power measuring point was chosen after the transformer of each WT, so the WF network was not modeled. No mechanical losses were considered, ideal transformers were employed and the converter power losses were modeled through a static factor μ.

Using these model conditions three symmetric wind speed distribution across the WF were employed. They were described through a wind factor which defines the maximum deviation from the average WF wind speed that a single WT of a row can experience.

In general terms it can be stated that the DFIG WT was the most efficient from an aerodynamic point of view, followed by the full-scale SPMSG, the RCC-IG and the SCIG

The new WT concept evaluated, RCC-IG WT, showed promising features under certain wind conditions – low wind factor.

Moreover the simulation speed was tested, showing a very fast performance for DFIG and full-scale SPMSG (few seconds). For SCIG and RCC-IG the simulation time needed was longer due to the solution of non-linear systems of equations (563s and 1381s respectively)

Chapter 10 Conclusions And Future work

10.1 Conclusions

In this report a first approach of the proposed method has been employed to evaluate annual energy production of the four proposed off-shore VSC-HVDC WF configurations (full scale SPMSG, DFIG, RCC-WRIG, SCIG). Results from simulations were evaluated and compared and reasonable results were obtained.

A new variable speed wind turbine concept based on RCC-WRIG were also evaluated, showing promising features under certain wind conditions.

It should be emphasized that specific results and conclusions can vary if WTs with different characteristics are employed or if e.g. the wind speed distribution across the WF varies. So the most important aspect of this report is that a proper evaluation method has been developed.

It should be noted that one the most difficult tasks involved in the development of this method was the search for proper modeling assumptions in order to simplify the system simulations.

It should be also stressed the modeling effort behind the original design of the RCC-IG WT steady state model. A similar design idea is also behind the SCIG WT steady state model.

10.2 Future work

Since more detailed models of the gear train, the transformers, the converters and the AC line have been derived but not implemented in simulation it is natural to propose the implementation of these components in the Simulink model as the next design step.

Other secondary future tasks could be:

- To include core losses in machines models.
- To consider several modulations methods for the converters.
- To consider different converter topologies.
- To derive and include a model of the DC-line transmission line in simulations.
- To develop WF dynamic models in order to be compared with the WF steady-state models.
- To optimize non-linear equations solvers in order to improve simulation speed.
- To implement the Simulink models in M-fuctions in order to develop a usable calculation tool based on a graphical interface.

Summarizing, a huge amount of work can be still done in this exciting field.

Chapter 11 REFERENCES

[1] Theodore Wildi, "Electrical Machines, Drives, and Power Systems", 5th ed. Prentice Hall, ISBN 0-13-093083-0, 2002.

[2] Albert Betz, "Das Maximum der theoretisch moglichen Ausnutzung des Windes durch Windmotoren, Zeitschrift fur das gesamte Turbinenwesen", Heft 26, September 26, 1920. (Theoretical possible maximum use of wind by wind-engines)"

[3] M. Godoy Simões, Felix A. Farret, "Renewable energy systems: design and analysis with induction generators", CRC Press LLC, ISBN 0-8493-2031-3, 2004.

[4] Diego M. Aguilera Forero, "Modelling and control of DC wind farms", Thesis for the degree of MSc in Enginnering, Institute of Energy Technology, Aalborg University, Denmark, 2003.

[5] Frede Blaabjerg, Zhe Chen, "Power Electronics for Modern Wind Turbines", Institute of Energy Technology, Aalborg University, Denmark, 2006.

[6] V. Aknmatov, A. Hejde Nielsen, "A Small Test Model of the Transmission Grid with a Large of shore Wind Farm for Education and Research at Technical University of Denmark", IEEE 2006

[7] Clemens Jauch, "Stability and Control of Wind Farms in Power Systems", Risø National Laboratory and Aalborg University, Risø-PhD-24(EN), ISBN 87-89179-63-3, 2006.

[8] Nicola Barberis Negra, "Offshore Wind Power: Grid Connection and Reliability", DONG Energy, Risø National Laboratory and Aalborg University, ISBN 978-87-89179-72-2, 2008.

[9] Sigrid Bolik, "Modelling and Analysis of variable speed Wind Turbines with Induction Generator during grid fault", PhD thesis in Electrical Engineering, Faculty of Science and Engineering, Aalborg University, 2004.

[10] Sigrid M. Bolik, *Grid requirements challenges for Wind Turbines,* Proceedings Fourth International Workshop on Large-Scale Integration of Wind Power and Transmission Networks for Offshore Wind Farms, October 2003, Billund, Denmark

[11] Julija Matevosyan, Thomas Ackermann, Sigrid Bolik, Lennart Söder, *Comparison of International Regulations for Connection of Wind Turbines to the Network*, NWPC '04, Grid Integration and Electrical Systems of Wind Turbines and Wind Farms, Chalmers University of Technology, 1-2 March 2004, Göteborg, Sweden.

[12] NECA, *National Electricity Code*, Version 1.0 Amendment 8.0, 1999 – 2003, Australia

[13] SP Transmission & Distribution, Scottish Hydro Electric, *Guidance Note for the connection of Wind Farms*, Issue No. 2.1.4, December 2002, Scotland

[15] W.L. Kling and J.G. Slootweg, "Wind turbines as Power Plants," in Proceedings of the IEEE/Cigre workshop on Wind Power and the Impacts on Power Systems, 17 - 18 June 2002, Oslo, Norway.

[16] GE Wind Energy GE Wind Turbine. Brochures. Available from http://www.gepower.com/prod_serv/products/wind_turbines/en/index.htm.

[17] Nordex wind turbine brochures. Available from http://www.nordexonline.com/en/products-services/wind-turbines.html.

[18]Vestas wind turbine brochures. Available from http://www.vestas.com/vestas/global/en/Products/Download_brochures/download brochurer.htm.

[19] Mohamed Ridha Khadraoui and Mohamed Elleuch, "Comparison between OptiSlip and Fixed Speed Wind Energy Conversion Systems", 5th International Multi-Conference on Systems, Signals and Devices, IEEE SSD 2008, pp 1-6.

[20] BTM Consults Aps. "International wind energy department word market update 2002," Forecast 2003–2007, 2003.

[21] M. P. Kazmierkowski, R. Krishnan, and F. Blaabjerg, *Control in Power Electronics- Selected Problems*. Academic Press, New York, 2002.

[22] Florin lov, Anca Daniela Hansen, Poul S0rensen and Nicolaos Antonio Cutululis, *"Mapping of grid faults and grid codes,"* Technical report of Risø National Laboratory, Technical University of Denmark Roskilde, Denmark, July 2007.

[23] Krause, P.C., Wasynczuk, O., Sudhoff, S.D. – Analysis of Electric Machinery, IEEE Press 1995, ISBN 0-7803-1101-9;

[24] J.T.G. Pierik, J. Morren, E.J. Wiggelinkhuizen, S.W.H de Haan, T.G. van Engelen, J. Bozelie, "Electrical and control aspects of offshore wind farms II (Erao II), Volume 1: Dynamic models of wind farms", Technical report of ECN&TUD, ECN-C-04-050, Netherlands, 2004.

[25] F. Iov, A.D. Hansen, P. Sørensen and F. Blaabjerg, "Wind Turbine Blockset in Matlab/Simulink. General Overview and Description of the Models", Aalborg University, March 2004, ISBN 87-89179-46-3.

[26] Rudervall R, Charpentier JP, Sharma R. High voltage direct current (HVDC) transmission systems technology review paper. Presented at Energy Week 2000, Washington, DC, 7–8 March 2000

[27] LM Fernández, F Jurado, JR Saenz, "Aggregated dynamic model for wind farms with doubly fed IG wind turbines" Renewable Energy, 2008.

[28] Adelina Agap, Adrian Constantin, Cristina Dragan, Borja Imanol Markinez, "Modeling Operation and Control of HVDC Connected Offshore Wind Farms", 3rd semester project, IET, Aalborg University, January 15, 2009.

[29] Douglas Westwood (2006): POWER: Pushing Offshore Wind Energy Regions. Trans-national Offshore Wind Supply Chain Study - Appendices. Douglas Westwood, UK, May 2006.

[30] Göran Dandanell, "Kriegers Flak - transnational use of offshore wind power" EWEA Policy Conference Large Scale Integration of Wind Energy Brussels, 7th of November 2006.

[31] F. Iov, P. Soerensen, A. Hansen, F. Blaabjerg, "Modelling and Control of VSC based DC Connection for Active Stall Wind Farms to Grid", IEE Japan Trans. on Industry Applications, 2006, Vol. 126-D, No. 5, pp. 622-629.

[32] F. Iov, R. Teodorescu, F. Blaabjerg, B. Andresen, J. Birk, J. Miranda, "Grid code compliance of grid-side converter in wind turbine systems", Proc. of PESC 2006 Conference, 18-22 June 2006, Jeju, South-Korea, 7 p., IEEE Catalog Number: 06CH37819C, ISBN: 1-4244-9717-7, ISSN 02-75-9306.

[33] F. Iov, M. Ciobotaru, F. Blaabjerg, "Power electronics control of wind energy in distributed power systems" Aalborg University, Institute of Energy Technology, PEDS'07 Conference, Thailand, 2007.
[34] Luis M. Fernández, J.R. Saenz, Francisco Jurado, "Dynamic models of wind farms with fixed speed wind turbines", Renewable Energy 31 (2006) 1203-30.

[35] Akhmatov V., Knudsen H., "An aggregate model of a grid-connected, large-scale, offshore wind farm and power system", Risø National Laboratory, 2001, Risø-R-1281.

[36] Ledesma P., Usaola J. Rodríguez J.L., "Transient stability of a fixed speed wind farm", Renewable Energy 28 (2003) 1341-55.

[37] Stavrakis G.S., Kariniotakis G.N., "A general simulation algorithm for the accurate assessment of isolated diesel wind turbines systems interaction" - Part I and II, IEEE Trans Energy Convers 1995, 10(3), 577-90.

[38] Danish Wind Industry Association. http://www.windpower.dk

[39] Ervin Spahic, Gerd Balzer, "Offshore Wind Farms – VSC-based HVDC Connection" ISBN: 978-5-93208-034-4, Power Tech, 2005 IEEE Russia.

[40] Gunnar Asplund, "Electric transmission system in change", PESC Conference, Rodhes (Greece), June 2008.

[41] N. Barberis Negra, J. Todorovic, T. Ackermann, "Loss evaluation of HVAC and HVDC transmission solutions for large offshore wind farms" Electric power systems research, **ISSN** 0378-7796.

[42] Anca D. Hansen, Florin Iov, Poul Sørensen, Nicolaous Cutululis, Clemens Jauch, Frede Blaabjerg. *Dynamic wind turbine models in power system simulation tool DIgSILENT*. Risø National Laboratory, Roskilde December 2003

[43] ABB AB, Grid Systems,"*HVDC. It's time to connect*", Technical description of HVDC Light technology.

[44] Siemens AG website. Power Transmission Solutions - HVDC Plus for off-shore applications. [cited 2008 October]. Available from: https://www.energy-portal.siemens.com/irj/portal/ptd/public/en/global-04/home?prodname=KN030112

[45] Lars Helle, "Modelling and Comparison of Power Converters for Doubly Fed Induction Generators in Wind Turbines", PhD. Thesis, Aalborg University, Institute of Energy Technology, ISBN 978-87-89179-66-7, April 2007.

[46] Lars Helle, Stig Munk-Nielsen, "Comparison of Converter Efficiency in Large Variable Speed Wind Turbines", Aalborg University, Institute of Energy Technology, APEC 2001.

[47] J.A.Baroudi, V.Dinavahi, A.M. Knight, "A review of power converter topologies for wind generators", 0-7803-8987-5/05/$20.00, IEEE, 2005.

[48] Florin Iov, "VSC based DC Transmission System for connecting Active Stall Wind Farms to Grid", Aalborg University, October 2004.

[49] Andreas Petersson *"Analysis, Modelling and Control of Doubly-Fed Induction Generators for Wind Turbines"*, Chalmers University of Technology, 2005, ISBN 91-7291-600-1.

[50] Tao Sun *"Power Quality of Grid-Connected Wind Turbines with DFIG and Their Interaction with the Grid"*, Institute of Energy Technology Aalborg University, Denmark, May 2004.

[51] R. Pena, J.C. Clare, G.M. Asher *"Doubly fed induction generator using back-to back PWM converters and its application to variable-speed wind-energy generation"* IEEE Proc.-Electr. Power Appl., Vol 143, No 3, May 1996, pp. 231-241.

[52] R. Datta, V.T. Ranganathan, *"Decoupled Control of Active and Reactive Power for a Grid-connected Doubly-fed Wound Rotor Induction Machine without Positioning Sensors",* IEEE Industry Applications Conference, 1999**,** Vol. 4, pp. 2623-2630.

[53]"Relationship between Space Vector Modulation and three-phase Carrier-Based PWM - A comprehensive analysis", IEEE TRANSACTIONS ON INDUSTRIAL ELECTRONICS, VOL. 49, NO. 1, FEBRUARY 2002, pag. 186-196, 0278–0046/02$17.00.

[54] A. E. Fitzgerald, Charles Kingsley Jr., Stephen D. Umans, *"Electrical Machinery"*, 6th ed. McGRAW-HILL, ISBN 0-07-366009-4, 2003.

[55] Kunio Koga, Ftyum Ueda, Toshikatsu Soncda,, "*Evaluations on operating performances of three typical V/f control schemes in PWM inverter drive induction motor system*", IEEE Industrial Electronics, Control and Instrumentation, 1991, Vol.1, pp. 701-706.

[56] Thomas Ackermann, *"Wind Power in Power Systems*", John Wiley & Sons, ISBN 0-470-85508-8, 2006.

[57] L. M. Fernández, C. A. García1, F. Jurado, *"Control System of Doubly Fed Induction Generators Based Wind TurbinesWith Production Limits"*, IEEE International Conference on Electric Machines and Drives, 2005, pp. 1936 - 1941 .

[58] Makund R. Patel, "*Wind and Solar Power Systems: Design, Analysis*", 2nd ed. Taylor & Francis, ISBN 0-8493-1570-0, 2006.

[59] T. Burton, D. Sharpe, N. Jenkins, E. Bossanyi, "*Wind Energy Handbook*", Jhon Wiley & Sons, ISBN 0-471-48997-2, 2001.

[60] A. McIver, D. G. Holmes, and P. Freere, "*Optimal control of a variable Speed wind turbine under dynamic wind conditions",* IEEE Industrial Application Society Annual Meeting, Vol. 3:pp. 1692–1698, 6.-10. October 1996.

[61] M. P. Papadopaulos and S. A. Papathanassiou, "*Dynamic characteristics of variable speed wind turbine configurations",* International Conference on Electrical Machines, Vol. 3:pp. 1723–1728, 2.-4. September 1998

[62] Anders Grauers, *"Efficiency of three wind energy generator Systems"*, IEEE Transactions on Energy Conversion, Vol. 11 No. 3:pp. 650–657, September 1996.

[63] R. Hoffmann and P. Mutschler, *"The influence of control strategies on the energy capture of wind turbines"*, IEEE Industrial Application Society Annual Meeting, Vol. 2:pp. 886–893, 8.-12. October 2000.

[64] Árpád Kelemen, Mária Imecs, "*Vector Control of AC Drives. Volume 1: Vector Control of Induction Machine Drives*", 1st Edition, OMIKK PUBLISHER, ISBN 963-593-140-9, 1991.

[65] Mihai Ciobotaru, Florin Iov, Yue Fan, Steffano Bifaretti, Pericle Zanchetta *"Advanced Power Converter for Universal and Flexible Management in Future Electricity Network"* UNIFLEX-PM, Project Number: 019794(SES6).

[66] Perera, P. D. Chandana, "*Sensorless Control of Permanent-Magnet Synchronous Motor Drives"*, Ph. D. Thesis in Electrical Engineering, Institute of Energy Technology, Aalborg University, 2002.

[67] "eCOG1X 3-Phase PMSM Control with Sensor Feedback", Cyan Technology application note, 2001.

[68] Victor R. Stefanovic, and Slobodan N. Vukosavic, "Space vector PWM Voltage Control with Optimized Switching Strategy", *IEEE IAS-1992 Ann. Meeting*, pp. 1025 -1033.

[69] Coy Studer, Ali Keyhani, "Study of cogging torque in permanent magnet machines", IEEE Industry Applications Conference, 1997. Thirty-Second IAS Annual Meeting, Vol.1:pp.42-49

[70] Young-Jin Lee, Young-Jin Yoon, Young-Ho Kim and Man-Hyung Lee, "A Study on the Sensorless PMSM Control using the Superposition Theory", *International Journal of the Korean Society of Precision Engineering Vol. 4, No. 2, March 2003*

[71] Adrian Vasile Timbuş, "Sensorless Control of PMSM", Master Thesis in Power Electronics and Drives, Institute of Energy Technology, Aalborg University, February/June 2003.

[72] Erwan Simon, *"Implementation of a Speed Field Oriented Control of 3-phase PMSM Motor using TMS320F240"*, TEXAS INSTRUMENTS Application report SPRA588, 1999.

Appendix A M-files

A.1 Aeromechanical Characteristic of a 2MW Wind Turbine

```
%Calculation of the Power and Torque in the Shaft for different Wind speeds
%and Generator speeds of a 2MW Wind Turbine

clc
clear all

%Cp parameters
c1=0.73;
c2=151;
c3=0.58;
c4=0.002;
c5=2.14;
c6=13.2;
c7=18.4;
c8=-0.02;
c9=-0.003;

Beta=0; %pitch angle [Degrees]
rho=1.225; %air density [Kg/m^3]
Pn=2e6; %nominal Power [W]
wn=1500; %nominal speed [rpm]
GearboxRT=1680/18.1; %Gearbox rate (DFIG=1680/18.1, VRCC=1516/18.1,
PMSG=1500/18.1)
R=40;%Blade radius [m]
vwind=[4:1:12]; %wind speed [m/s]
f=50; %grid frequency [Hz]
p=2; %pole pairs
ws=(f/p)*2*pi;%stator speed [rad/s]
omega=[1:25:1000*3]; %rotor speed [rpm]
romega=(omega*2*pi/60)/(GearboxRT); %calculate the turbine speed [rad/s]

%%

for k=1:length(vwind)
%calculation of the tip-speed ratio (lambda)
    lambda(k,:)=((omega.*2.*pi./60)./GearboxRT).*R./vwind(k);
%calculation of the Power coefficient
    lambda_i(k,:)=1./((lambda(k,:)+1e-5)+c8*Beta)-c9/(Beta^3+1);
    cp(k,:) = c1 .* (c2.*lambda_i(k,:) - c3*Beta - c4*Beta^c5 -c6).* exp( -
c7 .* lambda_i(k,:));
%calculation of the Powoer in the shaft
    Pshaft(k,:) = (0.5*rho*pi*R^2).*vwind(k).^3.*cp(k,:);

    T(k,:)=Pshaft(k,:)./romega; %returns the wind turbine torque
end


%%
```

```
Pshaft=1/2*(Pshaft+abs(Pshaft)); %only positive values of Pref
T=1/2*(T+abs(T))%only positive values of T
Pshaft_tr=Pshaft';
[w,f]=max(Pshaft_tr); %returns in w the maximum value for each column of
Pshaft_tr
Pshaft_3 = w; %Pshaft_3 is the vector with the maximum values of Pshaft_tr
ome=omega(f); %ome is the vector with the values of omega_ for each
position k in which there is the maximum value of Pshaft_tr

T_tr=T';
[w1,f1]=max(T_tr); %returns in w the maximum value for each column of T_tr
T_3 = w1; %T_3 is the vector with the maximum values of T_tr
ome1=omega(f1); %ome is the vector with the values of omega_ for each
position k in which there is the maximum value of Pshaft_tr


figure(1)
plot(omega/wn,Pshaft/Pn)
title('Pshaft-Omega curves')
xlabel('Omega [pu]')
ylabel('Power [pu]')
hold on
plot(ome/wn,Pshaft_3/Pn,'LineWidth',2,'color','black')
hold off

figure(2)
plot(omega,T)
title('Wind Torque for different Wind speeds')
xlabel('omega [rad/s]')
ylabel('Torque [Nm]')
hold on
plot(ome1,T_3,'LineWidth',2,'color','black')
hold off
```

A.2 Wind speed annual distribution (Weibull)

```
%Calculation of the annual WEIBULL distribution of the Wind

clc
clear all

Vwind=[4:1:25]; %Wind speed [m/s]
%Weibull parameters for an off-shore Wind Farm
c=2;
a=11.38;
%Calculation of the distribution
P=365*24*(c./a.^c).*Vwind.^(c-1).*exp(-(Vwind./a).^c);
plot (Vwind,P)
hold on
hold off
Pa=zeros(1,26);
for t=2:1:26
    Pa(t)=P(t)+Pa(t-1);
end
```

```
    Pa=P(1)+Pa;
```

A.3 Full-scale SPMSG

A.3.1 Torque look-up table

```
%Calculation of the PMSG Torque Look-up table used in simulations.

clc
clear all

%Cp parameters
c1=0.73;
c2=151;
c3=0.58;
c4=0.002;
c5=2.14;
c6=13.2;
c7=18.4;
c8=-0.02;
c9=-0.003;

Beta=0; %Pitch angle [Degrees]
lambda =[0:0.5:20]; %tip-speed-ratio
vwind=[4:1:25]; %wind-speed [m/s]
GearBoxRT=1500/18.1; %Gearbox rate (DFIG=1680/18.1, VRCC=1516/18.1,
PMSG=1500/18.1
rho=1.225; %air density [Kg/m^3]
R=40; %radius of the rotor [m]
Tn=12862.3385850231*1.0442445; %nominal stator power [W
omega_n=1500; %nominal speed [rpm]
f=50; %frequency [HZ]
p=2; %pole pairs
ws=(f/p)*2*pi; %stator speed [rpm]
%%

%in next steps the calculation of the cp curve for different
%tip-speed-ratio for Beta=0 is done.

lambda_i=1./(lambda+c8.*Beta)-c9./(Beta.^3+1);
cp = c1 * (c2*lambda_i - c3*Beta - c4.*Beta.^c5 -c6).* exp( -c7 *
lambda_i);
cp=1/2*(cp+abs(cp)); %only positive values of Pref

figure(1)
plot(lambda,cp)
title('Cp-Lambda curves')
xlabel('Lambda')
ylabel('Cp')
%%

%In this section the calculation of the Maximum Torque Point look up table
valiues is done
```

```
%Find the value of the cp max for Beta equal to zero. i is the position
%where cp is max.
[cpmax i]=max(cp);
%lambda(i) is the lambda optimum
lambda_opt=lambda(i);
omega=lambda_opt.*vwind/R;
%next we introduce the pitch control limiting the rotor speed to its
%nominal value 18.1 rpm.
for u=1:length(omega)
    if omega(u)>18.1*2*pi/60
        omega(u)=18.1*2*pi/60;
    end
end
omega_gen=omega*GearBoxRT;
%A new lambda and cp must be calculate.
Lambda2=omega*R./vwind;
lambda_i1=1./(Lambda2+c8.*Beta)-c9./(Beta.^3+1);
cp = c1 * (c2*lambda_i1 - c3*Beta - c4.*Beta.^c5 -c6).* exp( -c7 *
lambda_i1);
%calculate the value of Pshaft and Torque for optimal lambda and max cp,
for different
%rotor speed
Pshaftr = ((0.5*rho*pi*R^2)*R^3.*(omega).^3./(Lambda2).^3).*cp;
Tshaft=Pshaftr./omega_gen;

for u=1:length(Tshaft)
    if Tshaft(u)>Tn
        Tshaft(u)=Tn;
    end
end
Pt=Tshaft.*omega_gen;


figure (2)
xlabel('Wind speed [m/s]','FontSize', 16)
ylabel('Power [W]','FontSize', 16)
plot(vwind,omega/(18.1*2*pi/60))
hold on
plot(vwind,Pt/2e6,'color','red')
hold on
plot(vwind,Pshaftr/2e6, 'color', 'green')
hold off

figure (3)
xlabel('Wind speed [m/s]','FontSize', 16)
ylabel('Torque [N/m^2]','FontSize', 16)
plot(vwind,Tshaft,'color','green')
hold on
```

A.4 DFIG

A.4.1Power look-up table

```
%Calculation of the DFIG Power Look-up table used in simulations.
```

```
clc
clear all

%Cp parameters
c1=0.73;
c2=151;
c3=0.58;
c4=0.002;
c5=2.14;
c6=13.2;
c7=18.4;
c8=-0.02;
c9=-0.003;

Beta=0; %Pitch angle [Degrees]
lambda =[0:0.5:20]; %tip-speed-ratio
vwind=[4:1:25]; %wind-speed [m/s]
GearBoxRT=1680/18.1; %Gearbox rate (DFIG=1680/18.1, VRCC=1516/18.1,
PMSG=1500/18.1
rho=1.225; %air density [Kg/m^3]
R=40; %radius of the rotor [m]
Pn=1.7859e+006; %nominal stator power [W]
omega_n=1500; %nominal speed [rpm]
f=50; %frequency [HZ]
p=2; %pole pairs
ws=(f/p)*2*pi; %stator speed [rpm]
%%

%in next steps the calculation of the cp curve for different
%tip-speed-ratio for Beta=0 is done.

lambda_i=1./(lambda+c8.*Beta)-c9./(Beta.^3+1);
cp = c1 * (c2*lambda_i - c3*Beta - c4.*Beta.^c5 -c6).* exp( -c7 *
lambda_i);
cp=1/2*(cp+abs(cp)); %only positive values of Pref

figure(1)
plot(lambda,cp)
title('Cp-Lambda curves')
xlabel('Lambda')
ylabel('Cp')
%%

%In this section the calculation of the MPP look up table values is done

%Find the value of the cp max for Beta equal to zero. i is the position
%where cp is max.
[cpmax i]=max(cp);
%lambda(i) is the lambda optimum
lambda_opt=lambda(i);
omega=lambda_opt.*vwind/R;
%next we introduce the pitch control limiting the rotor speed to its
%nominal value 18.1 rpm.
for u=1:length(omega)
    if omega(u)>18.1*2*pi/60
        omega(u)=18.1*2*pi/60;
    end
```

```
end
omega_gen=omega*GearBoxRT;

%A new lambda and cp must be calculate.
s=(ws-omega_gen)/ws;
Lambda2=omega*R./vwind;
lambda_i1=1./(Lambda2+c8.*Beta)-c9./(Beta.^3+1);
cp = c1 * (c2*lambda_i1 - c3*Beta - c4.*Beta.^c5 -c6).* exp( -c7 *
lambda_i1);
%calculate the value of Pshaft for optimal lambda and max cp,for different
%rotor speed
Pshaft = ((0.5*rho*pi*R^2)*R^3.*(omega).^3./(Lambda2).^3).*cp;
Pshaft2=Pshaft;

%Power in the stator and rotor are calculated.

Ps=Pshaft./(1-s);
for u=1:length(Ps)
    if Ps(u)>Pn
        Ps(u)=Pn;
    end
end
Pr=s.*Ps;
Pshaft1=Ps-Pr;
Ps1=Pshaft1./(1-s);
Pr1=s.*Ps1;

WP(:,1)=vwind;
WP(:,2)=s;
WP(:,3)=omega_gen*(60/(2*pi));
WP(:,4)=Ps;
WP(:,5)=Pr;
WP(:,6)=Pshaft;


figure (2)
plot(vwind,Pshaft,'+')
title('Pshaft-Wind speed curve')
xlabel('Wind speed [m/s]', 'FontSize', 16)
ylabel('Power [W]')
hold on
plot(vwind,Ps,'color','green')
hold on
plot(vwind,Pshaft1,'color','black')
hold on
plot(vwind,Pr,'color','red')
hold off
```

A.5 SCIG

M-functions used to calculate the reference stator power applied to the SCIG generator. Next figure shows the simulink model used to calculate the reference rotor speed (wr) and the reference stator power (Ps).

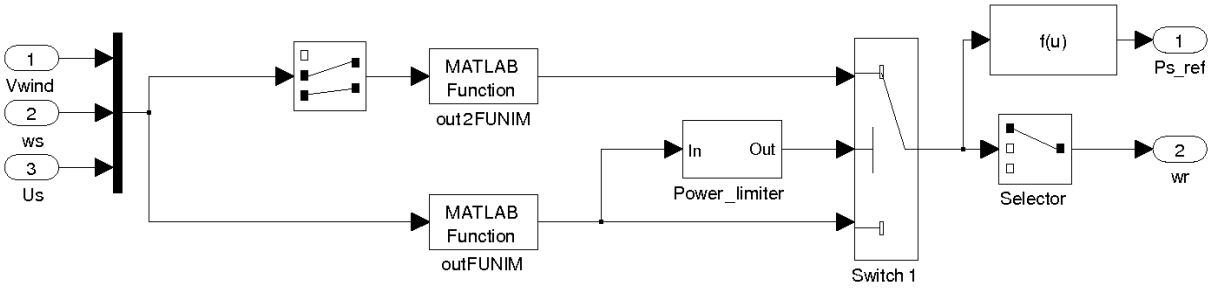

0.1 Simulink model of the power-speed reference calculation

A.5.1 outFUNIM

```
function [X] = outFUNIM(Vwind,ws,Us)

%INITIAL ELECTRICAL PARAMETERS
Rs=2.2e-3; %Stator resistance [Ohm]
Rr=2.8e-3; %Rotor resistance referred to the stator [Ohm]
L_s=83e-6; %Stator inductance [H]
Lr=83e-6; %Rotor inductance referred to the stator [H]
Lm=2.6e-3; %Mutual inductance [H]
p=2; %pole pairs
Rfe=0; %Mutual resistance [H]
Nph=3; %Number of phases
R1=Rs;
R2p=Rr;
X1=ws*L_s;
X2p=ws*Lr;
Xm=ws*Lm;

%note: MACHINE ELECTRICAL EQUATIONS BY USE OF THEVENIN'S THEOREM
%EQUIVALENT VOLTAGE SOURCE
V1eq=Us*Xm/(sqrt((R1^2)+(X1+Xm)^2));
%EQUIVALENT STATOR IMPEDANCE
Z1eq=Xm*(sqrt((R1)^2+(X1)^2))/(sqrt((R1)^2+(X1+Xm)^2));

%%%OPERATING POINT ESTIMATION%%%
opts = optimset('Display','off');
wr_out = fsolve(@(wr) myfun3IM(wr,Vwind,ws,R2p,X2p,Nph,V1eq,Z1eq), 1.01*ws,
opts);
s_out=(ws-wr_out)/ws;
%%%MACHINE ELECTRICAL EQUATIONS%%%
%ROTOR CURRENT RESPECT TO STATOR
I2p_out=V1eq/(Z1eq+(sqrt((R2p/s_out)^2+(X2p)^2)));
%ELECTROMECHANICAL TORQUE
Tr_out=(Nph/(ws/p))*(R2p/s_out)*(I2p_out^2);

X(1,:)=wr_out;
X(2,:)=Tr_out;
X(3,:)=s_out;
end
```

A.5.2 out2FUNIM

```
function [X] = out2FUNIM(ws,Us)

%INITIAL ELECTRICAL PARAMETERS
Rs=2.2e-3; %Stator resistance [Ohm]
Rr=2.8e-3; %Rotor resistance referred to the stator [Ohm]
L_s=83e-6; %Stator inductance [H]
Lr=83e-6; %Rotor inductance referred to the stator [H]
Lm=2.6e-3; %Mutual inductance [H]
p=2; %pole pairs
Rfe=0; %Mutual resistance [H]
Nph=3; %Number of phases

R1=Rs;
R2p=Rr;
X1=ws*L_s;
X2p=ws*Lr;
Xm=ws*Lm;


%note: MACHINE ELECTRICAL EQUATIONS BY USE OF THEVENIN'S THEOREM
%EQUIVALENT VOLTAGE SOURCE
V1eq=Us*Xm/(sqrt((R1^2)+(X1+Xm)^2));
%EQUIVALENT STATOR IMPEDANCE
Z1eq=Xm*(sqrt((R1)^2+(X1)^2))/(sqrt((R1)^2+(X1+Xm)^2));

%%%OPERATING POINT ESTIMATION%%%

opts = optimset('Display','off');
wr_out = fsolve(@(wr) myfun4IM(wr,ws,R2p,X2p,Nph,V1eq,Z1eq), 1.01*ws,
opts);
s_out=(ws-wr_out)/ws;
%%%MACHINE ELECTRICAL EQUATIONS%%%
%ROTOR CURRENT RESPECT TO STATOR
I2p_out=V1eq/(Z1eq+(sqrt((R2p/s_out)^2+(X2p)^2)));
%ELECTROMECHANICAL TORQUE
Tr_out=(Nph/(ws/p))*(R2p/s_out)*(I2p_out^2);

X(1)=wr_out;
X(2)=Tr_out;
X(3)=s_out;
end
```

A.5.3 myfun3IM

```
function Fx3 = myfun3IM(wr,Vwind,ws,R2p,X2p,Nph,V1eq,Z1eq)

p=2; %pole pairs

%%%MACHINE ELECTRICAL EQUATIONS%%%
```

```
s=(ws-wr)/ws;
%ROTOR CURRENT RESPECT TO STATOR
I2p=V1eq/(Z1eq+(sqrt((R2p/s)^2+(X2p)^2)));
%ELECTROMECHANICAL TORQUE
T1=(Nph/(ws/p))*(R2p/s)*(I2p^2);

%%%TURBINE AERODYNAMIC EQUATIONS%%%

%AERODYNAMIC PARAMETERS
c1=0.73;
c2=151;
c6=13.2;
c7=18.4;
c9=-0.03;
R=40;
rho=1.225;
A=pi*(R^2);
Gbox=1500*1.010/18.1;
omeg_r=wr/(Gbox*p);
%POWER COEFFICIENT FOR THETA = 0
Cp=(((c1*c2*Vwind)/(omeg_r*R))-c1*c2*c9-c1*c6)*exp(c7*c9-
(c7*Vwind/(omeg_r*R)));
%AEROMECHANICAL TORQUE
Taero=-0.5*rho*A*(Vwind^3)*(1/omeg_r)*Cp;
%GEAR-BOX
T2=Taero/Gbox;

%FUNCTION TO SOLVE
Fx3 = T1-T2;
end
```

A.5.4 myfun4IM

```
function Fx4 = myfun4IM(wr,ws,R2p,X2p,Nph,V1eq,Z1eq)

%%%MACHINE ELECTRICAL EQUATIONS%%%

s=(ws-wr)/ws;
%ROTOR CURRENT RESPECT TO STATOR
I2p=V1eq/(Z1eq+(sqrt((R2p/s)^2+(X2p)^2)));
p=2;
%ELECTROMECHANICAL TORQUE
T1=(Nph/(ws/p))*(R2p/s)*(I2p^2);

%%%TURBINE AERODYNAMIC EQUATIONS%%%

%AERODYNAMIC PARAMETERS
Gbox=1500*1.01/18.1;
omeg_r=wr/(Gbox*p);
Pshaft=-(2e6*1.01);
%AEROMECHANICAL TORQUE
Taero=Pshaft*(1/omeg_r);
%GEAR-BOX
T2=Taero/Gbox;
```

```
%FUNCTION TO SOLVE
Fx4 = T1-T2;
end
```

A.6 RCC

A.6.1 Mechanical Characteristic for the maximum and minimum resistance

```
%Calculation of the mechanical characteristic of an RCC for the maximum and
%minimum resistance

clear all
clc

%parameters
ws=50*2*pi; %Stator speed [rad/s]
Us=690; %Stator voltage [V]
Rs=2.2e-3; %Stator Resistance [Ohm]
Rr=2.8e-3; %Rotor Resistance referred to the stator [Ohm]
L_s=83e-6; %Stator Inductance [H]
Lr=83e-6; %Rotor Inductance referred to the stator [H]
Lm=2.6e-3; %Mutual Inductance [H]
p=2; %pole pairs
Rfe=0; %Mutual resistance [Ohm]
Nph=3; %Number of phases
s=0:0.001:1; %Slip
R1=Rs;
R2p=[Rr,0.0141648929889758];
X1=ws*L_s;
X2p=ws*Lr;
Xm=ws*Lm;

%Calculation of the torque for different rotor resistances
V1eq=Us*Xm/(sqrt((R1^2)+(X1+Xm)^2));
Z1eq=Xm*(sqrt((R1)^2+(X1)^2))/(sqrt((R1)^2+(X1+Xm)^2));
for t=1:length(R2p)
I2p(t,:)=V1eq./(Z1eq+(sqrt((R2p(t)./s).^2+(X2p)^2)));
T1(t,:)=(Nph/ws)*(R2p(t)./s).*(I2p(t,:).^2);
end

figure(1);
plot(s,T1);
title('Torque characteristic for different rotor Resistance', 'FontSize',
16)
xlabel('slip', 'FontSize', 16)
ylabel('Torque [N/m^2]', 'FontSize', 16)
hold off
```

A.6.2 Power look-up table

```
%Calculation of the RCC Power Look-up table used in simulations.

clc
clear all

%Cp parameters
c1=0.73;
c2=151;
c3=0.58;
c4=0.002;
c5=2.14;
c6=13.2;
c7=18.4;
c8=-0.02;
c9=-0.003;

Beta=0; %Pitch angle [Degrees]
lambda =[0:0.5:20]; %tip-speed-ratio
vwind=[4:1:25]; %wind-speed [m/s]
GearBoxRT=1500*1.01/18.1; %Gearbox rate (DFIG=1680/18.1, VRCC=1516/18.1,
PMSG=1500/18.1)
rho=1.225; %air density [Kg/m^3]
R=40; %radius of the rotor [m]
Pn=2020000; %nominal stator power [W]
omega_n=1500; %nominal speed [rpm]
f=50; %frequency [HZ]
p=2; %pole pairs
ws=(f/p)*2*pi; %stator speed [rpm]
%%

%in next steps the calculation of the cp curve for different
%tip-speed-ratio for Beta=0 is done.

lambda_i=1./(lambda+c8.*Beta)-c9./(Beta.^3+1);
cp = c1 * (c2*lambda_i - c3*Beta - c4.*Beta.^c5 -c6).* exp( -c7 *
lambda_i);
cp=1/2*(cp+abs(cp)); %only positive values of Pref

figure(1)
plot(lambda,cp)
title('Cp-Lambda curves')
xlabel('Lambda')
ylabel('Cp')
%%

%In this section the calculation of the MPP look up table values is done

%Find the value of the cp max for Beta equal to zero. i is the position
%where cp is max.
[cpmax i]=max(cp);
%lambda(i) is the lambda optimum
lambda_opt=lambda(i);
omega=lambda_opt.*vwind/R;
%next we introduce the pitch control limiting the rotor speed to its
%nominal value 18.1 rpm.
for u=1:length(omega)
    if omega(u)>18.1*2*pi/60
        omega(u)=18.1*2*pi/60;
    end
```

```
end
omega_gen=omega*GearBoxRT;
%A new lambda and cp must be calculate.
s=(ws-omega_gen)/ws;
Lambda2=omega*R./vwind;
lambda_i1=1./(Lambda2+c8.*Beta)-c9./(Beta.^3+1);
cp = c1 * (c2*lambda_i1 - c3*Beta - c4.*Beta.^c5 -c6).* exp( -c7 *
lambda_i1);
%calculate the value of Pshaft for optimal lambda and max cp, for different
%rotor speed
Pshaft = ((0.5*rho*pi*R^2)*R^3.*(omega).^3./(Lambda2).^3).*cp;
Pshaft2=Pshaft;
%values in per unit
Pshaft=Pshaft/Pn;
omega_pu=omega_gen*(60/(2*pi))/omega_n;

for u=1:length(Pshaft)
    if Pshaft(u)>1
        Pshaft(u)=1;
    end
end
WP(:,1)=vwind;
WP(:,2)=s;
WP(:,3)=omega_gen*(60/(2*pi));
WP(:,4)=Pshaft;

figure (2)
plot(vwind,Pshaft)
title('Pshaft-Wind speed curve')
xlabel('Wind speed [m/s]')
ylabel('Power [pu]')
hold off
```

A.6.3 Control functions

A.6.3.1 outFUNRr

```
function [X] = outFUNRr(Vwind,ws,Us,select)

%INITIAL ELECTRICAL PARAMETERS
Rs=2.2e-3; %Stator resistance [Ohm]
Rr=2.8e-3; %Rotor resistance referred to the stator [Ohm]
L_s=83e-6; %Stator inductance [H]
Lr=83e-6; %Rotor inductance referred to the stator [H]
Lm=2.6e-3; %Mutual inductance [H]
p=2; %pole pairs
Rfe=0; %Mutual resistance [H]
Nph=3; %Number of phases

R1=Rs;
X1=ws*L_s;
X2p=ws*Lr;
Xm=ws*Lm;
Rmax=5*Rr;
Rmin=Rr;

%note: MACHINE ELECTRICAL EQUATIONS BY USE OF THEVENIN'S THEOREM
```

```
%EQUIVALENT VOLTAGE SOURCE
V1eq=Us*Xm/(sqrt((R1^2)+(X1+Xm)^2));
%EQUIVALENT STATOR IMPEDANCE
Z1eq=Xm*(sqrt((R1)^2+(X1)^2))/(sqrt((R1)^2+(X1+Xm)^2));

%%%OPERATING POINT ESTIMATION%%%
R2p=Rmax*(select-2)-Rmin*(select-3);
opts = optimset('Display','off');
wr_out = fsolve(@(wr) myfun3Rr(wr,Vwind,ws,R2p,X2p,Nph,V1eq,Z1eq), 1.01*ws,
opts);
R_out=R2p;
s_out=(ws-wr_out)/ws;
%%%MACHINE ELECTRICAL EQUATIONS%%%
%ROTOR CURRENT RESPECT TO STATOR
I2p_out=V1eq/(Z1eq+(sqrt((R_out/s_out)^2+(X2p)^2)));
%ELECTROMECHANICAL TORQUE
Tr_out=(Nph/(ws/p))*(R_out/s_out)*(I2p_out^2);

X(1,:)=wr_out;
X(2,:)=Tr_out;
X(3,:)=R2p;
X(4,:)=s_out;
end
```

A.6.3.2 out2FUNRr

```
function [X] = out2FUNRr(ws,Us,select)

%INITIAL ELECTRICAL PARAMETERS
Rs=2.2e-3; %Stator resistance [Ohm]
Rr=2.8e-3; %Rotor resistance referred to the stator [Ohm]
L_s=83e-6; %Stator inductance [H]
Lr=83e-6; %Rotor inductance referred to the stator [H]
Lm=2.6e-3; %Mutual inductance [H]
p=2; %pole pairs
Rfe=0; %Mutual resistance [H]
Nph=3; %Number of phases

R1=Rs;
X1=ws*L_s;
X2p=ws*Lr;
Xm=ws*Lm;
Rmax=5*Rr;
Rmin=Rr;

%note: MACHINE ELECTRICAL EQUATIONS BY USE OF THEVENIN'S THEOREM
%EQUIVALENT VOLTAGE SOURCE
V1eq=Us*Xm/(sqrt((R1^2)+(X1+Xm)^2));
%EQUIVALENT STATOR IMPEDANCE
Z1eq=Xm*(sqrt((R1)^2+(X1)^2))/(sqrt((R1)^2+(X1+Xm)^2));

%%%OPERATING POINT ESTIMATION%%%
R2p=Rmax*(select-2)-Rmin*(select-3);
opts = optimset('Display','off');
wr_out = fsolve(@(wr) myfun4Rr(wr,ws,R2p,X2p,Nph,V1eq,Z1eq), 1.01*ws,
opts);
R_out=R2p;
```

```
s_out=(ws-wr_out)/ws;
%%%MACHINE ELECTRICAL EQUATIONS%%%
%ROTOR CURRENT RESPECT TO STATOR
I2p_out=V1eq/(Z1eq+(sqrt((R_out/s_out)^2+(X2p)^2)));
%ELECTROMECHANICAL TORQUE
Tr_out=(Nph/(ws/p))*(R_out/s_out)*(I2p_out^2);

X(1)=wr_out;
X(2)=Tr_out;
X(3)=R2p;
X(4)=s_out;
End
```

A.6.3.3 smaxFUNRr

```
function [s_max] = smaxFUNRr(Tr_opt,ws,Us)

%INITIAL ELECTRICAL PARAMETERS
Rs=2.2e-3; %Stator resistance [Ohm]
Rr=2.8e-3; %Rotor resistance referred to the stator [Ohm]
L_s=83e-6; %Stator inductance [H]
Lr=83e-6; %Rotor inductance referred to the stator [H]
Lm=2.6e-3; %Mutual inductance [H]
p=2; %pole pairs
Rfe=0; %Mutual resistance [H]
Nph=3; %Number of phases

R1=Rs;
X1=ws*L_s;
X2p=ws*Lr;
Xm=ws*Lm;
Rmax=5*Rr;
Rmin=Rr;

%note: MACHINE ELECTRICAL EQUATIONS BY USE OF THEVENIN'S THEOREM
%EQUIVALENT VOLTAGE SOURCE
V1eq=Us*Xm/(sqrt((R1^2)+(X1+Xm)^2));
%EQUIVALENT STATOR IMPEDANCE
Z1eq=Xm*(sqrt((R1)^2+(X1)^2))/(sqrt((R1)^2+(X1+Xm)^2));

%%%s_max CALCULATIONS%%%
R2p=Rmax;
opts = optimset('Display','off');
s_max=fsolve(@(s) myfun1Rr(s,Tr_opt,ws,V1eq,Z1eq,R2p,X2p,Nph), -0.06,
opts);
end
```

A.6.3.4 smaxFUNRr

```
function [s_min] = sminFUNRr(Tr_opt,ws,Us)

%INITIAL ELECTRICAL PARAMETERS
```

```
Rs=2.2e-3; %Stator resistance [Ohm]
Rr=2.8e-3; %Rotor resistance referred to the stator [Ohm]
L_s=83e-6; %Stator inductance [H]
Lr=83e-6; %Rotor inductance referred to the stator [H]
Lm=2.6e-3; %Mutual inductance [H]
p=2; %pole pairs
Rfe=0; %Mutual resistance [H]
Nph=3; %Number of phases

R1=Rs;
X1=ws*L_s;
X2p=ws*Lr;
Xm=ws*Lm;
Rmax=5*Rr;
Rmin=Rr;

%note: MACHINE ELECTRICAL EQUATIONS BY USE OF THEVENIN'S THEOREM
%EQUIVALENT VOLTAGE SOURCE
V1eq=Us*Xm/(sqrt((R1^2)+(X1+Xm)^2));
%EQUIVALENT STATOR IMPEDANCE
Z1eq=Xm*(sqrt((R1)^2+(X1)^2))/(sqrt((R1)^2+(X1+Xm)^2));

%%%s_min CALCULATIONS%%%
R2p=Rmin;
opts = optimset('Display','off');
s_min=fsolve(@(s) myfun2Rr(s,Tr_opt,ws,V1eq,Z1eq,R2p,X2p,Nph), -0.02,
opts);
end
```

A.6.3.5 myfun1Rr

```
function Fx1 = myfun1Rr(s,Tr_opt,ws,V1eq,Z1eq,R2p,X2p,Nph)

%ROTOR CURRENT RESPECT TO STATOR
p=2;
I2p_Rmax=V1eq/(Z1eq+(sqrt((R2p/s)^2+(X2p)^2)));

%ELECTROMECHANICAL TORQUE
T_Rmax=(Nph/(ws/p))*(R2p/s)*(I2p_Rmax^2);
Fx1=T_Rmax-Tr_opt;

end
```

A.6.3.6 myfun2Rr

```
function Fx2 = myfun2Rr(s,Tr_opt,ws,V1eq,Z1eq,R2p,X2p,Nph)

%ROTOR CURRENT RESPECT TO STATOR
I2p_Rmin=V1eq/(Z1eq+(sqrt((R2p/s)^2+(X2p)^2)));

%ELECTROMECHANICAL TORQUE
T_Rmin=(Nph/(ws/p))*(R2p/s)*(I2p_Rmin^2);
```

```
Fx2=T_Rmin-Tr_opt;

end
```

A.6.3.7 myfun3Rr

```
function [s_nom] = snomFUNRr(Tr_opt,ws,Us)

%INITIAL ELECTRICAL PARAMETERS
Rs=2.2e-3; %Stator resistance [Ohm]
Rr=2.8e-3; %Rotor resistance refered to the stator [Ohm]
L_s=83e-6; %Stator inductance [H]
Lr=83e-6; %Rotor inductance referred to the stator [H]
Lm=2.6e-3; %Mutual inductance [H]
p=2; %pole pairs
Rfe=0; %Mutual resistance [H]
Nph=3; %Number of phases

R1=Rs;
X1=ws*L_s;
X2p=ws*Lr;
Xm=ws*Lm;
Rnom=0.008389638040363; %aprox 3*Rr

%note: MACHINE ELECTRICAL EQUATIONS BY USE OF THEVENIN'S THEOREM
%EQUIVALENT VOLTAGE SOURCE
V1eq=Us*Xm/(sqrt((R1^2)+(X1+Xm)^2));
%EQUIVALENT STATOR IMPEDANCE
Z1eq=Xm*(sqrt((R1)^2+(X1)^2))/(sqrt((R1)^2+(X1+Xm)^2));

%%%s_mon CALCULATIONS%%%
R2p=Rnom;
opts = optimset('Display','off');
s_nom=fsolve(@(s) myfun2Rr(s,Tr_opt,ws,V1eq,Z1eq,R2p,X2p,Nph), -0.035,
opts);
end
```

A.6.3.7 myfun4Rr

```
function Fx4 = myfun4Rr(wr,ws,R2p,X2p,Nph,V1eq,Z1eq)


%%%MACHINE ELECTRICAL EQUATIONS%%%

s=(ws-wr)/ws;
%ROTOR CURRENT RESPECT TO STATOR
I2p=V1eq/(Z1eq+(sqrt((R2p/s)^2+(X2p)^2)));
p=2; %pole pairs
%ELECTROMECHANICAL TORQUE
T1=(Nph/(ws/p))*(R2p/s)*(I2p^2);

%%%TURBINE AERODYNAMIC EQUATIONS%%%
```

```
%AERODYNAMIC PARAMETERS
Gbox=1500*1.03/18.1; %Gear box ratio
omeg_r=wr/(Gbox*p); %generator speed[rad/s]
Pshaft=-2.06e6; %nominal power[W]
%AEROMECHANICAL TORQUE
Taero=Pshaft*(1/omeg_r);
%GEAR-BOX
T2=Taero/Gbox;

%FUNCTION TO SOLVE
Fx4 = T1-T2;
end
```

A.6.4 Calculation of R2pmax

A.6.4.1 R2pmax

```
%Calculation of R2pmax
clear all
clc

%Electircal parameters
ws=50*2*pi; %stator speed [rad/s]
Us=690; %Stator voltage [V]
Rs=2.2e-3; %Stator resistance [Ohm]
Rr=2.8e-3; %Rotor resistance referred to the stator [Ohm]
L_s=83e-6; %Stator inductance [H]
Lr=83e-6; %Rotor inductance referred to the stator [H]
Lm=2.6e-3; %Mutual inductance [H]
p=2; %pole pairs
Rfe=0; %Mutual resistance [Ohm]
Nph=3; %number of phases

R1=Rs;
X1=ws*L_s;
X2p=ws*Lr;
Xm=ws*Lm;

smax=-0.03; %Changing this value R2pmax is obtain

V1eq=Us*Xm/(sqrt((R1^2)+(X1+Xm)^2));
Z1eq=Xm*(sqrt((R1)^2+(X1)^2))/(sqrt((R1)^2+(X1+Xm)^2));
T2=-2060000/(161.7920);
opts = optimset('Display','off');
R2pmax_out=fsolve(@(R2p) myfunR2p(smax,ws,T2,R2p,X2p,Nph,V1eq,Z1eq), 10e-
3,opts )

RatioR=R2pmax_out/Rr

I2pmax=V1eq/(Z1eq+(sqrt((R2pmax_out/smax)^2+(X2p)^2)));
Pmax=3*I2pmax^2*R2pmax_out;
```

```
smin=-0.0107;
I2pmin=V1eq/(Z1eq+(sqrt((Rr/smin)^2+(X2p)^2)));
Pmin=3*I2pmin^2*Rr;
RatioP=100*(Pmin-Pmax)/Pmin
M=(2e6-Pmin)/2e6
Y=(2e6-Pmax)/2e6
```

A.6.4.2 myfunR2p

```
function Fx = myfunR2p(smax,ws,T2,R2p,X2p,Nph,V1eq,Z1eq)

p=2; %pole pairs

%ROTOR CURRENT RESPECT TO STATOR
I2p=V1eq/(Z1eq+(sqrt((R2p/smax)^2+(X2p)^2)));

%ELECTROMECHANICAL TORQUE
T1=(Nph/(ws/p))*(R2p/smax)*(I2p^2);

Fx=T1-T2;

end
```

A.7 Converter Losses m-file

```
clc
clear all

phi=-pi/2:0.001:pi/2;
M=0:0.1:1;
Irms=500;
%Irms_max=966.18;
for t=1:1:length(M)
It_avg(:,t)=(sqrt(2)/(2*pi)+sqrt(6)*M(t).*cos(phi)/12)*Irms;
Id_avg(:,t)=(sqrt(2)/(2*pi)-sqrt(6)*M(t).*cos(phi)/12)*Irms;
if abs(phi)<pi/6
    It(:,t)=sqrt((-M(t)+3*pi-
4*M(t).*cos(phi)^2+8*sqrt(3)*M(t).*cos(phi))/(12*pi))*Irms;
    Id(:,t)=sqrt(0.5-(-M(t)+3*pi-
4*M(t).*cos(phi)^2+8*sqrt(3)*M(t).*cos(phi))/(12*pi))*Irms;
    else %<pi/2
    It(:,t)=sqrt((2*M(t).*(2+sqrt(3)*sin(2*abs(phi))./2-cos(phi).^2-
2*sin(abs(phi))+2*sqrt(3)*cos(phi))+3*pi)/(12*pi))*Irms;
    Id(:,t)=sqrt(0.5-(2*M(t).*(2+sqrt(3)*sin(2*abs(phi))./2-cos(phi).^2-
2*sin(abs(phi))+2*sqrt(3)*cos(phi))+3*pi)/(12*pi))*Irms;
    end
end
Isw_avg=sqrt(2)/pi*Irms

figure (1)
plot(phi,It_avg/Irms,'LineWidth',2)
```

```
xlim([-pi/2 pi/2])
set(gca,'XTick',-pi/2:pi/4:pi/2)
set(gca,'XTickLabel',{'-pi/2','-pi/4','0','pi/4','pi/2'})
xlabel('Load angle (rad)','FontSize',16)
ylabel('Average transistor current (pu)','FontSize',16)
set(gca,'FontSize',16)
hold off

figure (2)
plot(phi,Id_avg/Irms,'LineWidth',2)
xlim([-pi/2 pi/2])
set(gca,'XTick',-pi/2:pi/4:pi/2)
set(gca,'XTickLabel',{'-pi/2','-pi/4','0','pi/4','pi/2'})
xlabel('Load angle (rad)','FontSize',16)
ylabel('Average diode current (pu)','FontSize',16)
set(gca,'FontSize',16)
hold off

figure(3)
plot(phi,It/Irms,'LineWidth',2)
xlim([-pi/2 pi/2])
set(gca,'XTick',-pi/2:pi/4:pi/2)
set(gca,'XTickLabel',{'-pi/2','-pi/4','0','pi/4','pi/2'})
xlabel('Load angle (rad)','FontSize',16)
ylabel('RMS transistor current (pu)','FontSize',16)
set(gca,'FontSize',16)
hold off

figure(4)
plot(phi,Id/Irms,'LineWidth',2)
xlim([-pi/2 pi/2])
set(gca,'XTick',-pi/2:pi/4:pi/2)
set(gca,'XTickLabel',{'-pi/2','-pi/4','0','pi/4','pi/2'})
xlabel('Load angle (rad)','FontSize',16)
ylabel('RMS diode current (pu)','FontSize',16)
set(gca,'FontSize',16)
hold off

figure(5)
plot(phi,Isw_avg/Irms,'LineWidth',2)
xlim([-pi/2 pi/2])
set(gca,'XTick',-pi/2:pi/4:pi/2)
set(gca,'XTickLabel',{'-pi/2','-pi/4','0','pi/4','pi/2'},'FontSize',16)
xlabel('Load angle (rad)','FontSize',16)
ylabel('Switching current function (pu)','FontSize',16)
set(gca,'FontSize',16)
hold off

alfa=0:0.0001:2*pi;
A=2/sqrt(3);
B=1/6;
f=50;
M=1;
Sa=M*A*(sin(alfa*f)+B*sin(3*alfa*f));
figure(6)
plot(alfa,Sa,'LineWidth',2)
xlim([0 2*pi*0.02])
%set(gca,'XTick',0:pi/2:2*pi)
```

```
%set(gca,'XTickLabel',{'0','pi/2','pi','3pi/2','2pi'})
xlabel('Angle (rad)','FontSize',16)
ylabel('Modulation function','FontSize',16)
set(gca,'FontSize',16)
hold off
```

Appendix B Total aerodynamic power

Parameters		
Blade Radius [m]		40
Air density [kg/m3]		1,225
Omega fixed [rad/s]		1,570796327
Vwind (m/s)	Weibull	Paero available (W)
4	478,2482468	9,42E+07
5	557,6757975	2,15E+08
6	614,7158591	4,09E+08
7	648,6726081	6,85E+08
8	660,2597681	1,04E+09
9	651,4148634	1,46E+09
10	625,0265094	1,92E+09
11	584,6115392	2,40E+09
12	533,9802348	2,84E+09
13	476,9243574	3,23E+09
14	416,9551849	3,52E+09
15	357,1089802	3,71E+09
16	299,8269326	3,78E+09
17	246,9071714	3,73E+09
18	199,5190594	3,58E+09
19	158,2652481	3,34E+09
20	123,2750005	3,04E+09
21	94,31273614	2,69E+09
22	70,88800274	2,32E+09
23	52,35641272	1,96E+09
24	38,00478258	1,62E+09
25	27,11720727	1,30E+09
Sum=		4,89E+12